中央大学博士論文

Synthesis of Antiaromatic Compounds Utilizing Hyperconjugation and Anionic Charges

Shotaro Ito
伊藤　正太郎

博士（工学）

中央大学大学院
理工学研究科
応用化学専攻

令和４年度
２０２３年３月

Preface

This thesis is concerned with the synthesis of antiaromatic compounds containing an sp^3-hybridized atom utilizing hyperconjugation and anionic charges, which has been carried out under the direction of Dr. Takuya Kuwabara and Prof. Yoichi Ishii at Chuo University, from April 2017 to March 2023.

Firstly, I want to express my deepest gratitude to my parents, Akinori Ito and Misako Ito, for their constant help and love. This dissertation is not here without them.

I am grateful to Dr. Kuwabara for his guidance. He taught me what is research, and the meaning of “original”. I’m proud of being his first student in the current laboratory.

My sincere appreciation is toward Prof. Ishii. I decided to become a chemist in his class of organic chemistry when I was a sophomore. He taught me that chemistry is interesting, fascinating, valuable, and fun!

I would like to thank Dr. Tsuyoshi Kato of Université Paul Sabatier for giving me an opportunity to study in Toulouse for three months. He taught me the importance of bravery in changing a strategy.

All teaching will live forever in my research life. I will return the favor by contributing to the world using their teaching.

Shotaro Ito
Chuo University
March 2023

Contents

Chapter 1

General introduction

1-1 Antiaromaticity

Since Michael Faraday discovered benzene in 1825, aromaticity has played a pivotal role in chemistry.[1] According to Huckel's rule, (anti)aromatic compounds consist of a planar sp^2- and/or sp-hybridized carbon-based framework with a cyclic π-conjugation. Aromatic and antiaromatic compounds have (4n+2)π- and 4nπ-electrons, respectively. Generally, aromatic compounds are more stable than antiaromatics because unsaturated cyclic (4n+2)π-electrons species have the filled highest occupied molecular orbital (HOMO) while corresponding MOs for those with 4nπ-electrons are half-filled resulting in triplet character or Jahn-Teller distortion (Figure 1-1).[2]

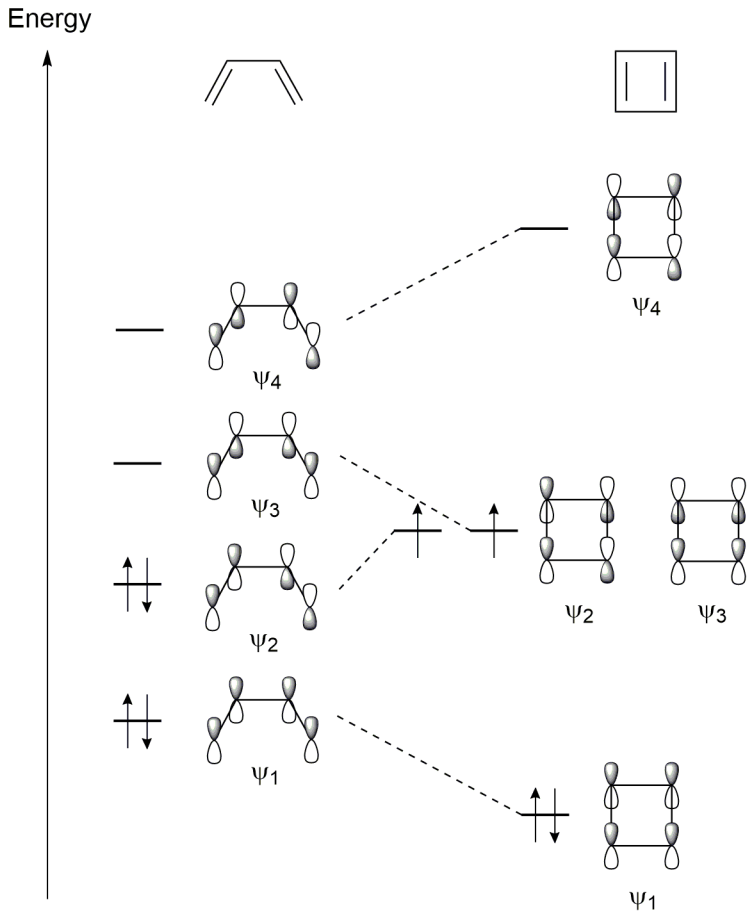

Figure 1-1. Energy diagrams and molecular orbitals of a butadiene (left) and a cyclobutadiene (right).

Because of low stability arising from a triplet character or a small singlet-triplet gap, synthetic studies of antiaromatic compounds are very limited than those for aromatics. Selected examples of synthetic research of 4nπ-electrons system in a simple carbon framework are illustrated in Scheme 1–4. The formation of cyclopropenyl anion **B** via the desilylation of **A** by fluoride ion in the gas phase had been reported (Scheme 1-1).[3] The most simple neutral antiaromatic compound, cyclobutadiene **D**, was first generated by the photolysis of α-pyrone **C** in an argon matrix (Scheme 1-2).[4] Treatment of bromocyclopentadiene **E** with SbF_5 generated cyclopentadienyl cation **F**, which has a triplet character as indicated by an ESR spectrum (Scheme 1-3).[5] Reaction between 7-methoxycycloheptatriene **G** and NaK yielded unsubstituted cycloheptatrienyl anion **H** (Scheme 1-4).[6] Generation of antiaromatic compounds is often confirmed by only trapping reactions, and structural research based on X-ray diffraction analysis is lagging behind.

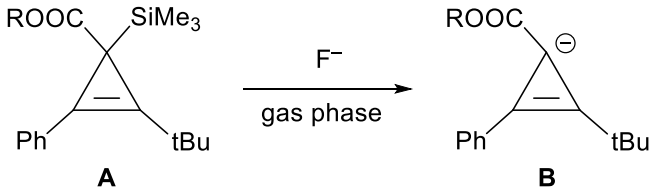

Scheme 1-1. Synthesis of cyclopropenyl anion **B**.

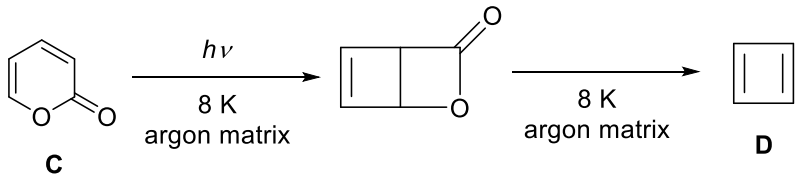

Scheme 1-2. Synthesis of cyclobutadiene **D**.

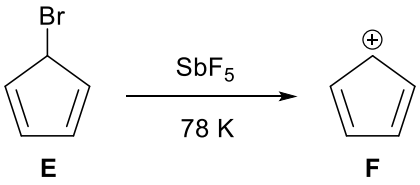

Scheme 1-3. Synthesis of cyclopentadienyl cation **F**.

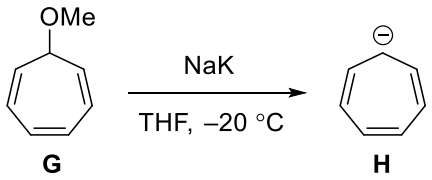

Scheme 1-4. Synthesis of cycloheptatrienyl anion **H**.

1-2 (Anti)aromaticity involving heavier group 14 elements

The concept of (anti)aromaticity is of significant importance to understand the properties of π-conjugated carbocyclic compounds. In the last few decades, introducing heavy group 14 elements into (anti)aromatic scaffolds has attracted considerable attention,[7] and heavier analogs of the cyclopropenyl cation (**I**),[8] the cyclobutadiene dianion (**J**),[9] the cyclopentadienyl anion (**K**)[9b,10] and dianion (**L**),[10a,11] benzene (**M**),[12] and the phenyl anion (**N**)[13] have been synthesized (Figure 1-2). Moreover, synthesis of an aromatic compound containing a lead atom, which is the nonradioactive heaviest group 14 element, is also reported. Saito's group isolated dilithioplumboles, which are lead analogs of **L**, and disclosed their aromatic nature.[14]

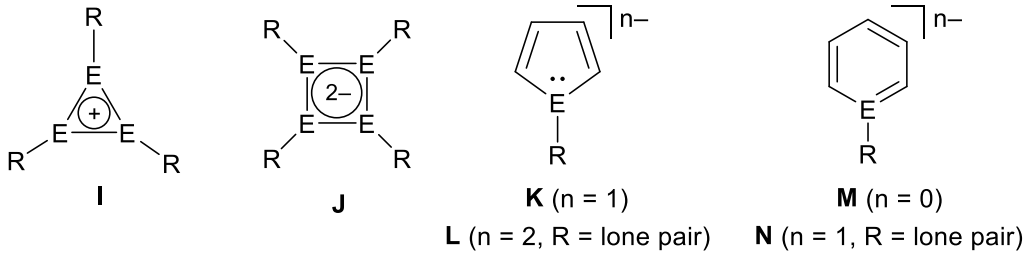

Figure 1-2. Heavier group 14 analogs of various aromatic compounds (**I**–**N**, E = Si, Ge, Sn, Pb).

In contrast, synthetic research of antiaromatic compounds is challenging due to thermodynamic instability. In 2011, the group of Matsuo and Tamao synthesized a silicon analog of a cyclobutadiene via reductive cleavages of Si–Br bonds of a tribromosilane by lithium naphthalenide (Scheme 1-5).[15] The product preferred rhombic charge-separated structure (compound **P**) than D_{4h} square structure (compound **O**), thus antiaromaticity originating from a delocalized 4π-electron system was not observed. To the best of the

author's knowledge, the first synthetic example of an antiaromatic compound containing silicon atoms was benzodisilacyclobutadiene **Q** reported by Iwamoto and coworkers (Scheme 1-6).[16] They revealed that extension of π-conjugated system reduces antiaromaticity of the disilacyclobutadiene moiety. Synthetic studies of antiaromatics involving heavier group 14 elements are limited to neutral species.

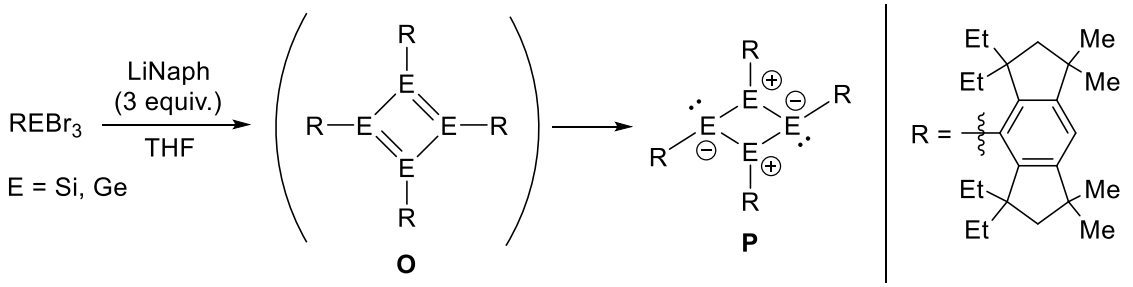

Scheme 1-5. Synthesis of heavy analogs of cyclobutadiene.

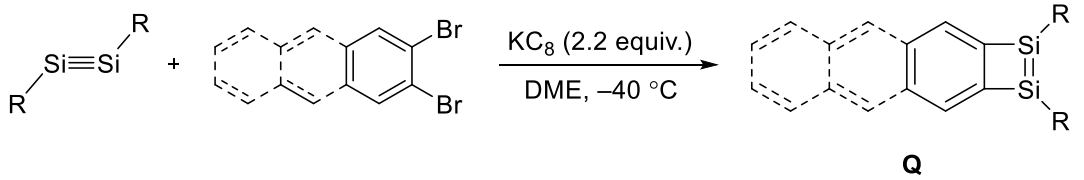

Scheme 1-6. Synthesis of disilacyclobutadiene derivatives.

1-3 Hyperconjugation and (anti)aromaticity

Hyperconjugation is an important factor to understand various phenomena in the field of organic chemistry.[17] There are two types of hyperconjugation as shown in Figure 1-3. An interaction between a σ and a π* orbital is called positive hyperconjugation, whereas that between a filled π orbital and a σ* orbital is negative hyperconjugation.

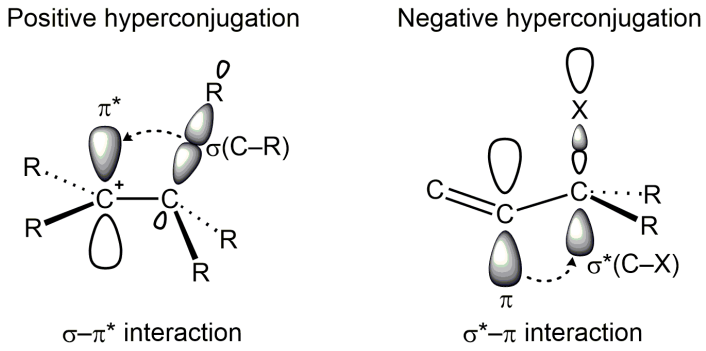

Figure 1-3. Positive and negative hyperconjugation

In contrast to enormous and historical investigations of both aromaticity and hyperconjugation, the studies of aromaticity involving hyperconjugation are very limited. According to Huckel's rule, (anti)aromatic compounds consist of a planar sp^2- and/or sp-hybridized carbon-based framework with a cyclic π-conjugation. Aromatic and antiaromatic compounds have (4n+2)π- and 4nπ-electrons, respectively. Because the Huckel's rule is the most widely used criteria for aromaticity, many chemists believe that (anti)aromatic rings should be composed of sp^2- and/or sp-hybridized atoms. Indeed, introducing an sp^3-hybridized atom into a π-conjugated system generates non-aromatic system due to a disrupted cyclic conjugation. In other words, the proposal of the synthesis of (anti)aromatic compounds involving sp^3-hybridized atom provides us with new alternatives of a design guideline for aromatic systems. Studies of some pseudo π-conjugated systems involving an sp^3-hybridized linkage, which is known as hyperconjugative aromatic compound[18] or σ*-aromatic compound,[19] were mainly conducted from the theoretical aspects.[20] Schleyer's group reported that planar cyclopolyenes ($C_nH_nCR_2$; n = 2, 4, 6, 8) have a potential to obtain hyperconjugative (anti)aromaticity depending on the electronegativity of the R groups (Figure 1-4).[20] For instance, theoretical calculation revealed that **R**, **U**, and **V** have pseudo aromaticity, while **S**, **T**, and **W** have pseudo antiaromaticity.

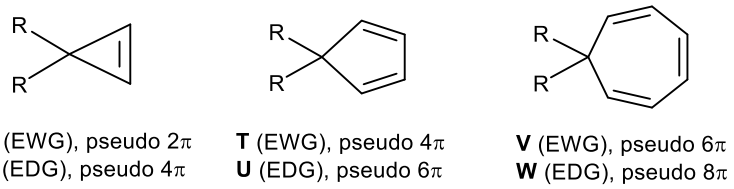

Figure 1-4. Cyclopolyenes and their pseudo (anti)aromaticity.

The concept of hyperconjugative (anti)aromaticity is also used to interpret some reactivities. For example, it is known that Diels–Alder reactions between 5-substituted cyclopentadienes and alkenes are accelerated by hyperconjugative antiaromaticity (Scheme 1-7).[21] Cyclopentadiene **X** obtains a higher reactivity toward an alkene when a σ*(C–X) is π-acceptor because of its pseudo 4π-antiaromatic character arising from the negative hyperconjugation between the σ*(C–X) orbital and adjacent 4π-butadiene moiety.

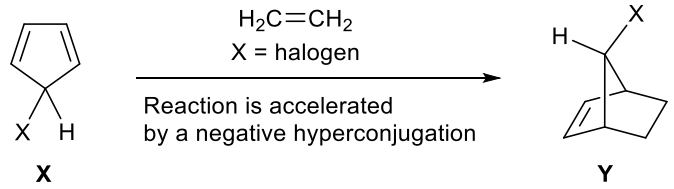

Scheme 1-7. Reaction of a cyclopentadiene and ethylene.

Other unique reactivities induced by hyperconjugative antiaromaticity are reported by Nyulászi and Réau's group (Scheme 1-8). Generally, phosphine is more thermodynamically unstable than its phosphine oxide.[22] However, some phosphole oxides and sulfides are less stable in comparison to the corresponding phospholes. For example, although phosphole **Z** is stable in THF under reflux, phosphole sulfide **AA** is quantitatively transformed into the corresponding phospholene **AB** via a migration of a hydrogen atom. They declared that the instability of **AA** is derived from the delocalized 4π-electron system on the five-membered ring via the negative hyperconjugation between the σ*(P–S) and endocyclic π-system.

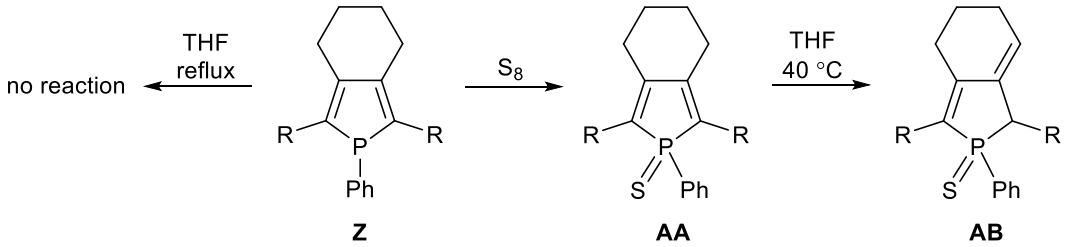

Scheme 1-8. Different stabilities of phosphole and phosphole sulfide in THF.

Several groups have reported the synthesis and structural discussion of hyperconjugative (anti)aromatic compounds (Figure 1-5). To the best of the author's knowledge, the first

structural discussion of (anti)aromaticity is reported by Kira's group in 1998.[19b] They revealed that when a silacyclopropene has electronegative substituents on the silicon atom of the three-membered ring, such as compound **AC**, the bond length of the C=C double bond is elongated, while those of the endocyclic Si–C bonds are shortened, which was interpreted as the result of a pseudo 2π-aromatic character. After the Kira's report, polyaurated indolium derivatives **AD**[23] and cyclopent-4-enyl cations bearing two sp^3-hybridized carbon atoms **AE**[24] were also concluded to have hypercojnugative aromaticity based on structural features. Importantly, Shinokubo's group reported that a Ni(II) phosphacorrole oxide **AF**[25] has a weak antiaromaticity involving the hyperconjugation between the π-clouds of the corrole fragment and σ*(P–O) orbital, which was evidenced by the NMR spectroscopy, structural features, NICS values as well as ACID plots.

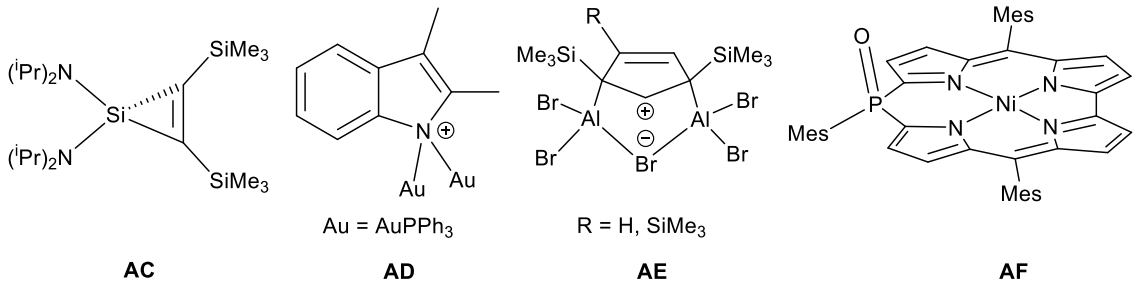

Figure 1-5. Selected examples of hyperconjugative aromatic (**AC**, **AD**, **AE**) and antiaromtic (**AF**) compounds.

1-4 Experimental evaluation of (anti)aromaticity based on NMR spectroscopy

Since antiaromatic compounds are unstable, experimental evaluations of their properties are always challenging, thus identification and quantification of them were mainly conducted theoretically. Especially, NICS (nucleus independent chemical shifts)[26] and ACID (anisotropy of the induced current density) plots[27] are widely used. However, what we have to bear in mind is that too much dependence on the theoretical methods without experimental support may lead to inadequate interpretations, as cautioned by some papers.[28] Therefore, experimental evaluations make arguments on (anti)aromaticity more reliable.

^{1}H NMR spectroscopy is one of the most frequently used experimental methods to describe (anti)aromaticity of compounds, because chemical shifts of ^{1}H NMR signals are

strongly affected by diatropic and paratropic ring currents of aromatic and antiaromatic compounds, respectively. Figure 1-6 shows ^{1}H NMR chemical shifts of seletcted (anti)aromatic compounds. The ^{1}H NMR signal of antiaromatic trisdehydro[12]annulene **AG** appears at high-field (δ 4.55) in comparison to that of aromatic hexakisdehydro[18]annulene **AH** (δ 7.02),[29] which can be attributable to the paratropic and the diatropic ring current of **AG** and **AH**, respectively. Importantly, ^{1}H NMR chemical shifts are also drastically different whether protons locate inside or outside the ring. For instance, the ^{1}H NMR signal inside and outside the π-scaffold of aromatic bisdehydro[14]annulene **AI**[30] resonates at characteristic high-field (δ −4.55) and low-field (δ 9.42), respectively. However, in the case of antiaromatic tridehydro[16]annulene **AJ**,[31] the exact opposite tendency to **AI** is observed because of the paratropic ring current (inside: δ 17.2, outside: δ 4.05). A similar relationship is also found in aromatic [18]annulene **AK** (inside: δ −1.92, outside: δ 8.88) and its dianionic antiaromatic species **AL** (inside: δ 28.8, outside: δ −1.13).[32]

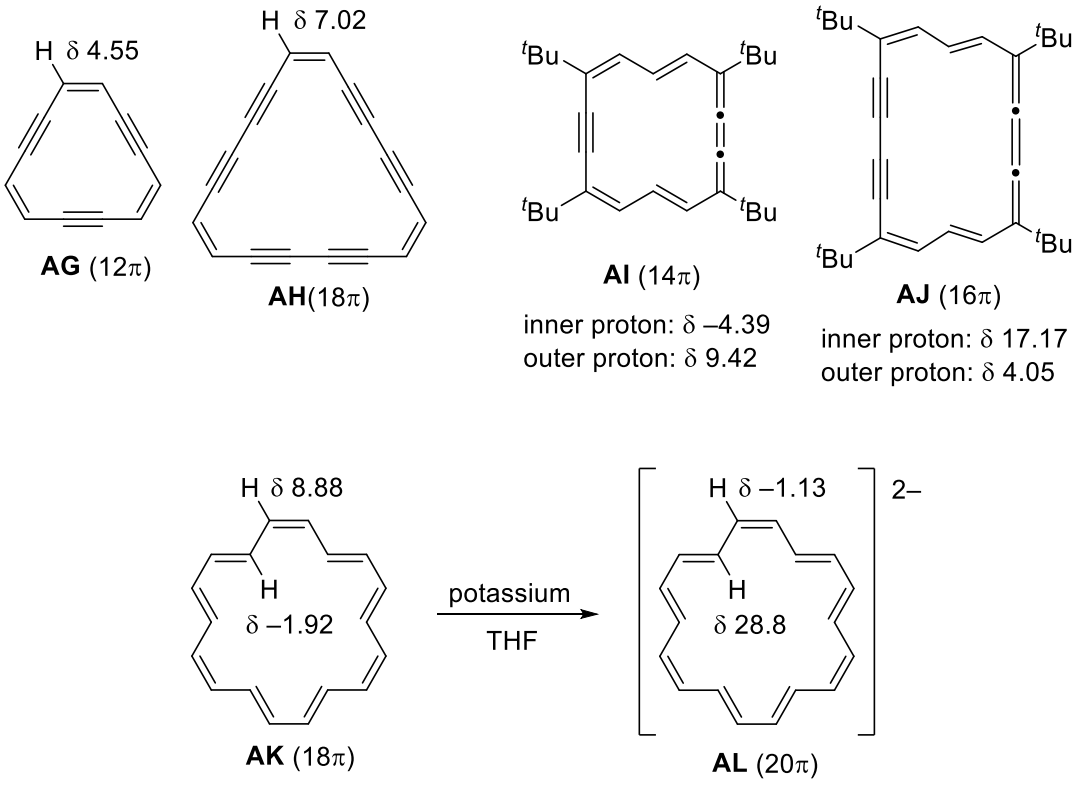

Figure 1-6. ^{1}H NMR chemical shifts of selected aromatic and antiaromatic compounds.

If a compound has lithium cations, ^{7}Li NMR spectroscopy is available for experimental evaluation of (anti)aromaticity, because ^{7}Li NMR chemical shifts are also affected by ring currents, as do ^{1}H NMR chemical shifts. For example, ^{7}Li NMR signals of lithium salts of anionic aromatic compounds, such as cyclopentadienyl anions,[33] heterole dianions,[34] metallole anions and dianions[35] appear at characteristic high-field (δ(^{7}Li) = −4 to −13), whereas those of general organolithium compounds (butyllithium, phenyllithium, etc) and free-lithium cations resonate at around 0 ppm.[36] In contrast, the signals of dilithium salts of benzene dianion (δ(^{7}Li) = 10.2)[36a] and *trans*-15,16-dimethyldihydropyrene dianion (δ(^{7}Li) = 3.2)[37] shifted to low-field, reflecting their antiaromaticity as in the case of **AJ** and **AL**.

1-5 This work

Introduction of heavier group 14 elements into aromatic skeletons have been attempted to explore novel properties that are not found in all-carbon framework aromatics. However, those research for antiaromatic compounds is challenging due to thermodynamic instability. In this doctoral thesis, both experimental and theoretical research of antiaromaticity involving heavier group 14 elements, a silicon atom or a tin atom, are demonstrated (Figure 1-7). In chapter 2, synthesis of Sn analogs of a cycloheptatrienyl anion and a further reduced dianionic species are reported. In chapter 3, the author succeeded in the synthesis of a silepinyl dianion, which is an antiaromatic compound containing an sp^{3}-hybridized silicon atom. In chapter 4, NMR-based evaluation of hyperconjugative antiaromaticity of a trimer of silepinyl dianions and a spirobi(silepinyldianion) is described. In chapter 5, face-to-face interaction between two silepinyl dianions resulting in weakened antiaromaticity is discussed.

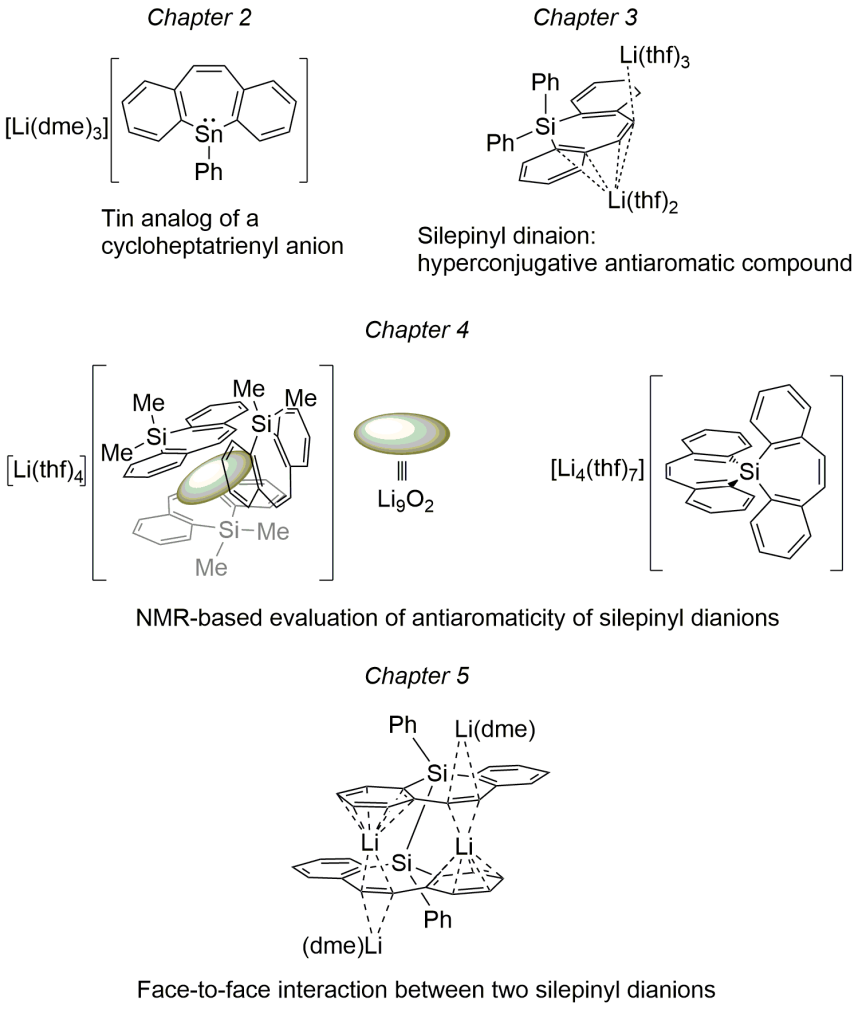

Figure 1-7. The outline for this doctoral thesis.

1-6 References

(1) M. Faraday, *Philos. Trans. R. Soc. London* **1825**, *115*, 440−466.

(2) K. B. Wiberg, *Chem. Rev.* **2001**, *101*, 1317−1331.

(3) R. K. Sachsf, S. R. Kass, *J. Am. Chem. Soc*. *1994*, *116*, 783-784.

(4) O. L. Chapman, C. L. McIntosh, J. Pacansky *J. Am. Chem. Soc.* **1973**, *95*, 614–617.

(5) M. Saunders, R. Berger, A. Jaffe, J. M. McBride, J. O'Neill, R. Breslow, J. M. Hoffmann, C. Perchonock, E. Wasserman, *J. Am. Chem. Soc.* **1973**, *95*, 3017–3018.

(6) H. J. Dauben and M. R. Rifi *J. Am. Chem. Soc.* **1963**, *85*, 3041–3042.

(7) (a) Tokitoh, N. *Bull. Chem. Soc. Jpn.* **2004**, *77*, 429−441. (b) Lee, V. Y.; Sekiguchi, A. *Angew. Chem., Int. Ed.* **2007**, *46*, 6596−6620. (c) Saito, M. *Coord. Chem. Rev.* **2012**,

256, 627−636. (d) Wei, J.; Zhang, W.-X.; Xi, Z. *Chem. Sci.* **2018**, *9*, 560−568. (e) Saito, M. *Bull. Chem. Soc. Jpn.* **2018**, *91*, 1009−1019.

(8) (a) Sekiguchi, A.; Tsukamoto, M.; Ichinohe, M. *Science* **1997**, *275*, 60−61. (b) Ichinohe, M.; Igarashi, M.; Sanuki, K.; Sekiguchi, A. *J. Am. Chem. Soc.* **2005**, *127*, 9978−9979.

(9) (a) Lee, V. Y.; Takanashi, K.; Matsuno, T.; Ichinohe, M.; Sekiguchi, A. *J. Am. Chem. Soc.* **2004**, *126*, 4758−4759. (b) Lee, V. Y.; Takanashi, K.; Kato, R.; Matsuno, T.; Ichinohe, M.; Sekiguchi, A. *J. Organomet. Chem.* **2007**, *692*, 2800−2810. (4) (a) Freeman, W. P.; Tilley, T. D.; Liable-Sands, L. M.; Rheingold, A. L. *J. Am. Chem. Soc.* **1996**, *118*, 10457−10468. (b) Freeman, W. P.; Tilley, T. D.; Yap, G. P. A.; Rheingold, A. L. *Angew. Chem., Int. Ed. Engl.* **1996**, *35*, 882−884. (c) Fekete, C.; Kovács, I.; Nyulászi, L.; Holczbauer, T. *Chem. Commun.* **2017**, *53*, 11064−11067. (d) Saito, M.; Kuwabara, T.; Ishimura, K.; Nagase, S. *Chem. Asian J.* **2011**, *6*, 2907−2910. (e) Saito, M.; Kuwabara, T.; Ishimura, K.; Nagase, S. *Bull. Chem. Soc. Jpn.* **2010**, *83*, 825−827. (f) Dong, Z.; Schmidtmann, M.; Müller, T. *Chem. Eur. J.* **2019**, *25*, 10858−10865.

(10) (a) Freeman, W. P.; Tilley, T. D.; Liable-Sands, L. M.; Rheingold, A. L. *J. Am. Chem. Soc.* **1996**, *118*, 10457−10468. (b) Freeman, W. P.; Tilley, T. D.; Yap, G. P. A.; Rheingold, A. L. *Angew. Chem., Int. Ed. Engl.* **1996**, *35*, 882−884. (c) Fekete, C.; Kovács, I.; Nyulászi, L.; Holczbauer, T. *Chem. Commun.* **2017**, *53*, 11064−11067. (d) Saito, M.; Kuwabara, T.; Ishimura, K.; Nagase, S. *Chem. Asian J.* **2011**, *6*, 2907−2910. (e) Saito, M.; Kuwabara, T.; Ishimura, K.; Nagase, S. *Bull. Chem. Soc. Jpn.* **2010**, *83*, 825−827. (f) Dong, Z.; Schmidtmann, M.; Müller, T. *Chem. - Eur. J.* **2019**, *25*, 10858−10865.T. Nomoto, S. Nakatsuji, M. Nakagawa, *Bull. Chem. Soc. Jpn.*, **1978**, **51**, 3345-3350.

(11) (a) Hong, J.-H.; Boudjouk, P.; Castellino, S. *Organometallics* **1994**, *13*, 3387−3389. (b) West, R.; Sohn, H.; Bankwitz, U.; Calabrese, J.; Apeloig, Y.; Mueller, T. *J. Am. Chem. Soc.* **1995**, *117*, 11608−11609. (c) West, R.; Sohn, H.; Powell, D. R.; Müller, T.; Apeloig, Y. *Angew. Chem., Int. Ed. Engl.* **1996**, *35*, 1002−1004. (d) Saito, M.; Haga, R.; Yoshioka, M.; Ishimura, K.; Nagase, S. *Angew. Chem., Int. Ed.* **2005**, *44*, 6553−6556. (e) Saito, M.; Kuwabara, T.; Kambayashi, C.; Yoshioka, M.; Ishimura, K.; Nagase, S. *Chem. Lett.* **2010**, *39*, 700−701. (f) Hong, J.-H. *Molecules* **2011**, *16*, 8033. (g) Kuwabara, T.; Guo, J.-D.; Nagase, S.; Minoura, M.; Herber, R. H.; Saito, M.

Organometallics **2014**, *33*, 2910−2913. (h) Dong, Z.; Reinhold, C. R. W.; Schmidtmann, M.; Müller, T. *Organometallics* **2018**, *37*, 4736−4743.

(12) (a) Wakita, K.; Tokitoh, N.; Okazaki, R.; Takagi, N.; Nagase, S. *J. Am. Chem. Soc.* **2000**, *122*, 5648−5649. (b) Nakata, N.; Takeda, N.; Tokitoh, N. *J. Am. Chem. Soc.* **2002**, *124*, 6914−6920. (c) Mizuhata, Y.; Fujimori, S.; Noda, N.; Kanesato, S.; Tokitoh, N. *Dalton Trans* **2018**, *47*, 14436−14444. (d) Kaiya, C.; Suzuki, K.; Yamashita, M. *Angew. Chem., Int. Ed.* **2019**, *58*, 7749−7752.

(13) (a) Mizuhata, Y.; Fujimori, S.; Sasamori, T.; Tokitoh, N. *Angew. Chem., Int. Ed.* **2017**, *56*, 4588−4592. (b) Fujimori, S.; Mizuhata, Y.; Tokitoh, N. *Chem. Eur. J.* **2018**, *24*, 17039−17045. (c) Fujimori, S.; Mizuhata, Y.; Tokitoh, N. *Chem. Lett.* **2018**, *47*, 708−710.

(14) (a) Saito, M.; Sakaguchi, M.; Tajima, T.; Ishimura, K.; Nagase, S.; Hada, M. *Science* **2010**, *328*, 339−342. (b) Saito, M.; Nakada, M.; Kuwabara, T.; Minoura, M. *Chem. Commun.* **2015**, *51*, 4674−4676.

(15) (a) Suzuki, K.; Matsuo, T.; Hashizume, D.; Fueno, H.; Tanaka, K.; Tamao, K. *Science* **2011**, *331*, 1306−1309. (b) Suzuki, K.; Numata, Y.; Fujita, N.; Hayakawa, N.; Tanikawa, T.; Hashizume, D.; Tamao, K.; Fueno, H.; Tanaka, K.; Matsuo, T. *Chem. Commun.* **2018**, *54*, 2200−2203.

(16) Ishida, S.; Misawa, Y.; Sugawara, S.; Iwamoto, T. *Angew. Chem., Int. Ed.* **2017**, *56*, 13829−13832.

(17) Alabugin, I. V.; dos Passos Gomes, G.; Abdo, M. A. Hyperconjugation. *WIREs Comput. Mol. Sci.* **2019**, 9, No. e1389.

(18) L. Nyulászi and P. v. R. Schleyer, *J. Am. Chem. Soc.*, **1999**, *121*, 6872-6875.

(19) (a) A. Göller, H. Heydt and T. Clark, *J. Org. Chem.*, **1996**, *61*, 5840-5846; (b) S. Tsutsui, K. Sakamoto, C. Kabuto and M. Kira, *Organometallics*, **1998**, *17*, 3819-3821.

(20) I. Fernández, J. I. Wu and P. v. R. Schleyer, *Org. Lett.*, **2013**, *15*, 2990-2993.

(21) (a) B. J. Levandowski and K. N. Houk, *J. Am. Chem. Soc.* , **2016**, *138*, 16731-16736; (b) B. J. Levandowski, L. Zou and K. N. Houk, *J. Org. Chem.*, **2018**, *83*, 14658-14666; (c) B. J. Levandowski, N. S. Abularrage, K. N. Houk and R. T. Raines, *Org. Lett.*, **2019**, *21*, 8492-8495.

(22) (a) L. Nyulászi, O. Hollóczki, C. Lescop, M. Hissler and R. Réau, *Org. Biomol. Chem.*, **2006**, *4*, 996-998; (b) Z. Mucsi and G. Keglevich, *Eur. J. Inorg. Chem.*, **2007**,

4765-4771.

(23) (a) J. Yuan, T. Sun, X. He, K. An, J. Zhu and L. Zhao, *Nat. Commun.*, **2016**, *7*, 11489; (b) K. Xiao, Y. Zhao, J. Zhu and L. Zhao, *Nat. Commun.*, **2019**, *10*, 5639.

(24) S. Nees, T. Kupfer, A. Hofmann and H. Braunschweig, *Angew. Chem., Int. Ed.* , **2020**, *59*, 18809-18815.

(25) H. Omori, S. Hiroto, Y. Takeda, H. Fliegl, S. Minakata and H. Shinokubo, *J. Am. Chem. Soc.*, **2019**, *141*, 4800-4805.

(26) (a) Z. Chen, C. S. Wannere, C. Corminboeuf, R. Puchta and P. v. R. Schleyer, *Chem. Rev.*, **2005**, *105*, 3842-3888; (b) A. Stanger, *Eur. J. Org. Chem.*, **2020**, 3120-3127.

(27) D. Geuenich, K. Hess, F. Köhler and R. Herges, *Chem. Rev.*, **2005**, *105*, 3758-3772.

(28) (a) J. J. Torres, R. Islas, E. Osorio, J. G. Harrison, W. Tiznado and G. Merino, *J. Phys. Chem. A*, **2013**, *117*, 5529-5533; (b) C. Foroutan-Nejad, *Theor. Chem. Acc.*, **2015**, *134*, 8; (c) S. Van Damme, G. Acke, R. W. A. Havenith and P. Bultinck, *Phys. Chem. Chem. Phys.*, **2016**, *18*, 11746-11755; (d) G. Acke, S. Van Damme, R. W. A. Havenith and P. Bultinck, *Phys. Chem. Chem. Phys.*, **2019**, *21*, 3145-3153.A

(29) Lungerich, D.; Nizovtsev, A. V.; Heinemann, F. W.; Hampel, F.; Meyer, K.; Majetich, G.; v. R. Schleyer, P.; Jux, N. *Chem. Commun.* **2016**, *52*, 4710−4713.

(30) T. Nomoto, S. Nakatsuji, M. Nakagawa, *Bull. Chem. Soc. Jpn.*, **1978**, *51*, 3345-3350.

(31) S. Nakatsuji, M. Morigaki, S. Akiyama, M. Nakagawa, *Tetrahedron Letters*, **1975**, *16*, 1233-1236.

(32) Oth, J. F. M.; Woo, E. P.; Sondheimer, F. Unsaturated macrocyclic compounds. LXXXIX. Dianion of [18]annulene. *J. Am. Chem. Soc.* **1973**, *95*, 7337−7345.a

(33) (a) R. H. Cox, H. W. Terry and L. W. Harrison, *J. Am. Chem. Soc.*, **1971**, *93*, 3297-3298; (b) L. A. Paquette, W. Bauer, M. R. Sivik, M. Buehl, M. Feigel and P. v. R. Schleyer, *J. Am. Chem. Soc.*, **1990**, *112*, 8776-8789.a

(34) (a) G. E. Herberich, T. Wagner and H.-W. Marx, *J. Organomet. Chem.*, **1995**, *502*, 67-74; (b) T. Agou, T. Wasano, P. Jin, S. Nagase and N. Tokitoh, *Angew. Chem., Int. Ed.*, **2013**, *52*, 10031-10034; (c) V. Y. Lee, H. Sugasawa, O. A. Gapurenko, R. M. Minyaev, V. I. Minkin, H. Gornitzka and A. Sekiguchi, *J. Am. Chem. Soc.*, **2018**, *140*, 6053-6056; (d) J. Sarcevic, T. Heitkemper and C. P. Sindlinger, *Chem. Commun.*, **2022**, *58*, 246-249.

(35) (a) S.-B. Choi, P. Boudjouk and J.-H. Hong, *Organometallics*, **1999**, *18*, 2919-2921; (b) M. Saito and M. Yoshioka, *Coord. Chem. Rev.*, **2005**, *249*, 765-780; (c) M. Saito, T. Kuwabara, C. Kambayashi, M. Yoshioka, K. Ishimura and S. Nagase, *Chem. Lett.*, **2010**, *39*, 700-701; (d) T. Kuwabara, J.-D. Guo, S. Nagase, M. Minoura, R. H.

Herber and M. Saito, *Organometallics*, **2014**, *33*, 2910-2913; (e) C. Fekete, I. Kovács, L. Nyulászi and T. Holczbauer, *Chem. Commun.*, **2017**, *53*, 11064-11067; (f) J. Wei, W.-X. Zhang and Z. Xi, *Chem. Sci.*, **2018**, *9*, 560-568; (g) T. Kuwabara and M. Saito, in *Comprehensive Heterocyclic Chemistry IV*, eds. D. S. Black, J. Cossy and C. V. Stevens, Elsevier, Oxford, **2022**, pp. 798-832.

(36) (a) H. Sakurai, *Pure & Appl. Chem.*, **1994**, *66*, 1431-1438; (b) T. Chivers, A. Downard and G. P. A. Yap, *J. Chem. Soc., Dalton Trans.*, **1998**, 2603-2606. (12) Y. Zhu, Z. Zhou, Z. Wei and M. A. Petrukhina, *Organometallics*, **2020**, *39*, 4688-4695.

(37) (a) R. H. Mitchell, C. E. Klopfenstein and V. Boekelheide, *J. Am. Chem. Soc.*, **1969**, *91*, 4931-4932; (b) R. H. Cox, H. W. Terry and L. W. Harrison, *Tetrahedron Lett.*, **1971**, *12*, 4815-4818.

Chapter 2

Synthesis and antiaromaticity of lithium salts of a stannepinyl anion and a dianion

2-1 Introduction

As shown in section 1-2, synthetic studies of antiaromatics involving heavier group 14 elements are limited in neutral species. Cycloheptatrienyl anion **AM** (Figure 2-1) has the 8π-electron system, and its antiaromatic characters as well as instability have been revealed by both experimental studies (^{1}H NMR,[1] pKa values,[2] and high reactivities[3]) and theoretical calculations (NICS (nucleus independent chemical shift)[4] and ISE (isomerization stabilization energy)[5]). Although synthesis of heavier group 14 element analogs of cycloheptatrienyl cation such as silacycloheptatrienyl cation[6] has been reported, the cycloheptatrienyl anion analog had not been synthesized. In this chapter, the author presents the synthesis, structure, and discussion of the antiaromaticity of a stannepinyl anion and a further reduced dianionic compound.

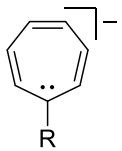

AM

Figure 2-1. Cycloheptatrienylanion **AM**.

2-2 Synthesis of a lithium stannacycloheptatrienide.

Because a Sn−Ph bond is reductively cleaved by lithium to form a Sn−Li bond,[7] 5,5-diphenyldibenzo[*b*,*f*]stannepin **1** was chosen as a precursor for a lithium stannacycloheptatrienide. Lithiation of (*Z*)-2,2-dibromostilbene **2**[8] with ^{n}BuLi followed by the addition of dichlorodiphenylstannane yielded **1** in 76% yield (Scheme 2-1). To synthesize a tin analog of the cycloheptatrienyl anion, a reduction of **1** with lithium was conducted (Scheme 2-1). When **1** was allowed to react with excess lithium at −10 °C for 30 min, the colorless solution turned orange, suggesting the generation of anionic species. Recrystallization of the orange solution at −40 °C provided yellow crystals which decomposed under reduced pressure to give a white powder. Preliminary X-ray diffraction analysis of the yellow crystals revealed that the crystallized product was the lithium stannacycloheptatrienide **3** with a contact ion pair structure (Figure 2-2, left). The lithium cation was coordinated by three diethyl ether molecules and the tin atom.

Recrystallization of the yellow crystals from 1,2-dimethoxyethane (DME) solution deposited thermally stable orange crystals of **4** adopting a solvent-separated ion pair structure (21% isolated yield), which is suitable for X-ray diffraction analysis (Figure 2-2, right). The lithium atom in **4** was coordinated by three DME molecules, and the distance between the lithium and the tin atom exceeded 6 Å, suggesting no bonding interaction between them.

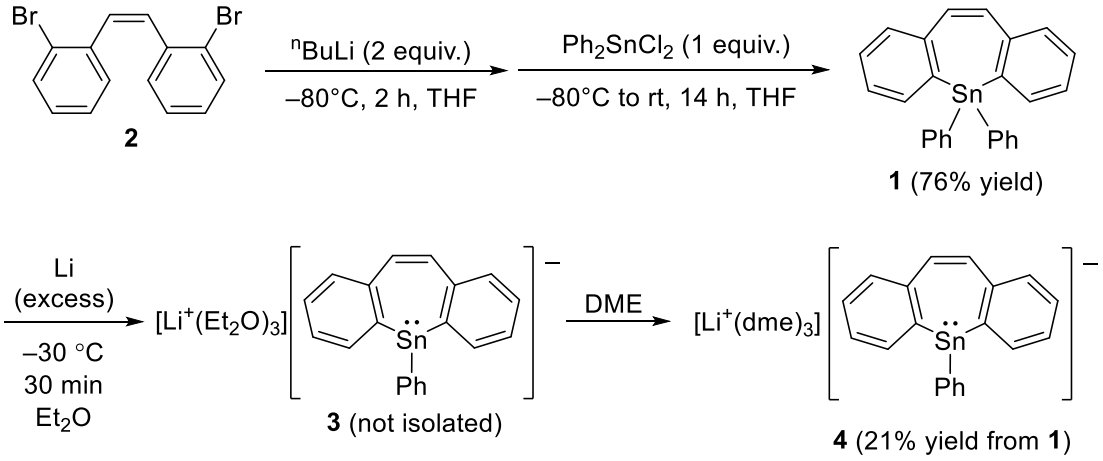

Scheme 2-1. Isolation of **1** and **4**.

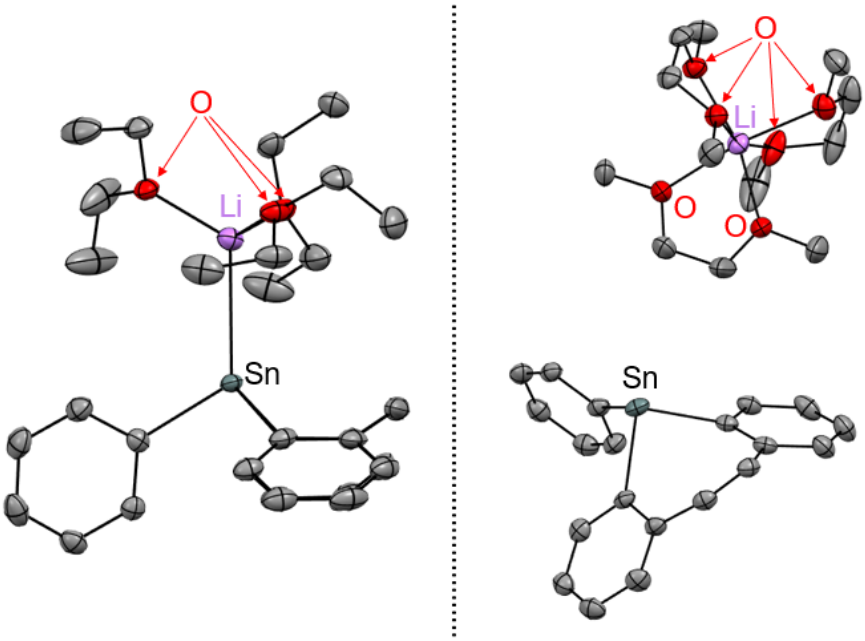

Figure 2-2. Whole structures of **3** (left) and **4** (right).

In the ^{1}H NMR spectrum of **4** in C_6D_6, the signal of the vinyl protons was observed at δ 7.08, which is in a region similar to that of precursor **1** (δ 6.88), suggesting the lack of paratropic ring currents in **4**. The $^{1}J_{Sn-C}$ coupling constants for the $^{13}C\{^{1}H\}$ NMR signals for C_α atoms and C_{ipso} atom of the Ph groups in **4** ($^{1}J_{Sn-C}$ = 125−160 Hz) became much smaller than those in **1** ($^{1}J_{Sn-C} \approx 500$ Hz). The $^{7}Li\{^{1}H\}$ NMR signal of **4** in C_6D_6 appeared at δ −1.17, which is closely related to those observed for [solvent-separated lithium cation][metallolyl anion] type compounds.[9] The $^{119}Sn\{^{1}H\}$ NMR signal of **4** was observed at higher field than that of **1** (δ −164 vs. δ −129) indicating that the anionic charge is localized on the tin atom of **4**.

Figure 2-3 illustrates the structural comparison between **1** and **4**. Although there are two independent molecules (denoted as **4a** and **4b**) in the unit cell of **4**, only the molecular structure of **4a** is shown in Figure 2-3 because the structural parameters for both **4a** and **4b** were almost identical. The stannepin ring in **1** has a boat-type structure with its θ1 (44.1°) and θ2 (37.7°), where θ1/θ2 are defined by the angles between the C1−C2−C5−C6 plane and the Sn−C1−C6/C2−C3−C4−C5 planes, respectively. The dibenzostannepin skeleton has a bent structure with a folding angle (θ3) of 111.3°, which is defined by the angle between the two fused benzene rings flanking the stannepin core. These structural properties are similar to those of other reported dibenzoheteropins with a group 14 element (Si[10] and Sn[11]). Three C−Sn−C angles of **4** ranging from 92.72(12) to 96.28(13)° are much smaller than those in **1** (100.54(12) to 111.64(12)°). The Sn−C_α bond lengths are 2.214(3)/2.220(3) Å, which are longer than those in **1** (2.121(3)/2.131(3) Å). The sum of the angles around the tin atom of **4** indicates a highly pyramidalized tin atom, as was found in a potassium triphenylstannide (290.6°).[12] These structural features suggest that the anionic charge is localized on the tin atom. Upon reduction, the angle θ1 became larger (from 44.1° (**1**) to 46.6° (**4a**) and 52.0° (**4b**)), whereas θ2 became smaller (from 37.7° (**1**) to 31.4° (**4a**) and 31.9° (**4b**)), and the folding angle (θ3) became wider (from 111.3° (**1**) to 126.7° (**4a**) and 124.4° (**4b**). As a result, the structure of the dibenzostannepin skeleton in **4** is similar to that of a neutral dibenzoarsepin that has a Ph group and a lone pair on the arsenic atom (θ1 = 55.0°, θ2 = 32.2°, θ3 = 125.1°).[13]

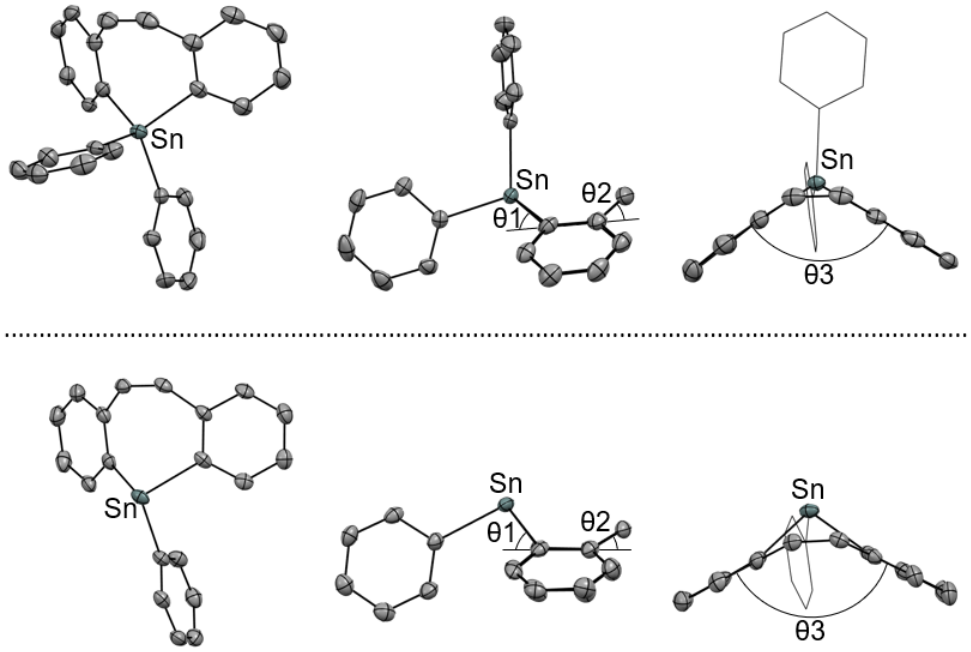

Figure 2-3. Whole structures of **1** (top) and anionic parts of **4** (bottom).

Table 2-1. Selected bond lengths of **1** and **4a**.

	1	**4a**
Sn1−C1/ Sn1−C6	2.121(3)/2.131(3)	2.214(3)/2.220(3)
C1−C2/C5−C6	1.411(4)/1.399(4)	1.427(5)/1.401(5)
C2−C3/C4−C5	1.490(5)/1.467(5)	1.471(5)/1.478(5)
C3−C4	1.352(5)	1.347(5)
C1−C7/C6−C14	1.396(4)/1.393(5)	1.400(5)/1.402(5)
C7−C8/C14−C13	1.393(4)/1.390(5)	1.388(5)/1.392(5)
C8−C9/C13−C12	1.393(4)/1.375(5)	1.380(5)/1.383(6)
C9−C10/C12−C11	1.386(5)/1.395(5)	1.386(5)/1.379(6)
C10−C2/C5−C11	1.396(5)/1.403(5)	1.404(5)/1.409(5)

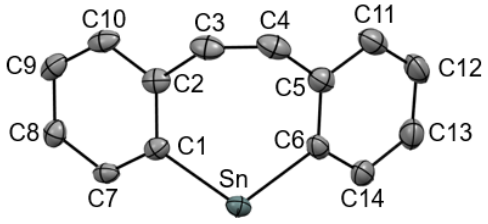

Elongation of the reaction time to 2 h generated a deep red solution, indicating that a further reduction product, probably dilithiostannepin **5** (Scheme 2-2), was generated. The trapping reaction was conducted using MeI, and dimethylstannepin **6**[14] was isolated in

63% yield as a colorless oil, indicating the generation of dilithiostannepin **5** in the deep red solution. However, unfortunately, **5** could not be isolated because of its thermal instability.

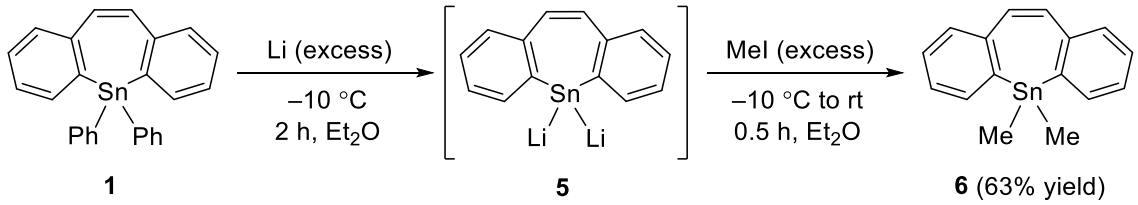

Scheme 2-2. Trapping reaction of **5** using MeI.

Notably, when the reduction of **1** with lithium was carried out at room temperature, a gray powder of tin metal was generated in the reaction mixture, suggesting a decomposition of **5** (Scheme 2-2). Indeed, the X-ray diffraction analysis of the yellow crystals obtained by recrystallization from the Et_2O solution at −30 °C revealed that the major product was (*E*)-2,2′-dilithiostilbene **7** (80% isolated yield), which forms a dimer in the crystalline state (Scheme 2-3). In stark contrast, dilithiostannoles, which are tin-containing aromatic compounds (**L** in Figure 1-2, E = Sn), are isolated by refluxing a mixture of the corresponding 1,1-diphenylstannoles and lithium in Et_2O.[15] The author estimated that the thermal instability of dilithiostannepin **5** in comparison to the dilithiostannoles can be attributable to the antiaromatic character due to the 16π-electron system. Theoretical calculations (details are written in Section 2-4-2) revealed that the $NICS(0)_{iso}$ values[16] for the seven- and six-membered rings of the lithium-free anion of **5** (denoted as **5′**) were calculated to be 6.7 and 9.9, respectively, indicating that **5′** has an antiaromatic character due to the 16π-electron system.

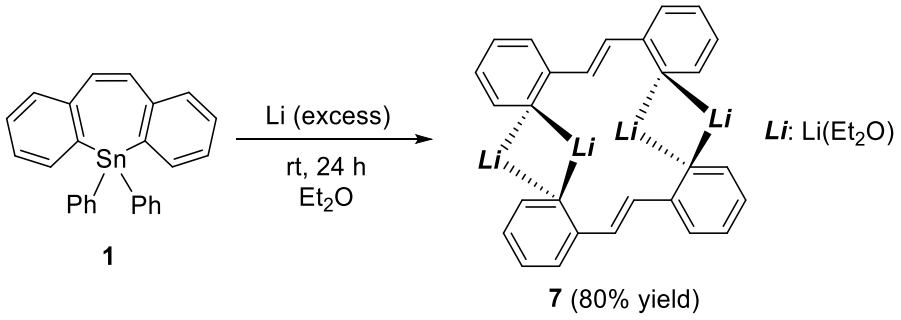

Scheme 2-3. Reduction of **1** with lithium at room temperature.

In conclusion, the author synthesized and characterized lithium dibenzostannepinide **4** which was concluded to be nonaromatic based on the NMR and X-ray diffraction studies. Moreover, a further reduced species, dilithiostannepin **5**, which seems to have antiaromaticity, was generated by a reduction of **1**, as evidenced by the trapping reaction.

2-3 Synthesis of a dilithium dinaphthostannepinide.

In section 2-2, a potential of antiaromaticity in a dilithiostannepin was suggested by its large negative $NICS(0)_{iso}$ values and less thermal stability in comparison to dilithiostannoles. However, the author failed to obtain experimental data to support the antiaromaticity in a dilithium salt of dibenzostannepinyl dianion due to its instability. Therefore, a π-extended dilithiostannepin was designed to improve the stability of such dianionic species. It is expected that a π-extension stabilizes the system by delocalization of anionic charges over a molecule. In this section, synthesis and discussion of antiaromaticity of dilithiostannepin based on NMR spectroscopy and theoretical calculations are demonstrated.

The author tried to synthesize stannylene **9** for a precursor of a stannepinyl dianion. ^{t}BuLi was added dropwise to a THF solution of dibromostilbene derivative **8** at −80 °C, then the mixture was treated with $SnCl_2$ to obtain a yellow powder. Recrystallization of the powder from a CS_2 solution deposited yellow crystals of tetramer **10** that was formed by tetramerization of **9** (Figure 2-4). The sum of the internal angles of the Sn_4 ring in **10** is 360°, indicating its high planarity. A related tetramer with a planar Sn_4 ring is reported by Schnepf.[17] In the ^{1}H NMR spectrum of **10** in C_6D_6, the signal of H_a shown in Figure 2-4 (right) appeared at characteristic high-field (δ 5.46). Assuming that the tetrameric structure remains intact in solution, this high-field shifted signal can be attributable to a diatropic ring current of an adjacent naphthalene unit.

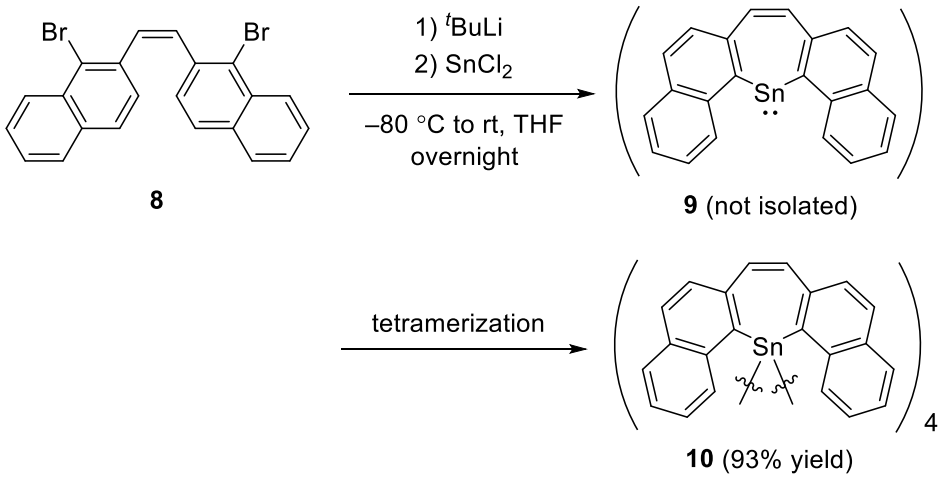

Scheme 2-4. Generation of stannylene **9** and its tetramerization to afford tetramer **10**.

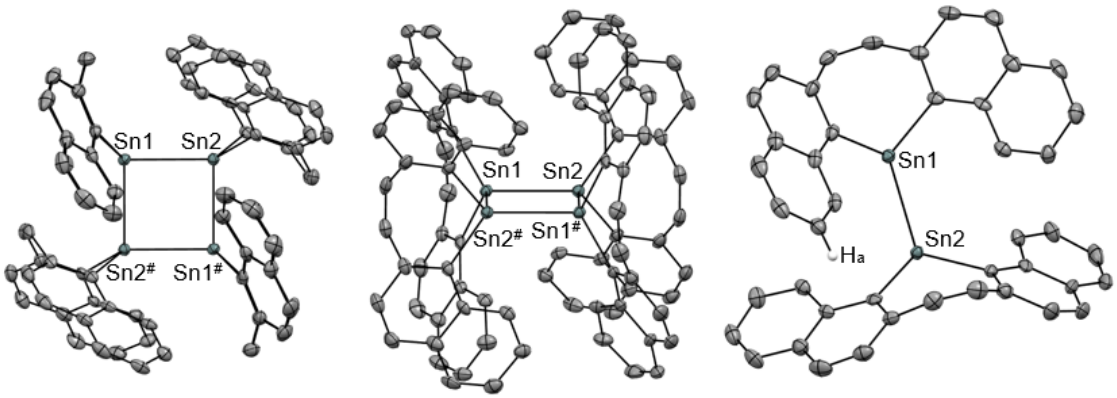

Figure 2-4. Whole structures of **10** (left and center), and a partial structure showing the H_a atom that is shielded by a diatropic ring current of the naphthalene unit (right).

The reaction of **10** and lithium at −80 °C in THF afforded black-purple powder **11** (Scheme 2-5). The ^{1}H NMR spectrum of the black-purple powder in THF-d_8 revealed consumption of the precursor and generation of a single product. The ^{1}H NMR signals of **11** appeared at characteristic high-field (δ 6.79 to 4.18), suggesting that the anionic charges are delocalized over the dinaphthostannepin scaffold. The ^{13}C NMR signal of the alpha carbon (C_α) that is bonded to the tin atom was broadened, the reason for which is not clear at this point. Interestingly, although the ^{1}H NMR spectra recorded at both room temperature and −100 ºC are almost identical, obvious temperature dependence was observed in the ^{7}Li{^{1}H} NMR spectra (Figure 2-5). There are two signals in the ^{7}Li{^{1}H} NMR chart of **11** in THF-d_8 at δ −0.26 and −2.62 with the same integral values. The

VT(variable temperature)-^{7}Li{^{1}H} NMR study revealed that the signal at δ −0.26 does not have temperature dependence, suggesting that the signal is assignable to free-lithium cations coordinated by THF molecules, while the signal at δ −2.62 is sharpened upon cooling. The author assumed that the high-field shift is attributable to paratropic ring currents of the stannepinyl dianion, and the temperature dependence is derived from ring inversion of the non-planar stannepin ring (*vide infra*) shown in Figure 2-6. Thus, the signal at δ −2.62 can be assignable to the lithium that interacts with the dianionic tin atom.

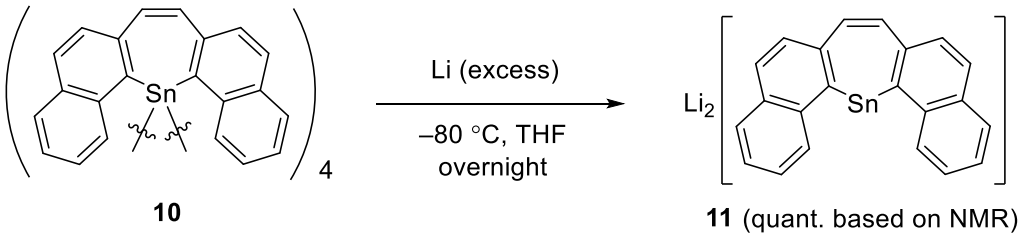

10 **11** (quant. based on NMR)

Scheme 2-5. Synthesis of dilithium dinaphthostannepinide **11**.

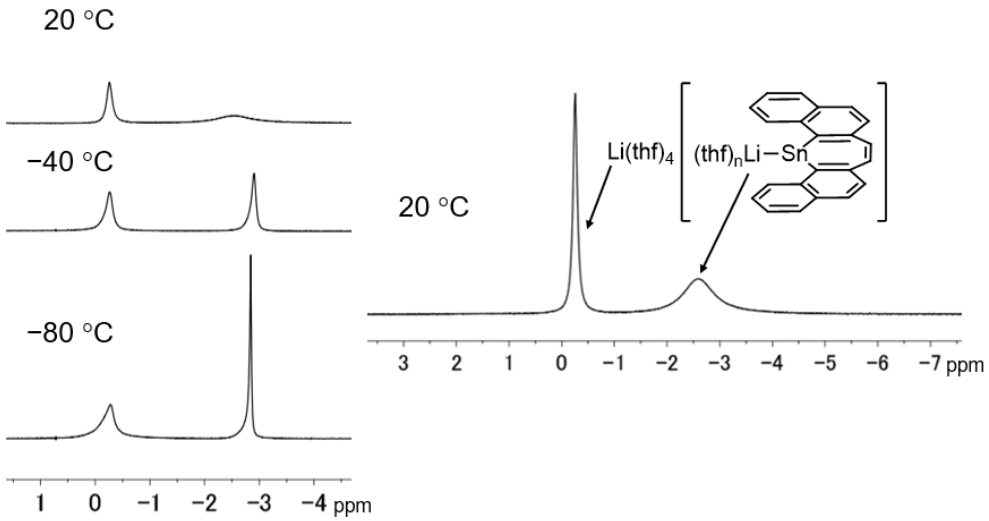

Figure 2-5. The VT-^{7}Li{^{1}H} NMR spectra of **11** recorded in THF-d_8, and the estimated assignment of the signals (right).

Since single crystals of **11** suitable for X-ray diffraction analysis could not be obtained, theoretical calculations were performed to better understand its structure and properties. The optimized structure and the NICS(0)$_{iso}$ values of the lithium-free dianion of **11** (denoted as **11′**) are shown in Figure 2-6 (top). The NICS(0)$_{iso}$ values were calculated to be positive large, indicating an antiaromatic character of **11′**. The HOMO and HOMO−1

of **11′** mainly demonstrate the filled p orbital and the s orbital of the tin atom, respectively, suggesting that two-electron reduction of the vacant p orbital of the tin atom in **9** proceeded to form **11**. Notably, the HOMO of **11** shows the orbital interaction between the filled p orbital of the tin atom and the π* orbital of the vinyl carbons, indicating that the anionic charges on the tin atom are delocalized to the carbon framework via p(Sn)-π*(C=C) interaction.

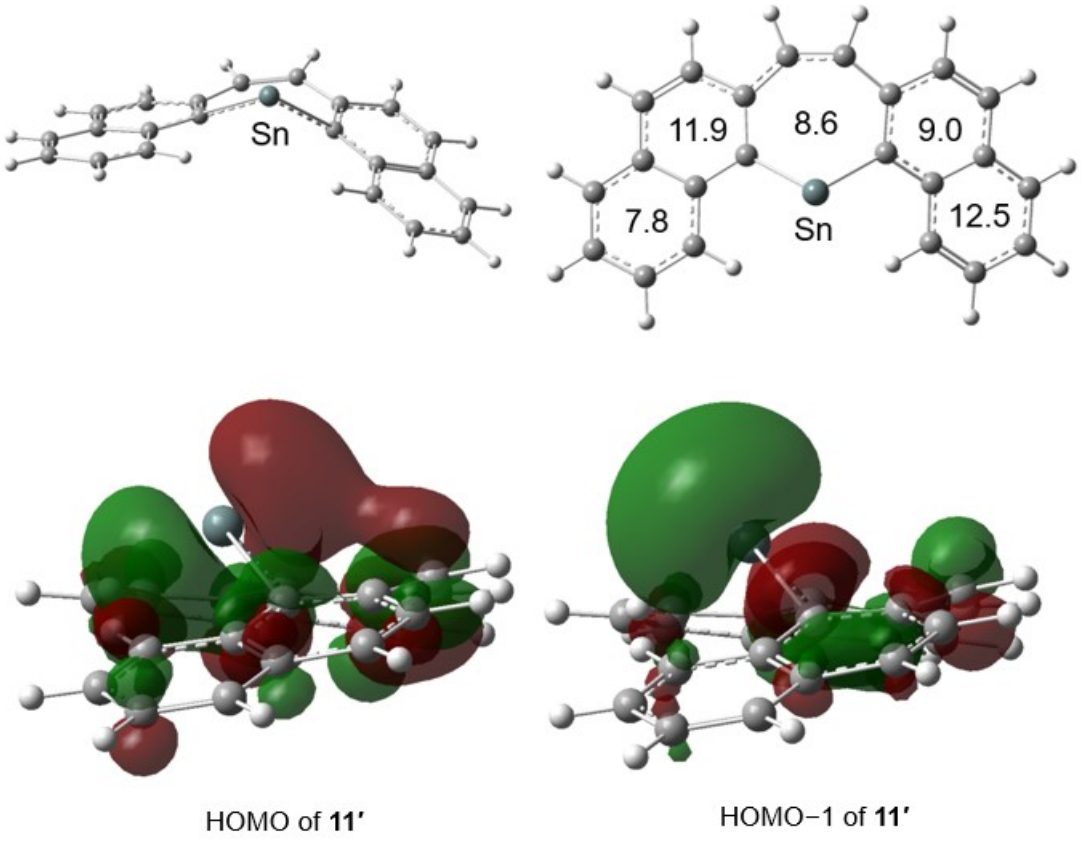

Figure 2-6. The optimized structure (top left) and the $NICS(0)_{iso}$ values (top right) of **11′**, and frontier molecular orbitals of **11′** (bottom).

In conclusion, the author synthesized thermally stable dilithium dinaphthostannepinide **11**. The ^{1}H NMR signals of **11** were observed at characteristic high-field, suggesting that the anionic charges are delocalized over the whole molecule. The $NICS(0)_{iso}$ values of **11′** obtained from the optimized structure were calculated to be large positive values, suggesting dilithium dinaphthostannepinide **11** has antiaromaticity derived from a 24π-electron system.

2-4 Experimental Section

2-4-1 Synthetic Procedures

All manipulations were carried out under an argon atmosphere by using standard Schlenk techniques or a glove box unless otherwise stated. Et_2O, THF, DME, C_6D_6, and THF-d_8 were distilled over potassium mirror. Ph_2SnCl_2 was purchased from Aldrich and recrystallized from hexane before used. 2,2′-Dibromostilbene **2** was synthesized according to the literature.[8] ^1H (500 MHz), $^{13}C\{^1H\}$ (126 MHz), $^7Li\{^1H\}$ (194 MHz) and $^{119}Sn\{^1H\}$ (187 MHz) NMR spectra were recorded on a JEOL ECA-500 spectrometer at 20°C unless otherwise stated. Chemical shifts are reported in δ and referenced to residual ^1H and ^{13}C signals of deuterated solvents as internal standards or to the $^7Li\{^1H\}$ and the ^{119}Sn NMR signal of LiCl in D_2O (δ=0.00) and $SnMe_4$ in C_6D_6 (δ=0.00), respectively, as external standards. Elemental analyses were performed on a Perkin Elmer 2400 series II CHN analyzer.

Synthesis of 5,5-diphenyldibenzo[b,f]stannepin 1.

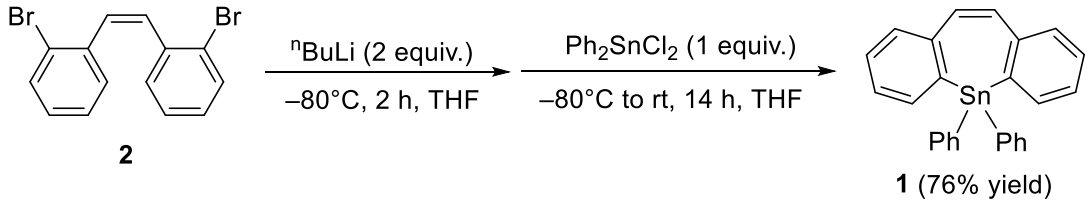

2 **1** (76% yield)

^{n}BuLi (1.6 M in hexanes, 10.0 mL, 16 mmol) was added to a THF solution (200 mL) of dibromostilbene **2** (2.47 g, 7.31 mmol) in THF at −78 ºC. After 2 hours, a THF solution (10 mL) of Ph_2SnCl_2 (2.52 g, 7.33 mmol) was added dropwise, then the mixture was allowed to gradually warm to room temperature and stirred for 14 hours at room temperature. The solvent was removed in vacuo, and materials insoluble in Et_2O were filtered off. The filtrate was concentrated and purified by recrystallization from Et_2O to yield **1** as colorless crystals (2.41 g, 5.35 mmol, 76% yield). m.p. 156 °C; ^1H NMR (500 MHz, $CDCl_3$): δ = 7.67–7.55 (m, 4H, *o-H of Ph*), 7.47 (dd, $^3J_{H–H}$ = 7 Hz, $^4J_{H–H}$ = 2 Hz, 2H, *CH*), 7.45-7.39 (m, 8H, *m- and p-H of Ph and Ar*), 7.36 (td, $^3J_{H–H}$ = 8 Hz, $^4J_{H–H}$ = 2 Hz, 2H, *CH*), 7.26 (t, $^3J_{H–H}$ = 8 Hz, 2H, *CH*), 6.88 (s, 2H, *vinyl*); $^{13}C\{^1H\}$ NMR (126 MHz, $CDCl_3$): δ=144.0 ($^2J_{Sn–C}$ = 29 Hz, 4°, *Cβ*), 139.9 ($^1J_{119Sn–C}$ = 502 Hz, $^1J_{117Sn–C}$ = 479

Hz, 4°, *Cα*), 137.8 ($^2J_{Sn–C}$ = 39 Hz, 3°, *o-C of Ph*), 136.2 ($^2J_{Sn–C}$ = 34 Hz, 3°), 136.1 ($^1J_{119Sn–C}$ = 552 Hz, $^1J_{117Sn–C}$ = 527 Hz, 4°, *ipso-C of Ph*), 134.2 ($^3J_{Sn–C}$ = 10 Hz, 3°, *vinyl*), 129.9 ($^3J_{Sn–C}$ = 45 Hz, 3°), 129.3 ($^4J_{Sn–C}$ = 10 Hz, 3°), 129.0 ($^4J_{Sn–C}$ = 10 Hz, 3°), 128.7 ($^3J_{Sn–C}$ = 53 Hz, 3°, m-C of Ph), 127.5 ($^3J_{Sn–C}$ = 49 Hz, 3°); ^{119}Sn{^{1}H} NMR (187 MHz, CDCl3): δ = −129; Elemental analysis calcd (%) for $C_{26}H_{20}Sn$: C 69.22, H 4.47; found: C 69.11, H 4.39.

Synthesis of lithium salt of 5-phenyldibenzo[*b*,*f*]stannepin anion 4.

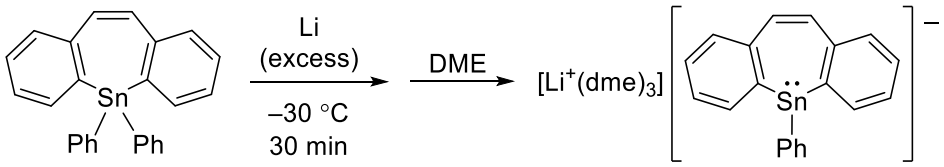

Lithium (60.0 mg, 8.64 mmol) was added to a solution of **1** (99.9 mg, 0.221 mmol) in Et_2O (4 mL) at −10 °C. After 0.5 hours, lithium was removed and cooling at −40 ºC deposited yellow crystals of **3**. After removing Et_2O by a syringe, the yellow crystals were dissolved in DME to give an orange solution, and cooling at −30 °C deposited **4** as orange crystals (30.1 mg, 0.0462 mmol, 21% yield). m.p. > 63 °C (decomp.); ^{1}H NMR (500 MHz, C_6D_6): δ = 8.32 (dd, 2H, $^3J_{H–H}$ = 8 Hz, $^4J_{H–H}$ = 1 Hz, *o-H of Ph*), 7.86-7.82 (m, 2H, *CH*), 7.51 (t, 2H, $^3J_{H–H}$ = 8 Hz, *m-H of Ph*), 7.39 (t, $^3J_{H–H}$ = 8 Hz, 1H, *pH of Ph*), 7.37 (dd, $^3J_{H–H}$ = 7 Hz, $^4J_{H–H}$ = 2 Hz, *CH*), 7.16 (td, $^3J_{H–H}$ = 7 Hz, $^4J_{H–H}$ = 2 Hz, 2H, CH), 7.14 (td, $^3J_{H–H}$ = 7 Hz, $^4J_{H–H}$ = 2 Hz, 2H, *CH*), 7.08 (s, 2H, *vinyl*), 2.96 (s, 30H, *DME*); ^{13}C{^{1}H} NMR (126 MHz, C_6D_6): δ = 161.0 ($^1J_{Sn–C}$ = 125 Hz, 4°, *Cα*), 160.3 ($^1J_{Sn–C}$ = 161 Hz, 4°, *ipso-C of Ph*), 143.7 ($^2J_{Sn–C}$ = 39 Hz, 4°, *Cβ*), 141.0 ($^2J_{Sn–C}$ = 59 Hz, 3°, *o-C of Ph*), 137.4 ($^2J_{Sn–C}$ = 21 Hz, 3°), 134.9 ($^3J_{Sn–C}$ = 16 Hz, 3°, *vinyl*), ($^3J_{Sn–C}$ = 68 Hz), 127.6 (3°), 127.4 (3°), 126.7 ($^3J_{Sn–C}$ = 60 Hz, 3°), 125.7 (3°, *p-C of Ph*), 124.5 (3°), 70.5 (*CH₂*), 58.7 (*CH₃*); ^{7}Li{^{1}H} NMR (194 MHz, C_6D_6): δ = −1.17; ^{119}Sn{^{1}H} NMR (187 MHz, C_6D_6): δ = −164.

Formation of 5,5-dilithiodibenzo[b,f]stannepin 5 and its trapping reaction using MeI.

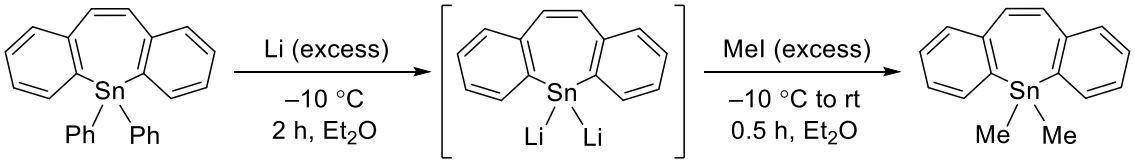

1 **5** **6** (63% yield)

Lithium (41.5 mg, 5.98 mmol) was added to a solution of **1** (50.7 mg, 0.112 mmol) in Et_2O (2 mL) at −10 °C. After 2 hours, lithium was removed and CH_3I (228 mg, 1.61 mmol) was added dropwise, then stirred for 0.5 hours at room temperature. The solvent was removed in vacuo, and the crude product was purified by preparative TLC (Hexane) to yield **6** as a colorless oil (23.0 mg, 0.0703 mmol, 63% yield). The ^{1}H NMR spectrum of **6** is identical to that reported in the literature.[29]

Reduction of 1 with lithium at room temperature.

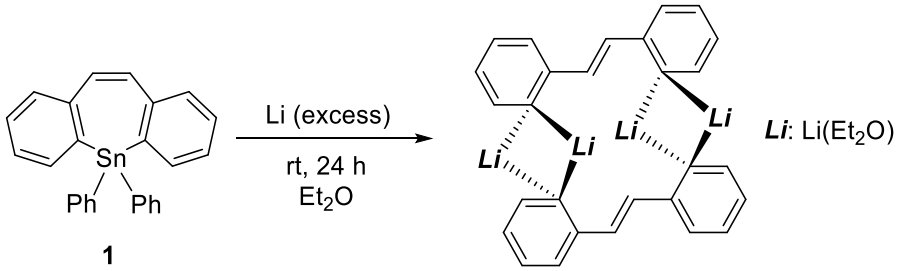

1 **7** (80% yield)

Lithium (80.7 mg, 11.6 mmol) was added to a solution of **1** (101.1 mg, 0.224 mmol) in Et_2O (4 mL) at room temperature. After stirring for 24 hours, gray powder was filtered off, and cooling the filtrate at −30 °C deposited **7** as yellow crystals (61.1 mg, 0.179 mmol, 80% yield). Due to the low solubility toward C_6D_6, Et_2O, and THF, NMR of **7** could not be measured. m.p. > 144 °C (decomp.); Elemental analysis calcd (%) for C44H60Li4O4: C 77.64, H 8.88; found: C 76.86, H 8.71.

Synthesis of tetramer of dinaphthostannylene 10.

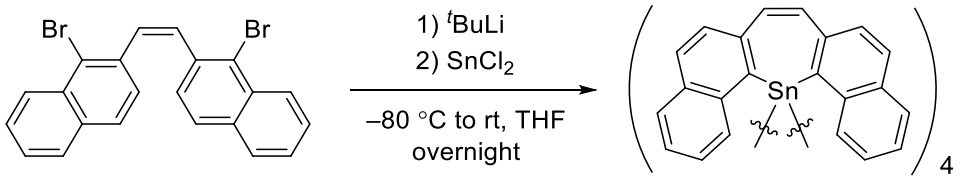

8 **10** (93% yield)

tBuLi (0.60 mL, 0.0935 mmol) was added to a THF solution (4 mL) of dibromostilbene derivative **8** (100.0 mg, 0.228 mmol) at −78 ºC. After 2 hours, the resulting black green solution was transferred to the Et_2O suspension (2 mL) of $SnCl_2$ (59.0 mg, 0.311 mmol) at −78 ºC, then the mixture was allowed to gradually warm to room temperature. The insoluble materials in the resulting red orange suspension were filtered and washed by THF to yield yellow powder of **10** (99.8 mg, 0.213 mmol, 93% yield). ^{1}H NMR (C_6D_6): δ = 7.94 (d, $^3J_{HH}$ = 8.0 Hz, 2H, *Ar*), 7.39 (d, $^3J_{HH}$ = 8.0 Hz, 2H, *Ar*), 7.20 (d, $^3J_{HH}$ = 7.7 Hz, 2H, *Ar*), 7.11 (br, 2H, *Ar*), 6.72 (br, 2H, *vinyl*), 6.53 (t (br), 2H, *Ar*), 5.46 (br, 2H, *Ar*).

Synthesis of dilithium dinaphthostannepinide 11.

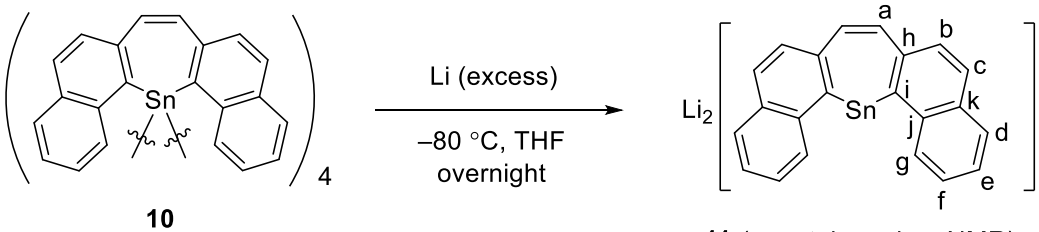

10 **11** (quant. based on NMR)

Lithium (30.0 mg, 4.32 mmol) was added to a solution of **10** (50.0 mg, 0.0326 mmol, 0.131 mmol) in THF (6 mL) at −78 ºC. After stirring overnight, lithium was removed and the solvent was removed in vacuo to yield **11** as a black powder (107.2 mg, quant. based on NMR, the author does not have any structural information such as the number of coordinating THF molecules in black powder of **11**). ^{1}H NMR (THF-d_8): δ 6.79 (d, 2H, $^3J_{HH}$ = 7.5 Hz, H_g), 6.46 (d, 2H, $^3J_{HH}$ = 7.0 Hz, H_d), 6.35 (d, 2H, $^3J_{HH}$ = 8.5 Hz, H_b), 6.33 (t, 2H, $^3J_{HH}$ = 6.5 Hz, H_f), 6.16 (d, 2H, $^3J_{HH}$ = 8.5 Hz, H_c), 5.76 (t, 2H, $^3J_{HH}$ = 6.5 Hz, H_e), 4.18 (s, 2H, *vinyl*); ^{13}C NMR (THF-d_8): δ 153.9 (C_k), 145.3 (C_j), 143.6 (C_k), 129.3 (C_i), 125.1 (C_d), 123.6 (C_h), 123.2 (C_b), 122.2 (C_c), 122.0 (C_f), 107.8 (C_e), 73.7 (*vinyl*); ^{7}Li NMR (THF-d_8): δ −0.26, −2.62.

2-4-2 Theoretical studies

Theoretical calculations were performed by using the Gaussian 09 program.[18] The structures of **4′**, **5′**, and **11′** were optimized at the B3LYP[19] level of theory with LanL2DZ with d polarization function (d exponent: 0.186)(Sn),[20] 6- 31+G(d) (C,H) basis sets.[21] Harmonic vibration frequency calculations at the same level were conducted to confirm all stationary points as local minima (without imaginary frequency). NICS and ^{1}H NMR chemical shifts were calculated by gause-independent atomic orbital (GIAO) calculation at the B3LYP level of theory using ATZP (Sn),[22] 6-311+G(2d,p) (C, H) basis sets based on the experimental structure **1** or the optimized structures (**4′**, **5′**, and **11′**).

2-4-3 Crystal data

	1	4	7
CCDC	1969348	1969350	1969351
formula	$C_{26}H_{20}Sn$	$C_{71}H_{98}Li_2O_{12}Sn_2$	$C_{44}H_{60}Li_4O_4$
fw	451.11	1394.75	680.68
crystal size	0.18 × 0.10 × 0.07	0.17 × 0.14 × 0.11	0.24 × 0.09 × 0.06
crystal system	triclinic	monoclinic	triclinic
space group	*P*-1	$P2_1/c$	*P*-1
a [Å]	9.261(2)	22.124(5)	8.922(4)
b [Å]	10.181(2)	11.326(2)	10.487(5)
c [Å]	11.221(3)	29.961(6)	12.159(6)
α [deg]	81.157(9)	90	107.265(9)
β [deg]	79.550(8)	109.578(4)	100.873(6)
γ [deg]	77.251(8)	90	100.681(3)
V [Å^3]	1007.5(4)	7073(3)	1031.0(9)
Z	2	4	1
ρ_{calcd} [g cm^{-3}]	1.487	1.310	1.096
F(000)	452	2904	768
μ [cm^{-1}]	12.8	7.63	0.66
transmission factors range	0.8939 – 1	0.8517 – 1	0.8904 – 1
index range	-12 ≤ h ≤ 11	-27 ≤ h ≤ 21	-11 ≤ h ≤ 8
	-13 ≤ k ≤ 12	-13≤ k ≤ 13	-8 ≤ h ≤ 13
	-14 ≤ l ≤ 14	-36 ≤ l ≤ 36	-13 ≤ h ≤ 13
no. reflections	8244	50516	7935
unique (R_{int})	4427 (0.0341)	13736 (0.0474)	4159 (0.0538)
$I > 2\sigma$(I)	3530	11267	2364
no. parameters	244	798	240
R_1 ($I > 2\sigma$(I))[a]	0.0336	0.0492	0.0622
wR_2 (all data)[b]	0.0752	0.1224	0.1387
GOF [c]	1.002	1.071	0.975
max diff peak / hole [e Å^{-3}]	0.665/-0.601	1.311/-1.073	0.271/-0.201

	10
CCDC	
formula	$C_{88}H_{56}Sn_4$
fw	1892.6
crystal size	0.16 × 0.11 × 0.04
crystal system	monoclinic
space group	*P*21/*n*
a [Å]	13.242(2)
b [Å]	21.632(3)
c [Å]	14.005(2)
α [deg]	90
β [deg]	108.514(2)
γ [deg]	90
V [Å^3]	3804.2(11)
Z	2
ρ_{calcd} [g cm^{-3}]	1.652
F(000)	1872
μ [cm^{-1}]	1.56
transmission factors range	0.8846 – 1
index range	-16 ≤ h ≤ 16
	-25 ≤ k ≤ 25
	-17 ≤ l ≤ 17
no. reflections	28969
unique (R_{int})	7708 (0.0566)
$I > 2\sigma(I)$	6464
no. parameters	469
R_1 ($I > 2\sigma(I)$)[a]	0.0445
wR_2 (all data)[b]	0.0887
GOF [c]	1.082
max diff peak / hole [e Å^{-3}]	1.051/-0.709

[a] $R1 = \Sigma||F_o| - |F_c||/\Sigma|F_o|$. [b] $wR2 = [\Sigma\{w(F_o^2 - F_c^2)^2\}/\Sigma w(F_o^2)^2]^{1/2}$, w = 1/[□$^2F_o^2$ + (aP)^2 + bP] (a and b are constants suggested by the refinement program; P = [max(F_o^2,0) + 2F_c^2]/3). [c]GOF = $[\Sigma w(F_o^2 - F_c^2)^2/(N_{obs} - N_{params})]^{1/2}$.

2-5 References

(1) (a) Staley, S. W.; Orvedal, A. W. *J. Am. Chem. Soc.* **1973**, *95*, 3382−3384. (b) Tolbert, L. M.; Ali, M. Z. *J. Org. Chem.* **1982**, *47*, 4793−4795. (c) Piekarski, A. M.; Mills, N. S.; Yousef, A. *J. Am. Chem. Soc.* **2008**, *130*, 14883−14890.

(2) Breslow, R.; Chang, H. W. *J. Am. Chem. Soc.* **1965**, *87*, 2200−2203.

(3) Staley, S. W.; Orvedal, A. W. *J. Am. Chem. Soc.* **1974**, *96*, 1618−1620.

(4) Gogonea, V.; Schleyer, P. v. R.; Schreiner, P. R. *Angew. Chem., Int. Ed.* **1998**, *37*, 1945−1948.

(5) Zhu, J.; An, K.; Schleyer, P. v. R. *Org. Lett.* **2013**, *15*, 2442−2445.

(6) (a) Nishinaga, T.; Izukawa, Y.; Komatsu, K. *J. Am. Chem. Soc.* **2000**, *122*, 9312−9313. (b) Nishinaga, T.; Izukawa, Y.; Komatsu, K. *Tetrahedron* **2001**, *57*, 3645−3656.

(7) (a) Saito, M.; Haga, R.; Yoshioka, M. *Chem. Commun.* **2002**, *0*, 1002−1003. (b) Saito, M.; Haga, R.; Yoshioka, M. *Chem. Lett.* **2003**, *32*, 912−913. (c) Saito, M.; Kuwabara, T.; Kambayashi, C.; Yoshioka, M.; Ishimura, K.; Nagase, S. *Chem. Lett.* **2010**, *39*, 700−701.

(8) (a) Dunne, E. C.; Coyne, É. J.; Crowley, P. B.; Gilheany, D. G. *Tetrahedron Lett.* **2002**, *43*, 2449−2453. (b) Mercier, L. G.; Piers, W. E.; Parvez, M. *Angew. Chem., Int. Ed.* **2009**, *48*, 6108−6111.

(9) (a) Saito, M.; Kuwabara, T.; Ishimura, K.; Nagase, S. *Chem. Asian J.* **2011**, *6*, 2907−2910. (b) Saito, M.; Kuwabara, T.; Ishimura, K.; Nagase, S. *Bull. Chem. Soc. Jpn.* **2010**, *83*, 825−827. (c) Saito, M.; Sakaguchi, M.; Tajima, T.; Ishimura, K.; Nagase, S.; Hada, M. *Science* **2010**, *328*, 339−342.

(10) (a) Corey, E. R.; Corey, J. Y.; Glick, M. D. *J. Organomet. Chem.* **1977**, *129*, 17−25. (b) Mercier, L. G.; Furukawa, S.; Piers, W. E.; Wakamiya, A.; Yamaguchi, S.; Parvez, M.; Harrington, R. W.; Clegg, W. *Organometallics* **2011**, *30*, 1719−1729. (c) Clegg, W.; Harrington, R. W.; Mercier, L. G.; Piers, W. E. *Acta Crystallogr., Sect. C: Cryst. Struct. Commun.* **2013**, *69*, 436−438.

(11) (a) Şeptelean, R.; Nemeş, G.; Petrar, P. M. *Rev. Roum. Chim.* **2014**, *59*, 997−1001. (b) Petrar, P. M.; Şeptelean, R.; Deak, N.; Gornitzka, H.; Nemeş, G. *J. Organomet. Chem.* **2015**, *787*, 14−18.

(12) Birchall, T.; Vetrone, J. A. *J. Chem. Soc., Chem. Commun.* **1988**, 877−879.

(13) Kawashima, I.; Imoto, H.; Ishida, M.; Furuta, H.; Yamamoto, S.; Mitsuishi, M.; Tanaka, S.; Fujii, T.; Naka, K. *Angew. Chem., Int. Ed.* **2019**, *58*, 11686−11690.

(14) Caruso, A., Jr.; Siegler, M. A.; Tovar, J. D. *Angew. Chem., Int. Ed.* **2010**, *49*, 4213−4217.

(15) (a) Saito, M.; Haga, R.; Yoshioka, M.; Ishimura, K.; Nagase, S. *Angew. Chem., Int. Ed.* **2005**, *44*, 6553−6556. (b) Saito, M.; Kuwabara, T.; Kambayashi, C.; Yoshioka, M.; Ishimura, K.; Nagase, S. *Chem. Lett.* **2010**, *39*, 700−701. (c) Kuwabara, T.; Guo, J.-D.; Nagase, S.; Minoura, M.; Herber, R. H.; Saito, M. *Organometallics* **2014**, *33*, 2910−2913.

(16) Schleyer, P. v. R.; Maerker, C.; Dransfeld, A.; Jiao, H.; Hommes, N. J. R. v. E. *J. Am. Chem. Soc.* **1996**, *118*, 6317−6318.

(17) Klink, R.; Schrenk, C.; Schnepf, A. *Dalton Trans.* **2014**, *43*, 16097−16104.

(18) Frisch, M. J.; Trucks, G. W.; Schlegel, H. B.; Scuseria, G. E.; Robb, M. A.; Cheeseman, J. R.; Scalmani, G.; Barone, V.; Mennucci, B.; Petersson, G. A.; Nakatsuji, H.; Caricato, M.; Li, X.; Hratchian, H. P.; Izmaylov, A. F.; Bloino, J.; Zheng, G.; Sonnenberg, J. L.; Hada, M.; Ehara, M.; Toyota, K.; Fukuda, R.; Hasegawa, J.; Ishida, M.; Nakajima, T.; Honda, Y.; Kitao, O.; Nakai, H.; Vreven, T.; Jr., J. A. M.; Peralta, J. E.; Ogliaro, F.; Bearpark, M.; Heyd, J. J.; Brothers, E.; Kudin, K. N.; Staroverov, V. N.; Kobayashi, R.; Normand, J.; Raghavachari, K.; Rendell, A.; Burant, J. C.; Iyengar, S. S.; Tomasi, J.; Cossi, M.; Rega, N.; Millam, J. M.; Klene, M.; Knox, J. E.; Cross, J. B.; Bakken, V.; Adamo, C.; Jaramillo, J.; Gomperts, R.; Stratmann, R. E.; Yazyev, O.; Austin, A. J.; Cammi, R.; Pomelli, C.; Ochterski, J. W.; Martin, R. L.; Morokuma, K.; Zakrzewski, V. G.; Voth, G. A.; Salvador, P.; Dannenberg, J. J.; Dapprich, S.; Daniels, A. D.; Farkas, Ö.; Foresman, J. B.; Ortiz, J. V.; Cioslowski, J.; Fox, D. J., GAUSSIAN 09, Revision C.01, Gaussian, Inc.: Wallingford CT.

(19) (a) Lee, C.; Yang, W.; Parr, R. G., *Phys. Rev. B* **1988**, *37,* 785-789; (b) Becke, A. D., *J. Chem. Phys.* **1993**, *98,* 5648-5652.

(20) Wadt, W. R.; Hay, P. J., *J. Chem. Phys.* **1985**, *82,* 284-298.

(21) Francl, M. M.; Pietro, W. J.; Hehre, W. J.; Binkley, J. S.; Gordon, M. S.; DeFrees, D. J.; Pople, J. A., *J. Chem. Phys.* **1982**, *77,* 3654-3665.

(22) (a) Martins, L. S. C.; de Souza, F. A. L.; Ceolin, G. A.; Jorge, F. E.; de Berrêdo, R.

C.; Campos, C. T., *Comput. Theo. Chem.* **2013**, *1013,* 62-69; (b) Martins, L. S. C.; Jorge, F. E.; Machado, S. F., *Mol. Phys.* **2015**, *113,* 3578-3586

Chapter 3

Synthesis of a hyperconjugative antiaromatic compound utilizing anionic charges

3-1 Introduction

As shown in Figure 1-5, the molecular design for hyperconjugative (anti)aromatic compounds reported to date relies on main-group elements as an sp^3-hybridized ring atom or substituents on the ring sp^3-carbons. This is reasonably explained by the energy diagrams illustrated in Figure 3-1. Generally, negative hyperconjugation does not occur efficiently because an energy gap between σ*(C–R) and π orbital is too large, and that is why a cyclopentadiene is nonaromatic. In contrast, because an energy level of a σ* orbital involving main-group element is low, some heterocyclic compounds such as phosphole oxides are considered to have weak antiaromaticity originating from delocalization of 4π-electron system via the σ*(P–O) orbital due to a small energy gap between π and σ* orbitals. From these backgrounds, the author focused on an anionic compound to create a novel hyperconjugative antiaromatic system, because the negative charges play crucial roles to raise the energy levels of the filled π-orbitals for effective hyperconjugation between the anionic π-system and σ*(E–R) orbital. Motivated by this idea, a dibenzo annulated silepin was selected as a precursor of the target molecule due to a high electron acceptability derived from an extended π-skeleton to readily yield dianionic species.

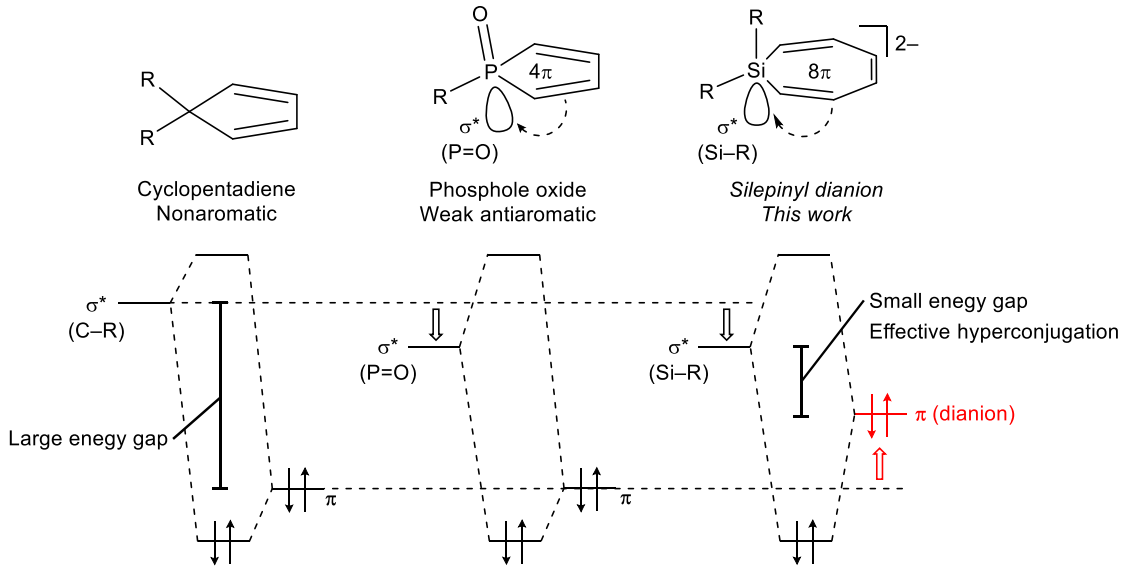

Figure 3-1. A mechanism of hyperconjugative antiaromaticity.

3-2 Synthesis, structure, and electronic properties of dibenzosilepinyl dianion

5,5-Diphenyl-*5H*-dibenzo[*b*,*f*]silepin **12**[1] was synthesized by a method similar to that for the corresponding stannepin analog. To generate the target compound, reaction of **12** and lithium was examined (Scheme 3-1). Treatment of **12** with lithium in THF afforded dilithium dibenzosilepinide **13** quantitatively. Recrystallization from a THF solution deposited black-purple crystals of **13** suitable for X-ray diffraction analysis.

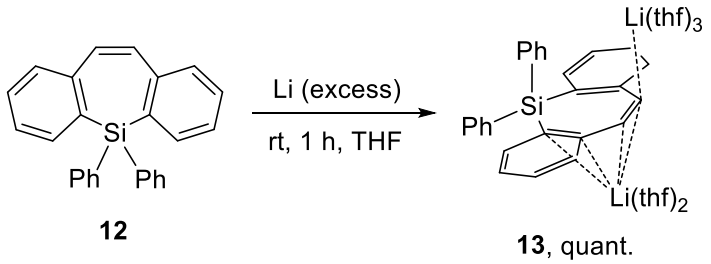

Scheme 3-1. Synthesis of **13**.

The crystal structures of **12** and **13** are shown in Figure 3-2. The folding angle, which is defined by the angle between the two six-membered rings flanking the silepin core, of **12** was 120.5° as was found in reported dibenzosilepins[2]. In contrast, the dibenzosilepinide core in **13** adopted a twisted structure: the twisted angle, which is defined as the angle between the two annulated six-membered rings, is 32.46°. The dibenzosilepinyl dianion coordinates the two lithium cations in an η^1- and η^4-fashions.

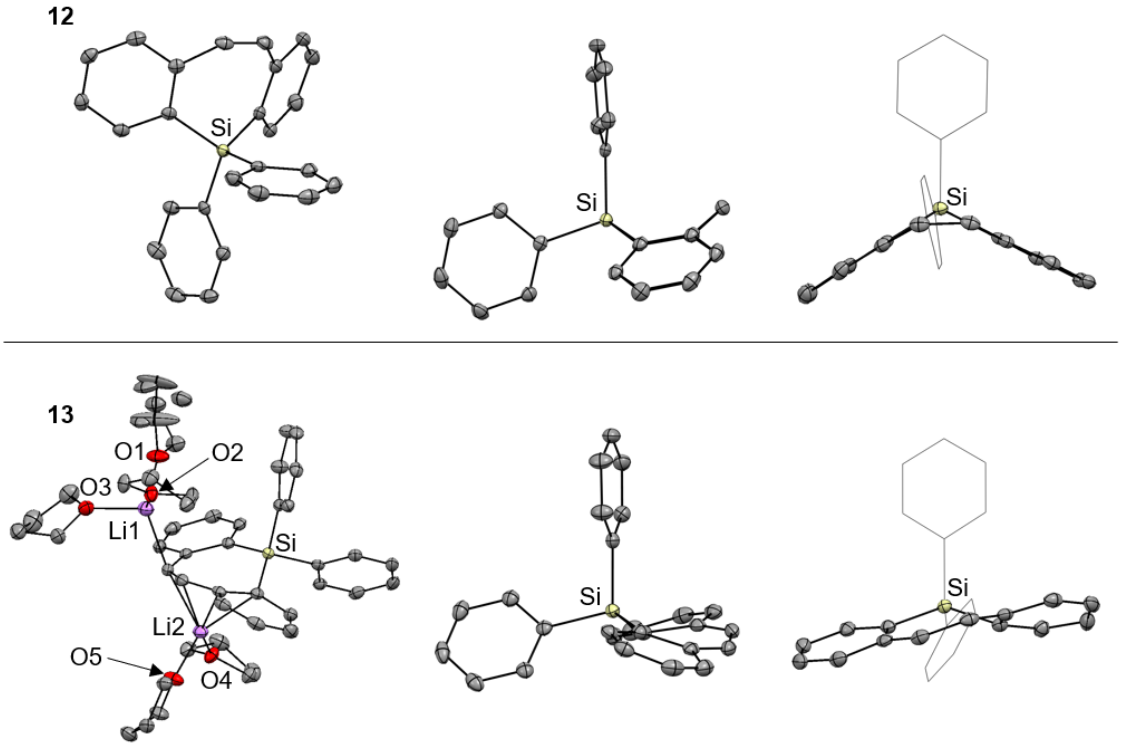

Figure 3-2. Whole molecular structures (left) and dibenzosilepin cores (middle and right) of **12** (top) and **13** (bottom).

Selected bond lengths and harmonic oscillator model of aromaticity (HOMA)[3] indices for **12** and **13** are listed in Table 3-1. The Si–Ph bond lengths of **13** are slightly elongated in comparison to those of **12** (1.8999(14) and 1.8976(14) for **13** vs. 1.8709(19) and 1.8748(19) Å for **12**), while the endocyclic Si–C bonds are shortened upon reduction (1.8470(14) and 1.8424(14) Å for **13** and 1.8680(18) and 1.8682(19) Å for **12**). These structural changes provide evidence for negative hyperconjugation between the π-electrons of the alpha carbon atoms (C_α) and the σ*(Si–Ph) orbitals. Thus, dilithium dibenzosilepinide **13** has a 16π-electron system involving negative hyperconjugation. Importantly, unlike **12**, there is bond alternation in the fused benzene rings of **13** (1.358(2)–1.387(2) Å for the shorter C–C group and 1.403(2)–1.4724(19) Å for the longer C–C group), indicating the loss of aromatic character of the benzene rings. Indeed, the HOMA values for the six-membered rings in **13** were 0.80 and 0.90, while the values of **12** is 0.99 and 0.98.

Table 3-1. Comparison of Si–C and C–C bond lengths of **12**, **13** and **14**, and HOMA values for the six-membered rings.

	12	**13**	**14**
Si−C1/ Si−C6	1.8682(19)/1.8680(18)	1.8424(14)/1.8470(14)	1.875(2)/1.880(3)
Si−C15/Si−C21	1.8709(19/1.8748(19)	1.8976(14)/1.8999(14)	1.870(3)/1.880(2)
C1−C2/C5−C6	1.416(2)/1.413(2)	1.4724(19)/1.4490(19)	1.408(3)/1.418(3)
C2−C3/C4−C5	1.476(3)/1.465(3)	1.390(2)/1.419(2)	1.503(3)/1.514(3)
C3−C4	1.341(3)	1.465(2)	1.519(4)
C1−C7/C6−C14	1.401(3)/1.402(3)	1.415(2)/1.4039(19)	1.405(3)/1.401(3)
C7−C8/C14−C13	1.389(3)/1.386(3)	1.382(2)/1.387(2)	1.388(3)/1.393(4)
C8−C9/C13−C12	1.391(3)/1.382(3)	1.420(2)/1.403(2)	1.382(4)/1.388(4)
C9−C10/C12−C11	1.379(3)/1.382(3)	1.358(2)/1.370(2)	1.384(4)/1.373(4)
C10−C2/C5−C11	1.403(3)/1.408(2)	1.457(2)/1.447(2)	1.394(3)/1.404(3)
HOMA values of Ring a/b	0.99/0.98	0.80/0.90	0.99/0.98

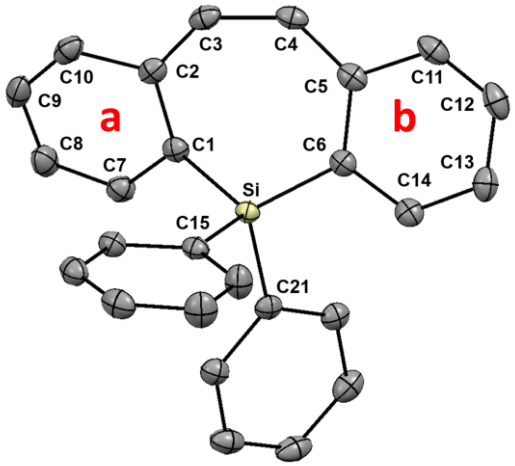

The ^{1}H NMR chart of **13** in THF-d_8 shows sharp signals assignable to the dibenzosilepinide core at a high-field region (δ 5.63, 5.34, 4.99, 4.22, and 2.88) in comparison to the signals of **12** (δ 7.45-7.27). The ^{29}Si{^{1}H} NMR signal of **13** was detected at δ −31.0, which is upfield-shifted relative to that of **12** (δ −13.9). In the ^{13}C{^{1}H} NMR spectrum of **13**, characteristic upfield-shifted signals, for instance, δ 78.4 (C_{vinyl}) and 103.8 (C_{α}), were observed. The ^{13}C{^{1}H} NMR signals for the dibenzosilepinide core in **13** were fully assigned, and the degree of upfield shifts can be reasonably explained by the resonance structures and the calculated NPA charges (Figure 3-3). These upfield shifts imply that the anionic charges are delocalized over the dibenzosilepinide scaffold by

negative hyperconjugation as well as classical π-conjugation.

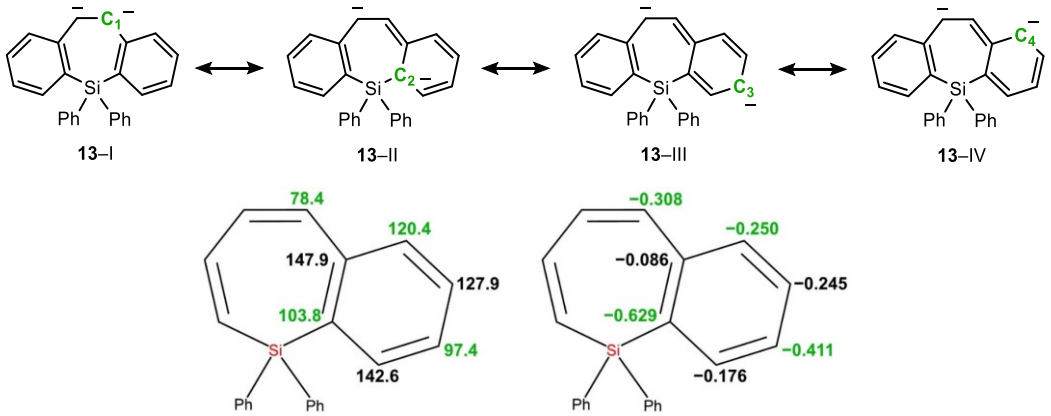

Figure 3-3. Dominant resonance structures (top), $^{13}C\{^{1}H\}$ NMR chemical shifts of **13** in THF-d_8 (bottom, left) and the NPA charges of **13′** (bottom, right).

Although ^{1}H NMR signals of the dibenzosilepin core appeared at high-field upon reduction, it is not clear whether these shifts are diagnostic for the antiaromaticity of **13** because both shielding effect by anionic charges and paratropic ring current induce upfield shifts. Thus, the author compared the ^{1}H NMR data of **13** and other dianionic compounds having aromaticity or antiaromaticity. (Table 3-2). The lithium salt of dibenzo[*a*,*e*]cyclooctatetraene dianion (**DBCOT**$^{2-}$)[4] and the lithium salt of phenanthrene dianions (**Phen**$^{2-}$, **Me$_2$Phen**$^{2-}$)[5] were selected as representatives for dianionic aromatic and antiaromatic compounds, respectively. The former compound shows ^{1}H NMR signals at common aromatic region (δ 6.98 (vinyl), 6.19 and 7.83 (fused benzene rings)) due to its 18π-electron system, despite its negative charges. In contrast, ^{1}H NMR signals of phenanthrene dianions appeared in high-field ranging from δ −1.14 to 2.75 for **Phen**$^{2-}$ and δ 1.23 to 4.32 for **Me$_2$Phen**$^{2-}$ due to the paratropic ring current as well as the negative charges. Considering that the ^{1}H NMR signals for **13** recorded in THF-d_8 at room temperature ranging from δ 2.88 to 5.63, it is estimated that **13** has a weak antiaromatic character originating from its 16π-electron system involving negative hyperconjugation. The reason for the smaller upfield shifts in **13** compared to those in **Phen**$^{2-}$ can be attributable to the negative hyperconjugation that is less effective than the classical π-conjugation.

Table 3-2. ^{1}H NMR chemical shifts for dilithium salts of dianionic compounds having (anti)aromaticity recorded in THF-d_8.

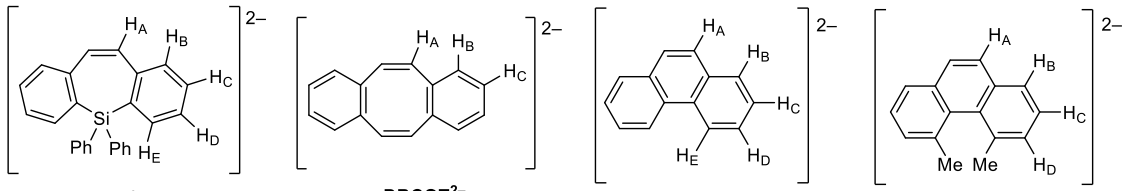

13^{2-} $\quad$ $DBCOT^{2-}$ $\quad$ $Phen^{2-}$ $\quad$ Me_2Phen^{2-}

13	**DBCOT^{2-}**	**Phen^{2-}**	**Me$_2$Phen^{2-}**
2.88 (H_A)	6.98 (H_A)	−1.14 (H_A)	1.23 (H_A)
4.22 (H_D)	6.19 (H_B or H_C)	0.62 (H_B)	2.40 (H_B)
4.99 (H_B)	7.83 (H_B or H_C)	0.80 (H_E)	3.62 (H_D)
5.34 (H_C)	–	1.69 (H_D)	4.32 (H_C)
5.63 (H_E)	–	2.75 (H_C)	–

VT(variable temperature)-^{1}H NMR measurements in THF-d_8 were conducted. In the spectra measured in THF-d_8, the signals of the fused benzene rings shifted to low-field by ca. 0.34–0.40 ppm upon heating from −80 °C to 60 °C (Figure 3-4). This temperature dependency suggests that antiaromaticity of **13** is weakened at higher temperatures, suggesting that the dibenzosilepinide core is more twisted at higher temperatures to minimize destabilization caused by its antiaromaticity. Indeed, planarity of antiaromatic compounds largely affect their ^{1}H NMR chemical shifts. For instance, as mentioned in the previous page, the ^{1}H NMR signals of **Me$_2$Phen^{2-}**, which is estimated to have a highly twisted structure due to the steric repulsion between the Me groups, underwent notable downfield shifts compared to those of non-substituted **Phen^{2-}** because a twisted structure interrupts effective π-conjugation.

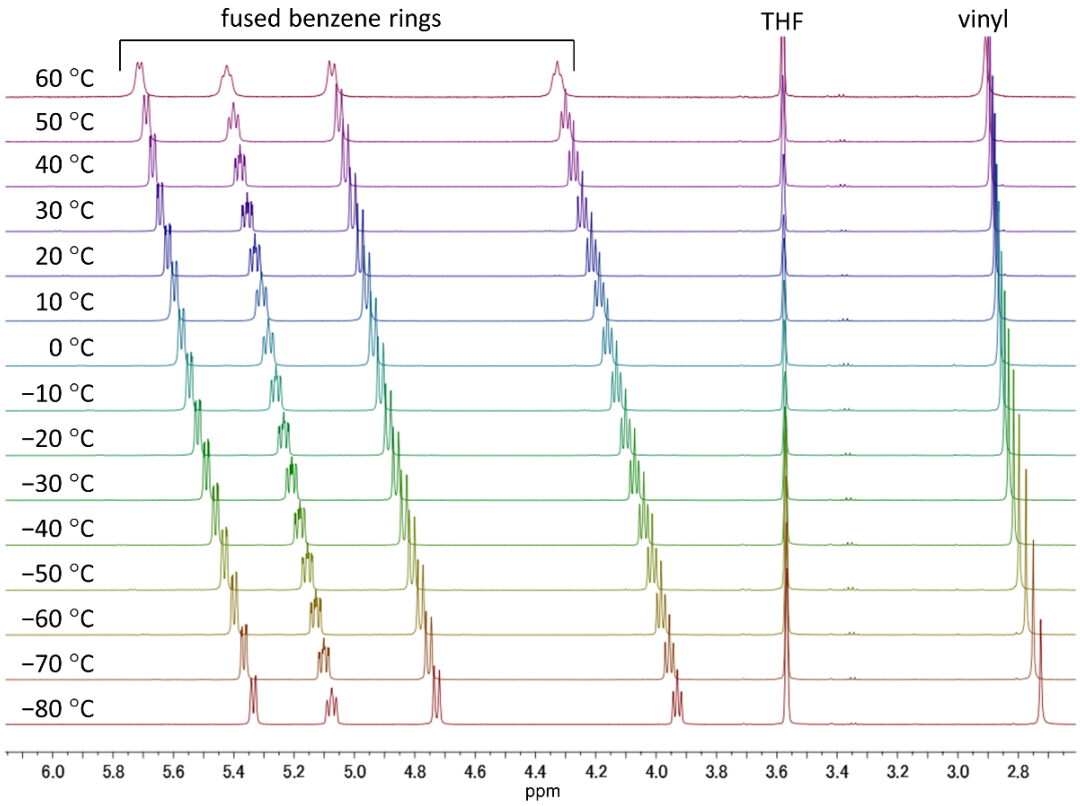

Figure 3-4. VT-^{1}H NMR spectra of **13** in the temperature range of −80 to 60 °C in THF-d_8.

Since ^{7}Li NMR chemical shift is widely employed as a magnetic criterion of (anti)aromaticity[6] (more specific information is demonstrated in Chapter 4), VT-^{7}Li{^{1}H} NMR studies of **13** in THF-d_8 were carried out. The author expected that the ^{7}Li nuclei in **13** resonate in a characteristic low-field region reflecting its paratropic ring current as in the case of a dilithium salt of benzene dianion (δ(^{7}Li) = 10.2).[7] However, each ^{7}Li{^{1}H} NMR spectrum in the temperature range of −100 to 20 °C shows a sharp signal at δ 0.1–0.2 without notable temperature dependency, suggesting that **13** exists as a solvent-separated ion pair in THF.

To gain more insight into the electronic properties of **13**, DFT calculations were conducted (details are written in Section 3-3-2). NICS-*X*-scan[8] and NICS$_{zz}$-scan[9] were performed for the lithium-free-dianion of **13** (denoted as **13′**) to clarify its magnetic properties (Figure 3-5). Since **13′** is non-planar, NICS(+1) and NICS(−1) were defined as illustrated in Figure 3-5a. According to the NICS-*X*-scans, flanking six-membered rings show antiaromatic characters with maximum NICS(±1)$_{zz}$ values of ca. 25 ppm. Moreover,

the NICS(−1)$_{zz}$ values for the silepin ring are also indicative of its weak antiaromaticity. Although the NICS(+1)$_{zz}$ values around the silepin ring (X = −1 to +0.5) were calculated to be nearly zero, it is obvious that these values were affected by the ring current of the pseudo axial Ph rings on the silicon atom, which is also suggested by the asymmetric NICS$_{zz}$-scan curve of ring B showing negative NICS$_{zz}$ values only at the distances from ca. +1 to +4 Å. The NICS$_{zz}$-scan curves for rings A and B displaying steady decreases from the large NICS(0)$_{zz}$ values of ca 45 ppm to the NICS(±5)$_{zz}$ values close to zero also support its antiaromatic nature.

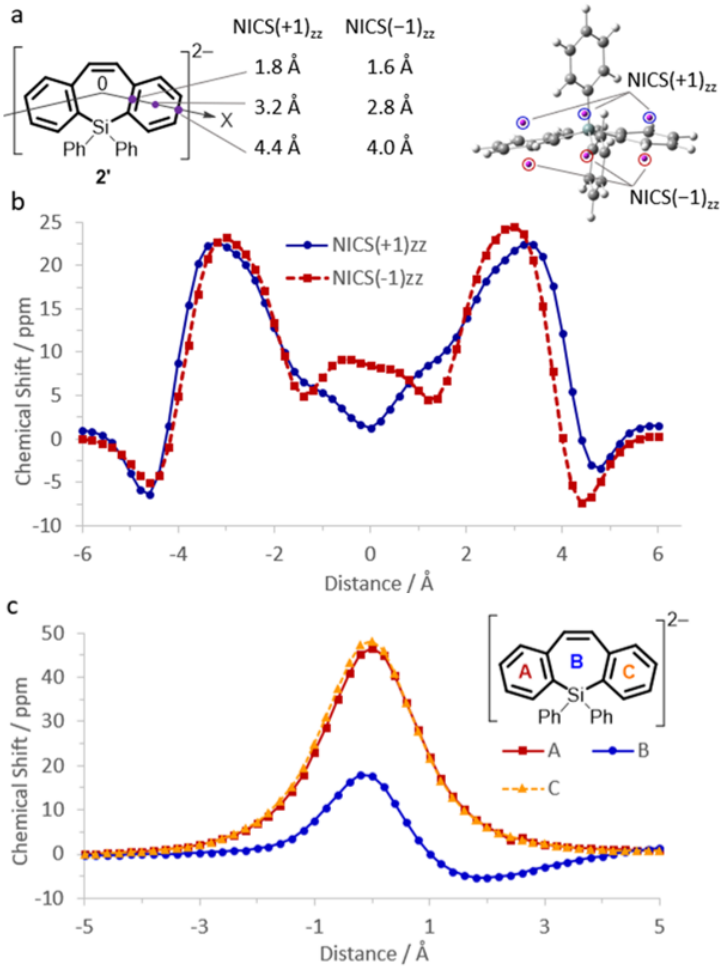

Figure 3-5. NICS calculations for **13′**. a: The X-axis for NICS-*X*-scan, positions for NICS(+1)$_{zz}$ and NICS(−1)$_{zz}$, and X values (in Å) at the purple dots for both NICS(+1) and NICS(−1). b: NICS-*X*-scan curves with 0.2 Å intervals at the heights of 1.0 Å above and below the rings. c: NICS$_{zz}$-scan curves with 0.2 Å intervals for rings A, B, and C.

The anisotropy of the induced current density (ACID) plot displaying paratropic (counterclockwise) ring currents over each ring (Figure 3-6) provides strong evidence for the antiaromaticity of **13′**.[10] On the contrary, in the ACID plot of **12**, diatropic (clockwise) ring currents were detected in the flanking six-membered rings, and no ring current was found in the silepin ring, which is a similar tendency to the results of the NICS calculations.

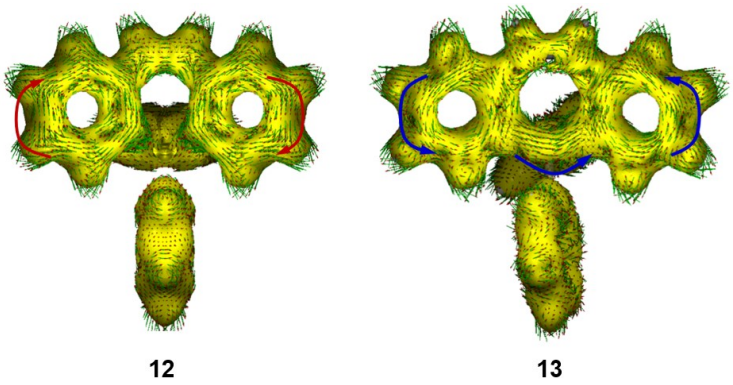

Figure 3-6. ACID plots of **12** (left) and **13′** (right) with isosurface of 0.03.

Natural bond orbital (NBO) calculations were conducted to prove the negative hyperconjugation in **13′**.[11] The Wiberg bond indices (WBI)[12] of the endocyclic Si–C bonds (0.77 and 0.76) are larger than those of the exocyclic Si–C bonds (0.71 and 0.70) in **13′**, whereas the WBI for all Si–C bonds in **12** are almost the same (0.72). The larger WBI for the endocyclic Si–C bonds in **13′** can be reasonably explained by the negative hyperconjugation. Moreover, the stabilization energy due to the negative hyperconjugation from filled π orbitals of C_α to σ*(Si–Ph) orbitals was calculated to be 9.88 and 8.97 kcal/mol for **13** and **13′**, respectively, by the second-order perturbation theory analysis. Thus, it could be concluded that **13′** is the first example of hyperconjugative antiaromatic compound having negative charges. The frontier molecular orbitals for **12** and **13′** are shown in Figure 3-7. Because compound **13′** is a two-electron reduced form of **12**, the HOMO of **12** and the HOMO–1 of **13′** resemble each other. However, the orbital overlap of the π-cloud and σ*(Si–Ph) was found in only in the HOMO−1 of **13′**, supporting hyperconjugation in **13**.

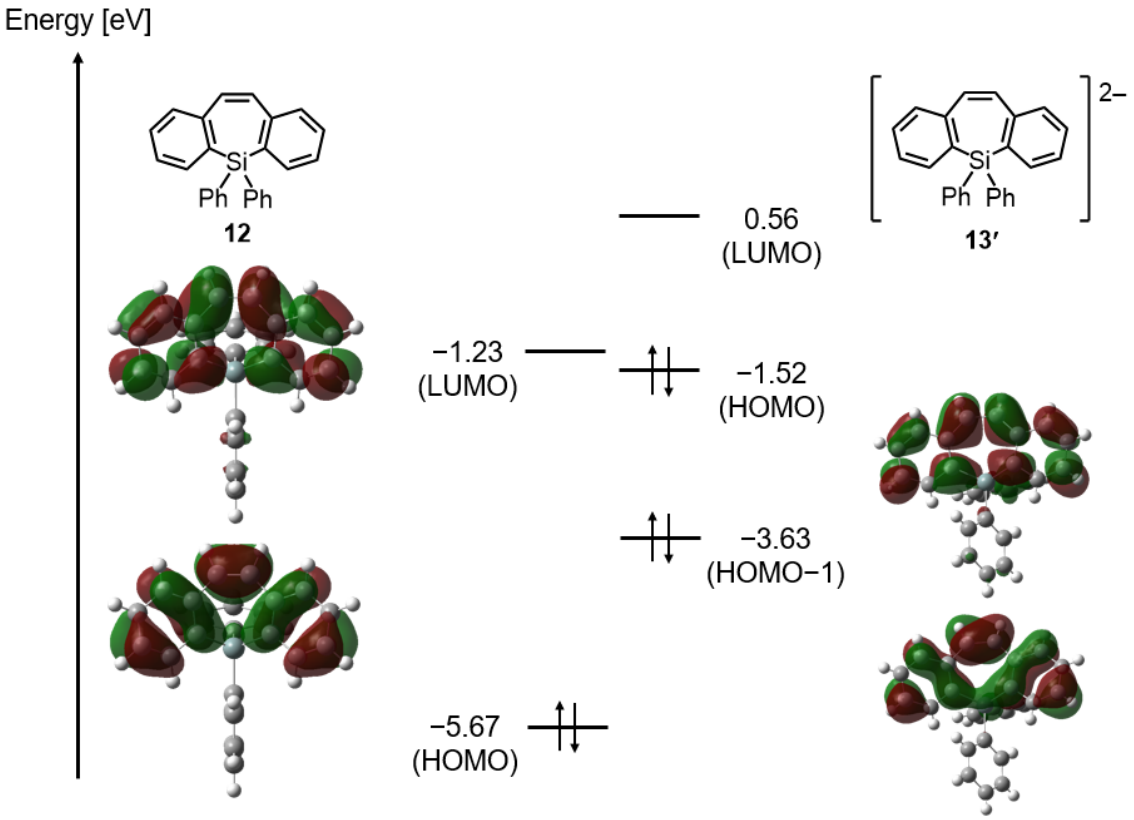

Figure 3-7. Frontier molecular orbitals and their enegy levels of **12** and **13′**

The reactivity of **13** toward oxidants and proton sources was investigated (Scheme 3-2). Reactions of **13** with O_2 or iodomethane regenerated neutral silepin **12** in high yields by two-electron oxidation. On the other hand, treatment of **13** and H_2O or EtOH resulted in the formation of protonated silepin **14**, which has been fully characterized by NMR, X-ray diffraction analysis (Figure 3-8), and elemental analysis.

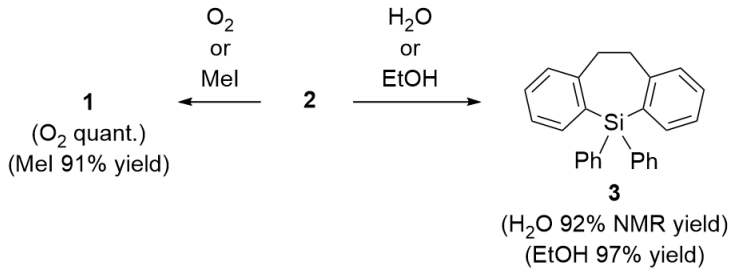

Scheme 3-2. Reactivities of **13**.

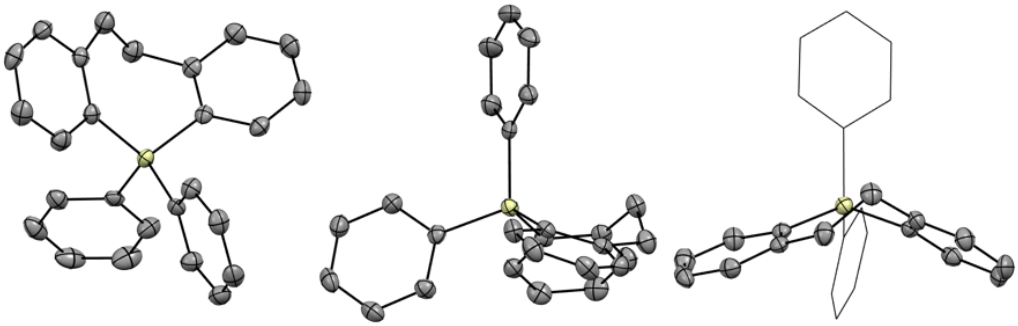

Figure 3-8. Crystal structures of **14**.

In conclusion, the author has successfully synthesized and characterized dilithium dibenzosilepinide **13**. Hyperconjugation between the π-electrons of C_α and the σ*(Si–Ph) orbitals in **13** was revealed by structural features, molecular orbitals, and second-order perturbation theory analysis, and its antiaromaticity was evidenced by NICS values as well as ACID plot. This is noteworthy as the first synthetic example of anionic hyperconjugative antiaromatic compound.

3-3 Experimental Section

3-3-1 Synthetic Procedures

General Procedure

All manipulations were carried out under an argon atmosphere by using standard Schlenk techniques or a glovebox unless otherwise stated. Et_2O, THF, DME, C_6D_6 and THF-d_8 were distilled over potassium mirror. Ph_2SiCl_2 was purchased from Tokyo Chemical Industry (TCI). 2,2′-Dibromostilbene was synthesized according to the literature.[13] ^1H (500 MHz), $^{13}C\{^1H\}$(126 MHz), $^7Li\{^1H\}$ (194 MHz), and $^{29}Si\{^1H\}$ (99 MHz) NMR spectra were recorded on a JEOL ECZ-500 spectrometer at 20°C unless otherwise stated. Chemical shifts are reported in δ and referenced to residual ^1H and ^{13}C signals of deuterated solvents as internal standards or to the $^7Li\{^1H\}$ and the ^{29}Si NMR signal of LiCl in D_2O ($\delta = 0.00$) and $SiMe_4$ in $CDCl_3$ ($\delta = 0.00$), respectively, as external standards. Elemental analyses were performed on a Perkin Elmer 2400 series II CHN analyzer. UV-vis absorption spectra were recorded on a SHIMADZU UV-1800 spectrophotometer.

Synthesis of diphenyldibenzosilepin 12.

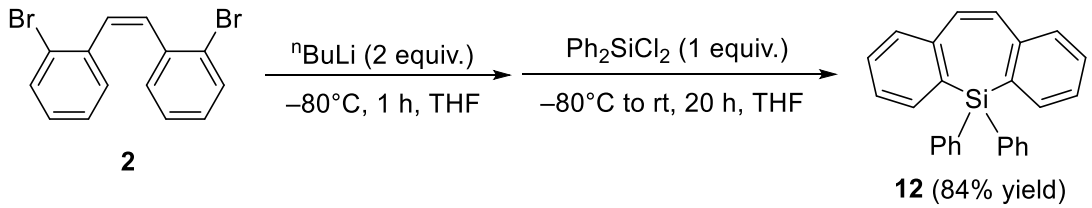

*n*BuLi (1.59 M in hexanes, 3.70 mL, 5.88 mmol) was added to a THF solution (100 mL) of dibromostilbene (0.998 g, 2.95 mmol) in THF at −80 °C. After 1 hour, Ph_2SiCl_2 (0.60 mL, 0.722 g, 2.85 mmol) was added dropwise, then the mixture was allowed to gradually warm to room temperature and stirred for 20 hours. The solvent was removed in vacuo, and materials insoluble in CH_2Cl_2 were filtered off. The filtrate was concentrated and purified by recrystallization from Et_2O to yield **12** as colorless crystals (0.890 g, 2.47 mmol, 84% yield). m.p. 203 °C; ^{1}H NMR (500 MHz, $CDCl_3$): δ = 7.45–7.40 (m, 8H, Ar), 7.38–7.33 (m, 8H, *Ar*), 7.30–7.27 (m, 2H, *Ar*), 6.79 (s, 2H, *vinyl*); ^{13}C{^{1}H} NMR (126 MHz, $CDCl_3$): δ = 142.5 (4°, C_α or C_β), 136.5 (3°), 136.0 (3°), 134.1 (4°, C_α or C_β), 133.1 (3°, *vinyl*), 132.8 (4°, C_{ipso} *of Ph*), 130.2 (3°), 129.8 (3°), 129.7 (3°), 127.9 (3°), 127.2 (3°); ^{29}Si{^{1}H} NMR (99 MHz, $CDCl_3$): δ = −13.9; Elemental analysis calcd (%) for $C_{26}H_{20}Si$ (**1**): C 86.62, H 5.59; found: C 86.24, H 5.55.

Synthesis of lithium salt of 5,5-diphenyldibenzo[*b*,*f*]silepinyl dianion 13.

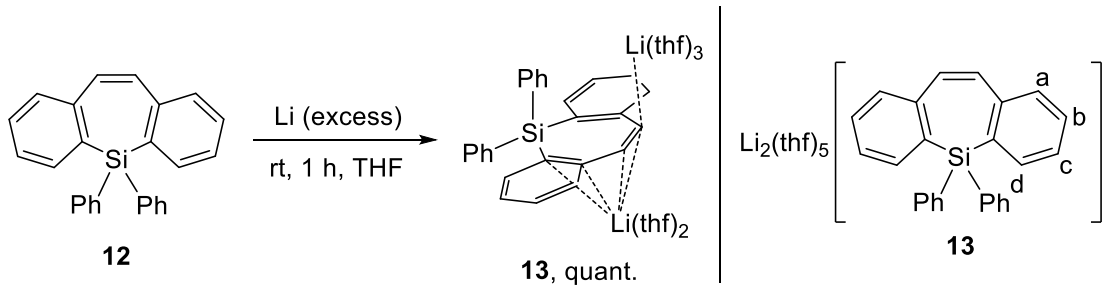

Lithium (16.6 mg, 2.39 mmol) was added to a solution of **12** (71.2 mg, 0.197 mmol) in THF (2 mL) at room temperature. After 1 hour, lithium was removed and the solvent was removed in vacuo to yield analytically pure **13** as black-purple powder (145.1 mg, 0.197 mmol, quant.) without any purifications. m.p. > 108 °C (decomp.); ^{1}H NMR (500 MHz, THF-d_8): δ = 7.63–7.60 (m, 4H, *Ph*), 7.14–7.10 (m, 6H, *Ph*), 5.63 (dd, $^3J_{H–H}$ = 7 Hz, $^4J_{H–}$

$_H$ = 2 Hz, 2H, *fused benzene-d*), 5.34 (td, $^3J_{H–H}$ = 7 Hz, $^4J_{H–H}$ = 2 Hz, 2H, *fused benzene-b*), 4.99 (d, $^3J_{H–H}$ = 8 Hz, 2H, *fused benzene-a*), 4.22 (t, $^3J_{H–H}$ = 7 Hz, 2H, *fused benzene-c*) , 2.88 (s, 2H, *vinyl*); $^{13}C\{^1H\}$ NMR (126 MHz, THF-d_8): δ = 147.9 (C_β), 143.4 (*ipso-Ph*), 142.6 (*fused benzene-d*), 137.4 (3°, *Ph*), 127.9 (*fused benzene-b*), 126.5 (3°, *para-Ph*), 126.3 (3°, *Ph*), 120.4 (*fused benzene-a*), 103.8 (C_α), 97.4 (*fused benzene-c*), 78.4 (*vinyl*); $^7Li\{^1H\}$ NMR (194 MHz, THF-d_8): δ = 0.21; $^{29}Si\{^1H\}$ NMR (99 MHz, THF-d_8): δ = −31.0. Elemental analysis calcd (%) for $C_{46}H_{60}SiLi_2O_5$ (**2**): C 75.18, H 8.23; found: C 74.91, H 8.32.

Reactivities of 13.

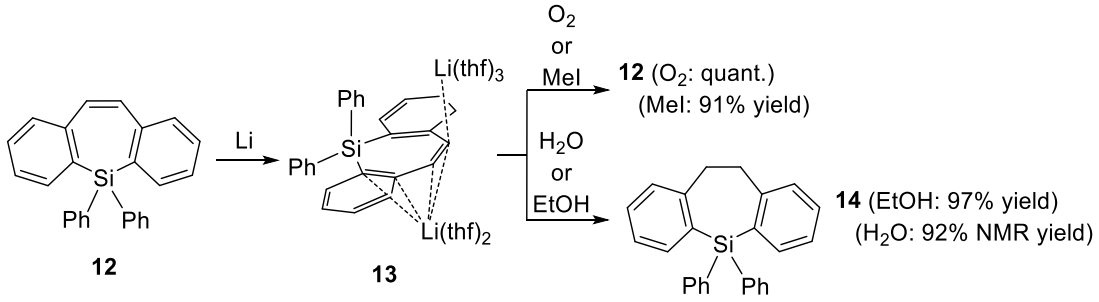

O_2 quench: Compound **13** was generated by the above method from **12** (30.0 mg, 0.0830 mmol) in THF (2 mL). After removal of excess lithium, O_2 gas was introduced to the Schlenk flask. The solvent was removed in vacuo to obtain white solids. Materials insoluble in CH_2Cl_2 were filtered off and the solvent was removed in vacuo to yield **12** as white powder (30.4 mg, 0.0841 mmol, quant.).

MeI quench: Compound **13** was generated by the above method from **12** (30.0 mg, 0.0830 mmol) in THF (2 mL). After removal of excess lithium, CH_3I (0.1 mL, 228 mg, 1.61 mmol) was added dropwise. After 0.5 h, the solvent was removed in vacuo, and materials insoluble in CH_2Cl_2 were filtered off. The solvent was removed in vacuo and crude product was purified by preparative TLC (Hexane:CH_2Cl_2 = 4:1) to yield **12** as a white powder (27.2 mg, 0.0753 mmol, 91% yield).

EtOH quench: Compound **13** was generated by the above method from **12** (30.4 mg, 0.0841 mmol). After removal of excess lithium, EtOH (0.1 mL, 78.9 mg, 1.71 mmol) was added dropwise. After 0.5 hour, the solvent was removed in vacuo, and materials

insoluble in CH_2Cl_2 were filtered off. The solvent was removed in vacuo to yield **14** as white powder (29.5 mg, 0.0815 mmol, 97% yield). m.p. 159 °C; ^{1}H NMR (500 MHz, $CDCl_3$): δ = 7.43–7.40 (m, 6H, *Ar*), 7.36–7.32 (m, 8H, *Ar*), 7.21 (d, $^3J_{H–H}$ = 7 Hz, 2H, *Ar*), 7.15 (t, $^3J_{H–H}$ = 7 Hz, 2H, *Ar*), 3.20 (s, 4H, *methylene*); ^{13}C{^{1}H} NMR (126 MHz, $CDCl_3$): δ = 150.5 (4°, C_α or C_β), 137.5 (3°), 136.2 (3°), 135.6 (4°), 133.1 (4°), 130.0 (3°), 129.5 (3°), 129.2 (3°), 127.9 (3°), 125.2 (3°), 36.8 (*methylene*); ^{29}Si{^{1}H} NMR (99 MHz, $CDCl_3$): δ = −12.7; Elemental analysis calcd (%) for $C_{26}H_{22}Si$ (**14**): C 86.14, H 6.12; found: C 85.90, H 5.83.

H_2O quench: Compound **13** was generated by the above method from **12** (30.1 mg, 0.0833 mmol). After removal of excess lithium, H_2O (0.1 mL, 100 mg, 5.55 mmol) was added dropwise. After 0.5 hour, $MgSO_4$ was added to the solution, then the solvent was removed in vacuo. $MgSO_4$ and materials insoluble in CH_2Cl_2 were filtered off. The solvent was removed in vacuo to yield mixture of **12** and **14** as white powder (29.9 mg, 92% NMR yield for **14**). Compounds **12** and **14** could not be separated by column chromatography or recrystallization due to their similar chemical properties.

3-3-2 Theoretical studies

Theoretical calculations were performed by using the *Gaussian* 16 Rev.C[14] for geometries and NICS values, and the Gaussian 09 Rev. E.01[15] for the anisotropy of the current (induced) density (ACID) analysis. The NICS and ACID data as well as molecular orbitals for **12**, **13**, and **13′** were calculated using optimized structures. The optimized structures of **12** and **13** are in good agreements with their X-ray structures. All local minima were confirmed by the vibrational frequency calculations with zero imaginary frequency, which was performed at the same levels for the optimization.

NICS and ACID calculations for **12**, and optimization and NBO calculations for **13** were performed at the B3LYP[16] level of theory using 6-31G(d) basis sets.[16] The NICS values, NPA charges, and ACID data for **13′** were calculated at the B3LYP level of theory using 6-31+G(d) basis sets. The external magnetic field of ACID calculations was applied in the direction almost orthogonal to three-ring planes, and current density vectors were plotted onto the isosurface of 0.03.

3-3-3 Crystal data

	12	13	14
CCDC	2100087	2100088	2100091
formula	$C_{26}H_{20}Si$	$C_{46}H_{60}Li_2O_5Si$	$C_{26}H_{22}Si$
fw	360.51	734.91	362.52
crystal size	0.08 × 0.07 × 0.06	0.15 × 0.09 × 0.07	0.09 × 0.05 × 0.05
crystal system	triclinic	monoclinic	monoclinic
space group	*P*-1	$P2_1/n$	$P2_1/n$
a [Å]	9.1512(14)	10.6771(12)	8.9514(18)
b [Å]	10.0552(16)	23.008(2)	19.204(4)
c [Å]	11.032(2)	16.8602(18)	11.397(2)
α [deg]	79.734(7)	90	90
β [deg]	81.052(8)	98.541(2)	98.546(4)
γ [deg]	74.730(8)	90	90
V [Å^3]	957.3(3)	4095.9(8)	1937.4(7)
Z	2	4	4
ρ_{calcd} [g cm^{-3}]	1.251	1.192	1.243
F(000)	380	1584	768
μ [cm^{-1}]	1.3	1.02	1.29
transmission factors range	0.8544– 1	0.8544– 1	0.8544 – 1
index range	-10 ≤ h ≤ 11	-10 ≤ h ≤ 13	-11 ≤ h ≤ 10
	-12 ≤ k ≤ 12	-29≤ k ≤ 29	10 ≤ h ≤ -24
	-12 ≤ l ≤ 13	-21 ≤ l ≤ 21	-24 ≤ h ≤ 24
no. reflections	7343	32961	15666
unique (R_{int})	3858 (0.0322)	9361 (0.0375)	4365 (0.0748)
$I > 2\sigma$(I)	2719	7798	3034
no. parameters	244	520	245
R_1 ($I > 2\sigma$(I))[a]	0.045	0.0494	0.0665
wR_2 (all data)[b]	0.1109	0.1285	0.1568
GOF [c]	1.009	1.053	1.048
max diff peak / hole [e Å^{-3}]	0.271/-0.359	0.285/-0.352	0.293/-0.358

[a] $R1 = \Sigma||F_o| - |F_c||/\Sigma|F_o|$. [b] $wR2 = [\Sigma\{w(F_o^2 - F_c^2)^2\}/\Sigma w(F_o^2)^2]^{1/2}$, w = 1/[$\square^2F_o^2 + (aP)^2 + bP$] (*a* and *b* are constants suggested by the refinement program; P = [max(F_o^2,0) + 2F_c^2]/3). [c]GOF = $[\Sigma w(F_o^2 - F_c^2)^2/(N_{obs} - N_{params})]^{1/2}$.

3-4 References

(1) J. Y. Corey, M. Dueber and B. Bichlmeir, *J. Organomet. Chem.*, 1971, **26**, 167-173.

(2) (a) E. R. Corey, J. Y. Corey and M. D. Glick, *J. Organomet. Chem.*, 1977, **129**, 17-25; (b) L. G. Mercier, S. Furukawa, W. E. Piers, A. Wakamiya, S. Yamaguchi, M. Parvez, R. W. Harrington and W. Clegg, *Organometallics*, 2011, **30**, 1719-1729; (c) W. Clegg, R. W. Harrington, L. G. Mercier and W. E. Piers, *Acta Crystallogr. Sec. C*, 2013, **69**, 436-438.

(3) T. M. Krygowski and M. K. Cyrański, *Chem. Rev.*, 2001, **101**, 1385-1420.

(4) Y. Zhu, Z. Zhou, Z. Wei and M. A. Petrukhina, *Organometallics*, 2020, **39**, 4688-4695.

(5) R. Frim, A. Mannschreck and M. Rabinovitz, *Angew. Chem., Int. Ed. Eng.*, 1990, **29**, 919-921.

(6) (a) R. H. Cox, H. W. Terry and L. W. Harrison, *J. Am. Chem. Soc.*, 1971, **93**, 3297-3298; (b) L. A. Paquette, W. Bauer, M. R. Sivik, M. Buehl, M. Feigel and P. v. R. Schleyer, *J. Am. Chem. Soc.*, 1990, **112**, 8776-8789; (c) A. Sekiguchi, Y. Sugai, K. Ebata, C. Kabuto and H. Sakurai, *J. Am. Chem. Soc.*, 1993, **115**, 1144-1146.

(7) H. Sakurai, *Pure Appl. Chem.*, 1994, **66**, 1431-1438.

(8) R. Gershoni-Poranne and A. Stanger, *Chem. Eur. J.*, 2014, **20**, 5673-5688.

(9) A. Stanger, *J. Org. Chem.*, 2006, **71**, 883-893.

(10) D. Geuenich, K. Hess, F. Köhler and R. Herges, *Chem. Rev.*, 2005, **105**, 3758-3772.

(11) E. D. Glendening, C. R. Landis and F. Weinhold, *J. Compt. Chem.*, 2013, **34**, 1429-1437.

(12) K. B. Wiberg, *Tetrahedron*, 1968, **24**, 1083-1096.

(13) L. G. Mercier, W. E. Piers and M. Parvez, *Angew. Chem., Int. Ed.*, 2009, **48**, 6108-6111.

(14) M. J. Frisch, G. W. Trucks, H. B. Schlegel, G. E. Scuseria, M. A. Robb, J. R. Cheeseman, G. Scalmani, V. Barone, G. A. Petersson, H. Nakatsuji, X. Li, M. Caricato, A. V. Marenich, J. Bloino, B. G. Janesko, R. Gomperts, B. Mennucci, H. P. Hratchian, J. V. Ortiz, A. F. Izmaylov, J. L. Sonnenberg, Williams, F. Ding, F. Lipparini, F. Egidi, J. Goings, B. Peng, A. Petrone, T. Henderson, D. Ranasinghe, V. G. Zakrzewski, J. Gao, N. Rega, G. Zheng, W. Liang, M. Hada, M. Ehara, K. Toyota, R. Fukuda, J. Hasegawa, M. Ishida, T. Nakajima, Y. Honda, O. Kitao, H. Nakai, T.

Vreven, K. Throssell, J. A. Montgomery Jr., J. E. Peralta, F. Ogliaro, M. J. Bearpark, J. J. Heyd, E. N. Brothers, K. N. Kudin, V. N. Staroverov, T. A. Keith, R. Kobayashi, J. Normand, K. Raghavachari, A. P. Rendell, J. C. Burant, S. S. Iyengar, J. Tomasi, M. Cossi, J. M. Millam, M. Klene, C. Adamo, R. Cammi, J. W. Ochterski, R. L. Martin, K. Morokuma, O. Farkas, J. B. Foresman and D. J. Fox, *Gaussian 16 Rev. C.01*, Gaussian, Inc., Wallingford, CT, 2016.

(15) M. J. Frisch, G. W. Trucks, H. B. Schlegel, G. E. Scuseria, M. A. Robb, J. R. Cheeseman, G. Scalmani, V. Barone, G. A. Petersson, H. Nakatsuji, X. Li, M. Caricato, A. Marenich, J. Bloino, B. G. Janesko, R. Gomperts, B. Mennucci, H. P. Hratchian, J. V. Ortiz, A. F. Izmaylov, J. L. Sonnenberg, D. Williams-Young, F. Ding, F. Lipparini, F. Egidi, J. Goings, B. Peng, A. Petrone, T. Henderson, D. Ranasinghe, V. G. Zakrzewski, J. Gao, N. Rega, G. Zheng, W. Liang, M. Hada, M. Ehara, K. Toyota, R. Fukuda, J. Hasegawa, M. Ishida, T. Nakajima, Y. Honda, O. Kitao, H. Nakai, T. Vreven, K. Throssell, J. J. A. Montgomery, J. E. Peralta, F. Ogliaro, M. Bearpark, J. J. Heyd, E. Brothers, K. N. Kudin, V. N. Staroverov, T. Keith, R. Kobayashi, J. Normand, K. Raghavachari, A. Rendell, J. C. Burant, S. S. Iyengar, J. Tomasi, M. Cossi, J. M. Millam, M. Klene, C. Adamo, R. Cammi, J. W. Ochterski, R. L. Martin, K. Morokuma, O. Farkas, J. B. Foresman and D. J. Fox, Gaussian 09 Rev. E.01, Gaussian, Inc., Wallingford CT, 2016.

(16) (a) C. Lee, W. Yang and R. G. Parr, *Phys. Rev. B*, 1988, **37**, 785-789; (b) A. D. Becke, *J. Chem. Phys.*, 1993, **98**, 5648-5652.

Chapter 4

Experimental evaluations of hyperconjugative antiaromaticity of dibenzosilepinyl dianions utilizing NMR spectroscopy

4-1 Introduction

As mentioned in Chapter 3, the author could not conclude that the origin of upfield shifted ^{1}H NMR signals in **13** (diPh dianion) is the paratropic ring currents arising from its hyperconjugative antiaromaticity because shielding effects are also derived from the negative charges. Therefore, the author believes that observations of deshielding effects (low-field shifts) of inside paratropic ring currents are crucial evidence of antiaromaticity in anionic compounds. In this chapter, the antiaromaticity of dibenzosilepinyl dianions is experimentally revealed by both ^{1}H and ^{7}Li NMR spectroscopy.

4-2 Synthesis of a trimer of dibenzosilepinyl dianions

Reaction of dimethylsilepin **15**[1] and lithium in THF afforded the dilithium salt $[(Li^{+})_2(thf)_5][\mathbf{15}^{2-}]$ (**16**) quantitatively, and recrystallization from a THF solution provided black crystals of **16** suitable for X-ray diffraction analysis (Scheme 4-1). To our surprise, during recrystallization of **2** from a toluene solution with additive of THF, black crystals of a cluster $[(Li^{+})(thf)_4][(\mathbf{15}^{2-})_3(Li_9O_2^{5+})]$ (**17-THF**), which can be understood as a complex of three dilithium dibenzosilepinide molecules and two Li_2O salts, were deposited. Since the phenyl derivative **13** reacts with excess oxygen gas to generate the corresponding neutral silepin and Li_2O,[2] the author estimated that the Li_2O salts in **17-THF** were generated by decomposition of **16** by O_2 gas during the recrystallization process. Indeed, **17-THF** was successfully synthesized in 29% yield from the reaction of **16** and 0.2 equivalents of O_2 gas in a toluene solution with THF additive in a good reproductivity. Moreover, the reaction of **15** in Et_2O followed by oxidation by O_2 gas led to the formation of $[(Li^{+})(Et_2O)_3][(\mathbf{15}^{2-})_3(Li_9O_2^{5+})]$ (**17-Et$_2$O**) in 36% yield.

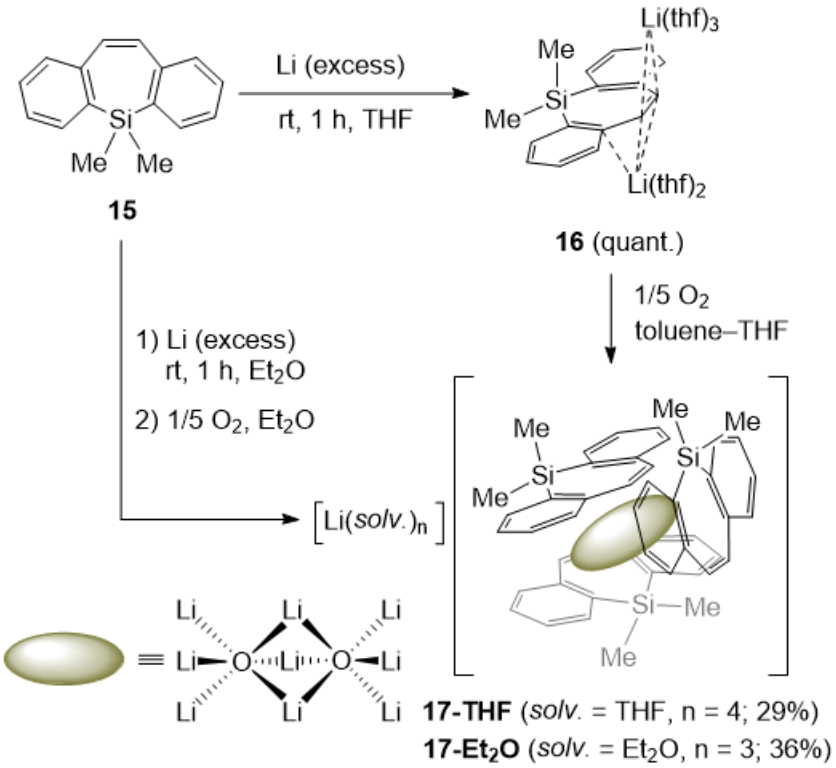

Scheme 4-1. Synthesis of dibenzosilepinyl dianion **16** and trimers **17**.

Crystal structures of **16** and **17-THF** are shown in Figure 4-1. Each lithium cation in **16** is coordinated by the dibenzosilepinyl dianion in η^2- and η^3-fashions as well as three and two molecules of THF, respectively. In **17-THF**, nine of the ten lithium cations form the Li_9O_2 cluster core that is encapsulated by the three dibenzosilepinde units, and the other is solvent-separated ion pair. The dibenzosilepinide scaffold in **16** has a slightly twisted structure as was found in **13**, most likely for an efficient overlap between the σ*(Si–Me) and the filled π orbitals of the endocyclic alpha carbon atoms (C_α). Each silepin ring in **17-THF** is composed of a planar C6 moiety (the sum of internal angles: 719°) and an out-of-plane Si atom; the average distance between the silicon atoms and the mean planes of the six carbon atoms is 0.82 Å. The reason for the non-planarity of the silepin rings seems to be steric repulsions between the pseudo equatorial Me groups and the vinyl protons of the adjacent silepin ring.

Negative hyperconjugation can be experimentally evaluated by comparing the Si–C_α and Si–Me bond lengths among neutral and dianionic silepins. Table 4-1 lists the bond lengths of the dibenzosilepin cores of **16**, **17-THF**, and a selected neutral silepin. To the best of

the author's knowledge, all structurally characterized neutral 5,5-dimethyl-5*H*-dibenzo[*b*,*f*]silepin derivatives have Si–Me bonds slightly shorter than their Si–C_α bonds (Si–Me: ca. 1.86 Å, Si–C_α: ca 1.87 Å).[1, 3] On the contrary, the Si–C_α bonds of **16** (1.862(5), 1.860(5) Å) and **17-THF** (1.871 Å (average)) are shorter than their Si–Me bonds (1.880(5) and 1.884(5) Å for **16**, and 1.879 Å (average) for **17-THF**. The reversal of the relationship between the Si–Me and Si–C_α bond lengths upon reduction can be attributable to the negative hyperconjugation between the π-electrons of the C_α and the σ*(Si–Me) orbitals causing elongation and shortening of the Si–Me and Si–C_α bonds, respectively. Therefore, these structural features indicate that dibenzosilepinyl dianion cores in **16** and **17-THF** have a pseudo 16π-electron system involving the negative hyperconjugation.

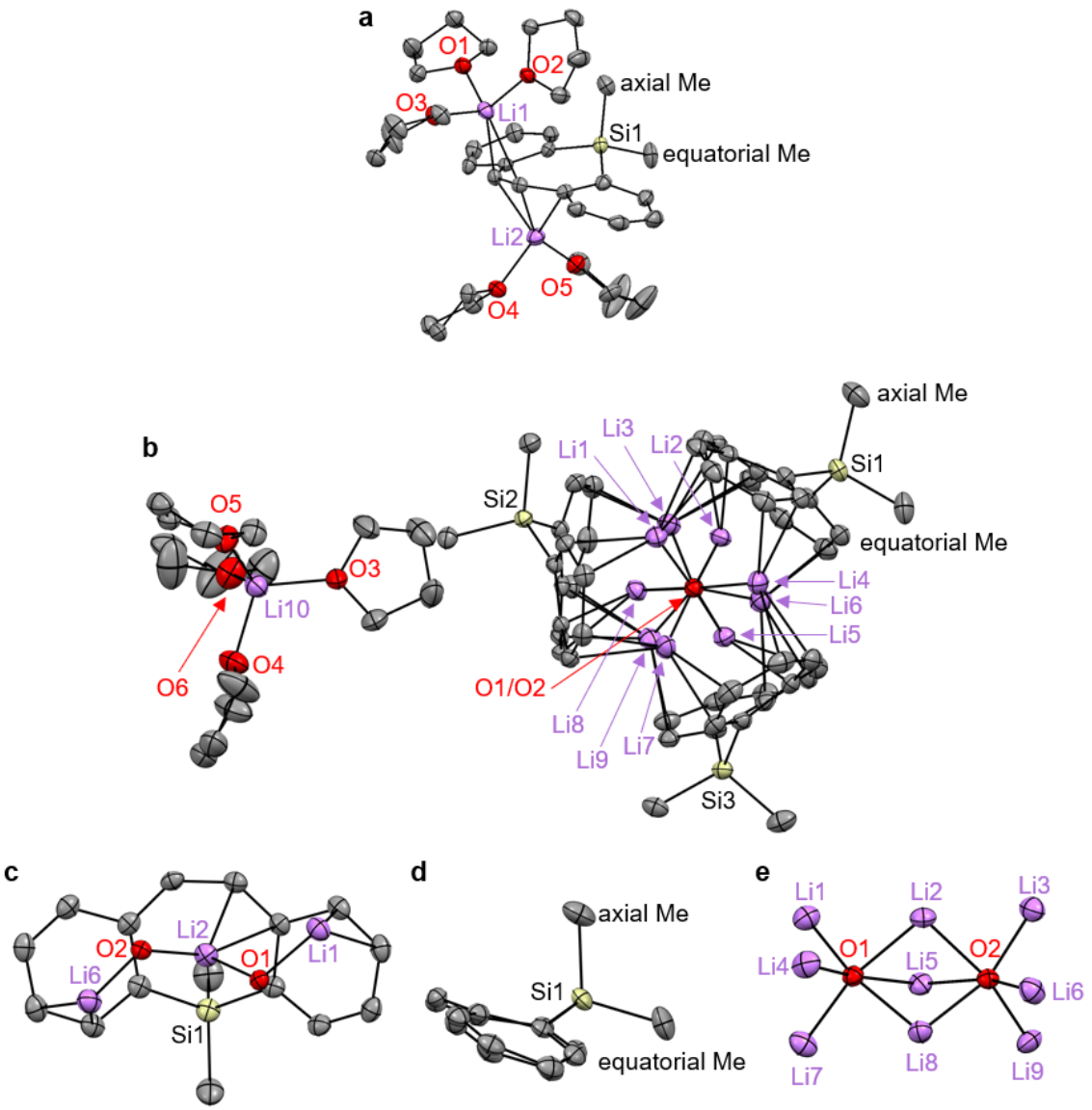

Figure 4-1. Whole structures of **16** (a) and **17-THF** (b), selected lithium cations coordinated by a dianionic moiety in **17-THF** (c), a dibenzosilepinyl dianion in **17-THF** (d), and the Li_9O_2 core structure in **17-THF** (e).

Table 4-1. Comparison of the Si–C and C–C bond lengths and HOMA values of **AN**[13], **16**, and **17-THF**.

	neutral silepin **AN**	**16**	**17-THF**
Si−C1/ Si−C6	1.872(3)/1.874(3)	1.848(4)/1.864(4)	1.868(3)/1.871(3)
Si−C15/Si−C21	1.860(3)/1.865(3)	1.884(4)/1.887(4)	1.878(3)/1.874(3)
C1−C2/C5−C6	1.404(4)/1.413(4)	1.474(5)/1.453(5)	1.487(3)/1.465(3)
C2−C3/C4−C5	1.470(4)/1.413(4)	1.404(5)/1.410(5)	1.395(3)/1.405(3)
C3−C4	1.343(4)	1.465(5)	1.461(3)
C1−C7/C6−C14	1.402(4)/1.391(4)	1.407(5)/1.388(5)	1.397(3)/1.409(3)
C7−C8/C14−C13	1.396(4)/1.406(4)	1.384(6)/1.393(5)	1.415(4)/1.405(4)
C8−C9/C13−C12	1.393(4)/1.397(4)	1.402(6)/1.412(5)	1.424(4)/1.416(4)
C9−C10/C12−C11	1.371(4)/1.377(4)	1.368(6)/1.361(5)	1.371(4)/1.379(4)
C10−C2/C5−C11	1.406(4)/1.401(4)	1.447(5)/1.446(5)	1.472(3)/1.461(4)
HOMA values of Ring a/b	0.99/0.99	0.84/0.88	0.75/0.84

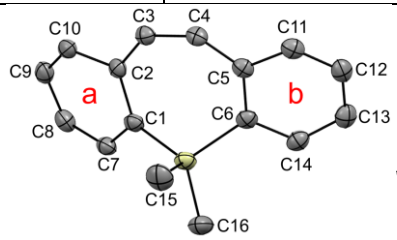

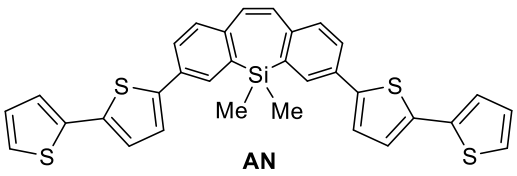

AN

In the ^{1}H NMR spectrum of **16** recorded in THF-d_8, the sharp signals of the dibenzosilepinide scaffold appeared at high-field (δ 5.81 to 2.81) relative to those of **15** (δ 7.56 to 6.96). Interestingly, the Me signal is also upfield shifted compared to that of **15** (δ 0.04 *vs.* 0.46), although the Me groups are not incorporated in the π-framework. The ^{29}Si{^{1}H} NMR signal of **16** was detected at δ −24.7, which is in the higher field in comparison to that of **15** (δ −11.1). These upfield shifts upon reduction imply that the negative charges are delocalized over the dibenzosilepinide core through hyperconjugation as well as classical π-conjugation.

The ^{1}H NMR spectrum of **17-THF** recorded in toluene-d_8 provides us evidence of antiaromaticity. In THF-d_8, **17-THF** exhibited a ^{1}H NMR spectrum identical to that of **16**, suggesting the trimer is dissociated into three monomeric dianions. In contrast, two distinct Me signals (δ 1.27 and 0.09) were observed in the ^{1}H NMR spectrum of **17-THF** in toluene-d_8, which indicates that the trimeric structure is maintained in toluene, and no ring inversion takes place within the ^{1}H NMR time scale. Importantly, one of the Si−Me signals of **17-THF** was observed at unusually low-field (δ 1.27), despite its dianionic

character that usually causes shielding effects. Although experimental assignment of these two Me signals failed because acquisition of ^{13}C NMR, HMBC, HMQC, and NOESY spectra was hampered by its low solubility in toluene-d_8, GIAO (Gauge-Including Atomic Orbitals) calculations of the anionic part of **17-THF** (denoted as **17′**) revealed that the average chemical shift for the pseudo axial Me protons (0.70 ppm) is in the lower field by approximately 1 ppm relative to that for the pseudo equatorial Me (−0.35 ppm), suggesting that the downfield shifted Me signal of **17-THF** can be assigned to the pseudo axial Me, the protons of which are situated above the silepin ring as shown in Figure 4-1(d). Therefore, the origin of the low-field shift should be the paratropic ring currents of the dibenzosilepin rings.

The author obtained more conclusive evidence for the antiaromatic character of the dibenzosilepinyl dianion from $^{7}Li\{^{1}H\}$ NMR studies (Figure 4-2). Both $^{7}Li\{^{1}H\}$ NMR spectra of **16** and **17-THF** in THF-d_8 showed a signal at δ 0.3, indicating that both of them exist as a solvent-separated ion pair of monomeric dilithium dibenzosilepinide in THF. Importantly, the $^{7}Li\{^{1}H\}$ NMR spectrum of **17-THF** in toluene-d_8 exhibits three distinct signals at δ 6.3, 4.4, and 0.6 with an integral ratio of 3:6:1, respectively. According to the integral ratio, the signals at δ 6.3 and 4.4 can be assignable to the inner three and outer six lithium cations in the Li_9O_2 cluster, respectively, and the signal at δ 0.6 to the solvent-separated lithium cation. GIAO calculations suggest that these downfield shifts observed for the Li_9O_2 cluster arises from π-coordination of the dibenzosilepinyl dianions (*vide infra*). Note that a lithium nucleus tightly coordinated by butadiene moieties in an anionic lithocene $[Li\{(SnC_4Et_4)_2\}]^-$ resonates in high-field (−7.1 ppm) due to strong shielding effects.[4] Therefore, the author concluded that the downfield shifted $^{7}Li\{^{1}H\}$ NMR signals are caused by the paratropic ring currents of the antiaromatic dibenzosilepinyl dianions.

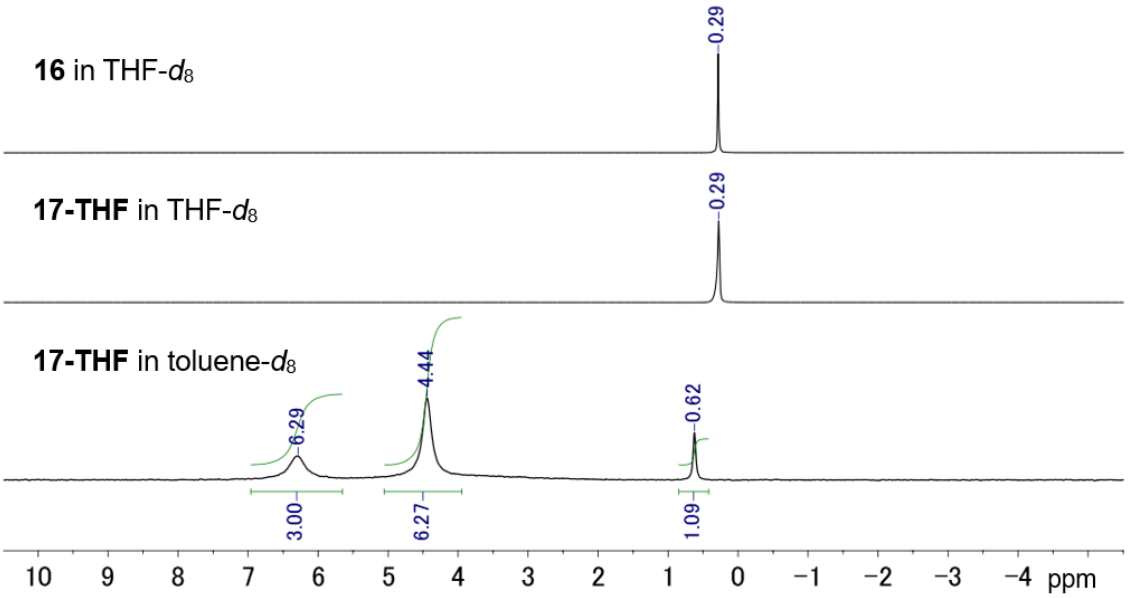

Figure 4-2. The $^{7}Li\{^{1}H\}$ NMR spectra of **16** recorded in THF-d_8 (top), and **17-THF** recorded in THF-d_8 (middle) and in toluene-d_8 (bottom).

To gain more insight into the electronic properties, DFT calculations were conducted at the B3LYP/6-31+G(d) level of theory (details are written in Section 4-3-2). The $NICS_{zz}$-*X*-scan[5] and $NICS_{zz}$-scan[6] curves illustrated in Figure 4-3 support the antiaromatic character of lithium-free dianion of **16** (denoted as $\mathbf{15^{2-}}$) with sufficiently positive large $NICS_{zz}$ values (for instance, $NICS(0)_{zz}$ were ca 44 and 20 for six- and seven-membered rings, respectively). The negative $NICS(n)_{zz}$ values of ring C, in the range of n = ca. +2.8 to +4.5, are likely due to the interactions between the dummy atoms and the spatially close pseudo axial methyl group.

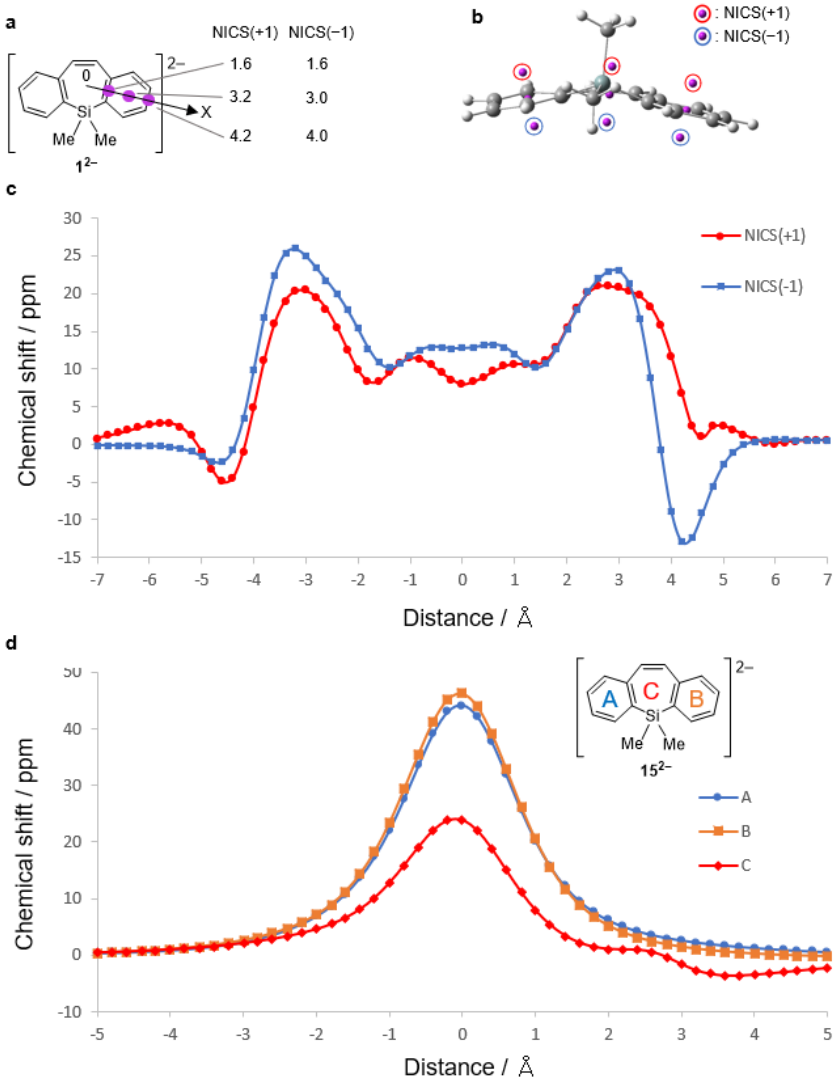

Figure 4-3. NICS calculations for $\mathbf{15}^{2-}$. a: The X-axis for NICS-*X*-scan, positions for NICS(+1)$_{zz}$ and NICS(−1)$_{zz}$, and X values (in Å) at the purple dots for both NICS(+1) and NICS(−1). b: NICS-*X*-scan curves with 0.2 Å intervals at the heights of 1.0 Å above and below the rings. c: NICS$_{zz}$-scan curves with 0.2 Å intervals for rings A, B, and C.

Since the *z*-axis was not vertical to any dibenzosilepinyl dianions of **17′** and its lithium-free model structure $(\mathbf{15}^{2-})_3$, NICS$_{iso}$ values were used instead of NICS$_{zz}$ values for the discussions (Figure 4-4). The NICS (n)$_{iso}$ values of **17-THF**, where n = −1 to −4, could not be estimated accurately because of magnetic interactions between the dummy atoms and the Li_9O_2 core. The negative NICS (n)$_{iso}$ values (n = −2 to −3.5) for the ring C are due to the pseudo axial methyl groups close to the dummy atoms, as was found in the NICS$_{zz}$-scan curve for $\mathbf{15}^{2-}$. Relatively large NICS$_{iso}$ values (NICS(0)$_{iso}$ = 9.2–15.6 and 6.0 for

six- and seven-membered rings, respectively) were obtained for **17′**, which agrees with the results of the $^{7}Li\{^{1}H\}$ NMR studies. In contrast, all $NICS_{iso}$ values of lithium-free **$(15^{2-})_3$** were calculated to be small (less than 5 ppm for $NICS(0)_{iso}$), suggesting that $NICS_{iso}$ values of the trimers are strongly affected by the Li_9O_2 core. This phenomenon indicates that the Li_9O_2 core has an important role in the antiaromatic character of the trimeric cluster, but the reason for which is not clear at this point.

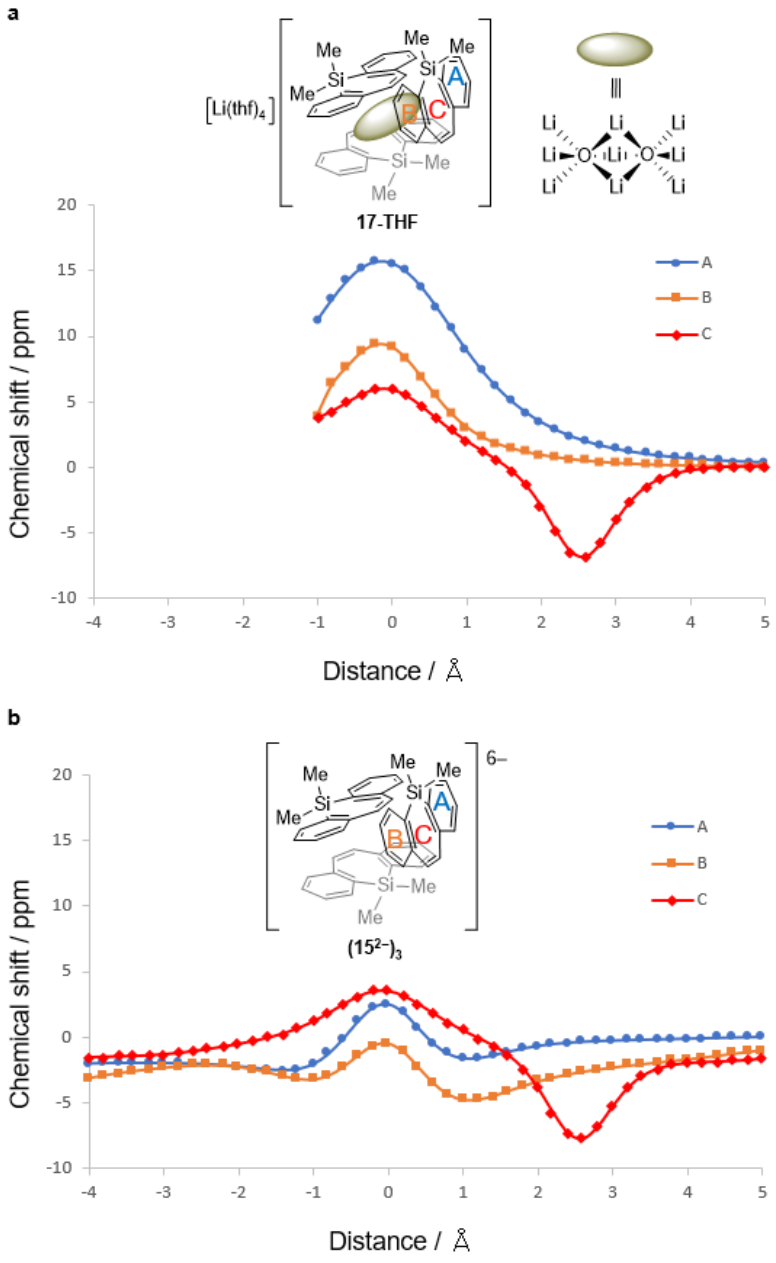

Figure 4-4. $NICS_{iso}$-scan curves for **17-THF** (a) and **$(15^{2-})_3$** (b).

Next, the author calculated the ^{7}Li NMR chemical shifts for $[Li(thf)_4]^+$, **17′**, and the dibenzosilepin-free central core $[Li_9O_2]^{5+}$ as shown in Figure 4-5. The calculated chemical shifts of **17′** were 4.8 and 2.0, whereas those of $[Li_9O_2]^{5+}$ were −0.1 and −2.0 ppm, when the chemical shift of $[Li(thf)_4]^+$ was set to the corresponding experimental value of 0.6 ppm in **17-THF**. Therefore, the downfield shifts of the trimer are attributable to the paratropic ring currents of the dibenzosilepinyl dianion.

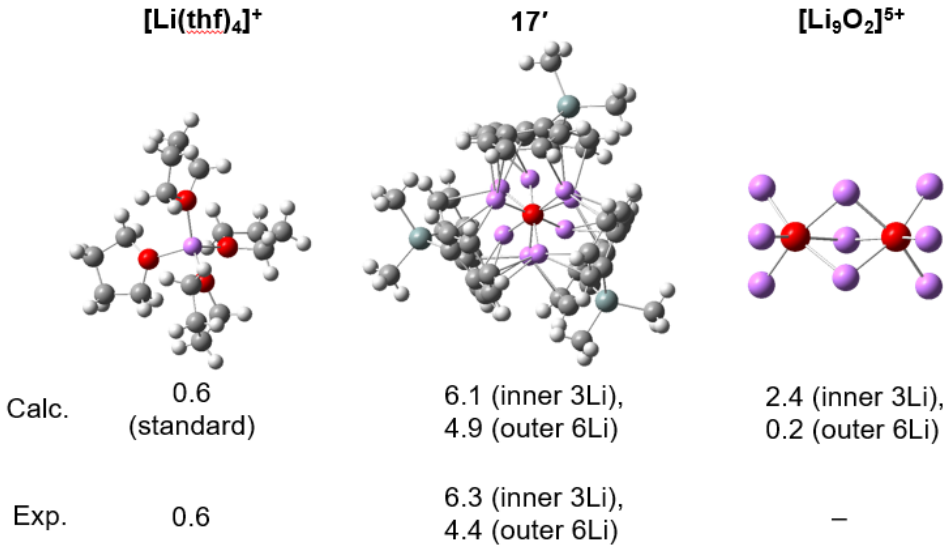

Figure 4-5. Calculated (top) and experimental (bottom) chemical shifts of ^{7}Li NMR of $[Li(thf)_4]^+$, **17′** and $[Li_9O_2]^{5+}$.

Frontier molecular orbitals (MOs) of **15**, **16**, and **17′** and their energy levels are shown in Figure 4-6. Since **16** is the dianionic form of **15**, the LUMO and HOMO of **15** are similar to the HOMO and HOMO−1 of **16**, respectively. Moreover, because **17′** can be regarded as a trimeric cluster of **16**, the HOMO, HOMO−1, HOMO−2 in **17′** correspond to the HOMO of **16,** and the HOMO−3, −4, −5 to the HOMO−1 of **16**. Bonding interactions between the silepin rings are found only in the HOMO−1, −2, −4, −5, but not in HOMO nor HOMO−3, which occurred in the two sets of degenerated MO pairs (HOMO−1/HOMO−2, and HOMO−4/HOMO−5).

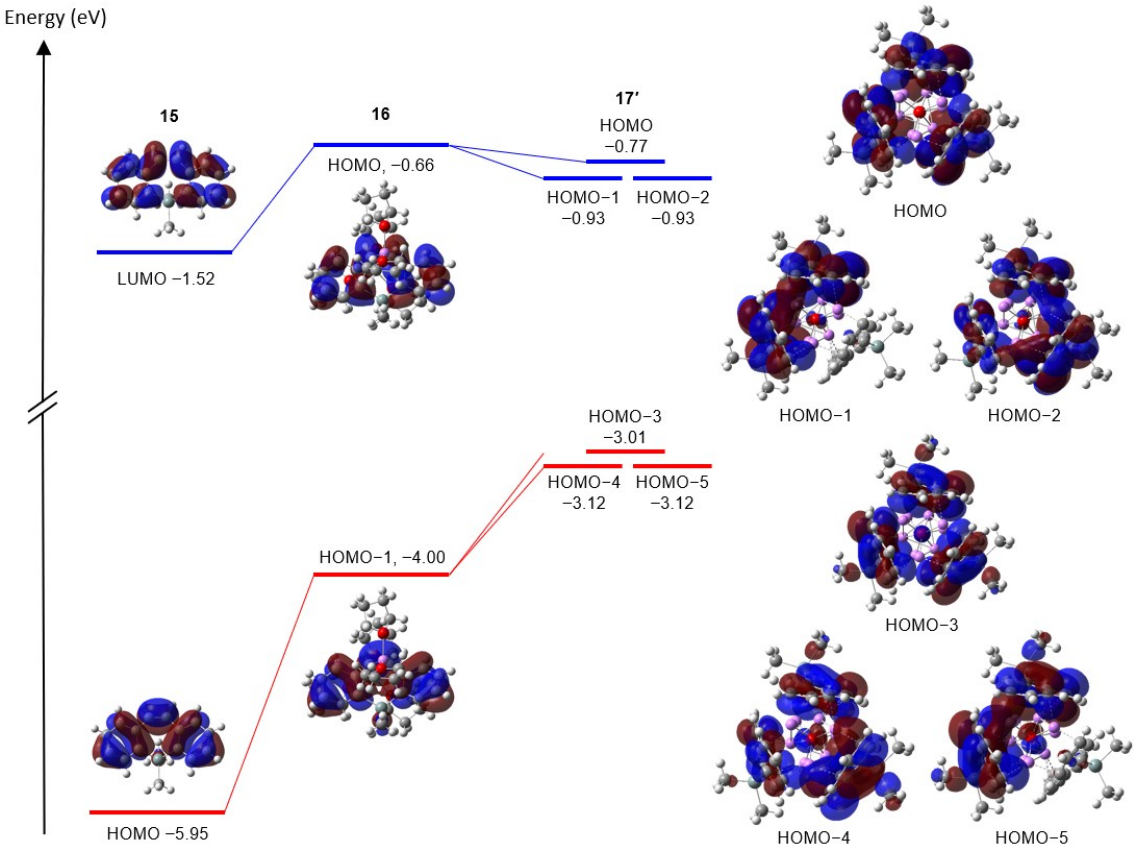

Figure 4-6. Energy diagrams for frontier molecular orbitals of **15**, **16**, and **17′** (isovalues: 0.02 for **15**, **16**; 0.013 for **17′**).

In conclusion, the author successfully synthesized and characterized dilithium dibenzosilepinide **16** and trimer **17-THF** encapsulating the Li_9O_2 core. The NMR studies revealed that the trimeric structure is maintained in toluene-d_8, and the antiaromatic character of **17-THF** has been elucidated by both experimental and theoretical $^{7}Li\{^{1}H\}$ NMR spectra with explicit downfield shifts due to the paratropic ring currents.

4-3 Synthesis of a tetraanion equivalent of spirobi(dibenzosilepin)

Aiming to prove hyperconjugative antiaromaticity of a dibenzosilepinyl dianion based on ^{1}H NMR spectroscopy, the author designed a tetraanion of spirobi(dibenzosilepin) **AO** (Figure 4-7). In **AO**, it is expected that only the ^{1}H NMR signal of the H_e appears at low-field as in the case of **AJ** and **AL** shown in Figure 1-6, because of the paratropic ring

currents of the silepin rings. In this section, synthesis of a spirobi(dibenzosilepin) and its tetraanionic form is demonstrated.

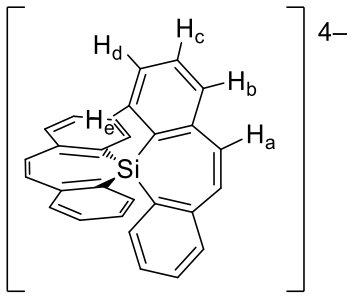

AO

Figure 4-7. The structure of tetrabenzospirosilepinyl tetraanion **AO**.

*n*BuLi was added dropwise to a THF solution of dibromostilbene derivative **2** at −80 °C, then the mixture was treated with 0.5 equivalents of $SiCl_4$ to obtain spirobisilepin **18**. Compound **18** was fully characterized by ^{1}H, $^{13}C\{^{1}H\}$, and $^{29}Si\{^{1}H\}$ NMR and X-ray diffraction analysis as well as elemental analysis. This is the first synthesis and isolation of a spirobisilepin. Next, spirobisilepin **18** was reacted with lithium in THF at room temperature to generate tetralithium salt **19** quantitatively (Scheme 4-2). Recrystallization from a THF solution provided black crystals of **19** suitable for X-ray diffraction analysis.

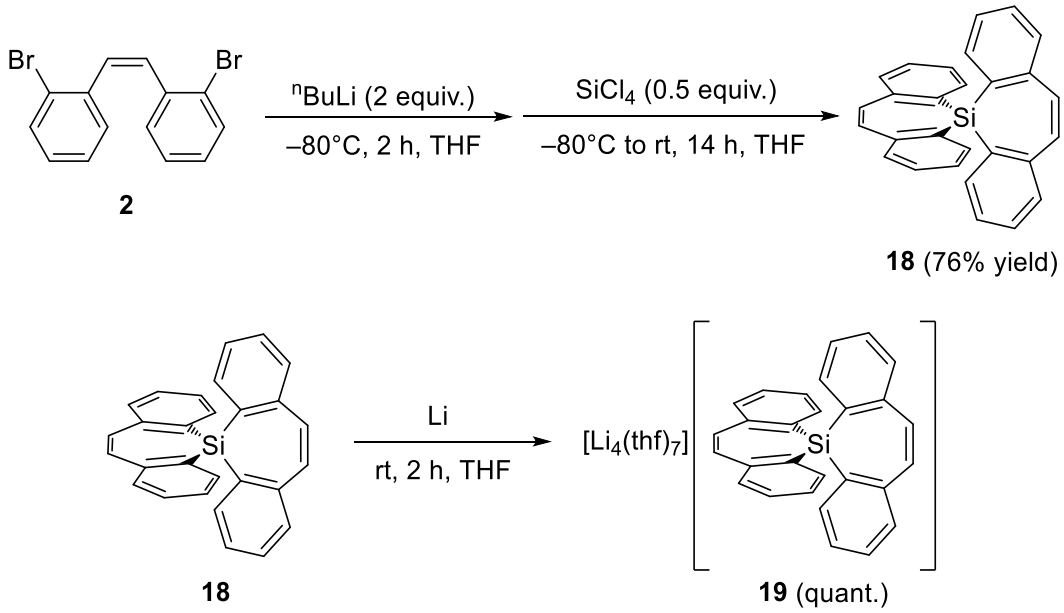

Scheme 4-2. Synthesis of **18** and **19**.

The ^{1}H NMR signals of dibenzosilepinyl dianion moiety in **13** (diPh dianion) and **19** are shown in Figure 4-8. The signals of H_b, H_c, and H_d of **19** shifted to low-field in comparison to those of **13** in a range of 0.15 to 0.17 ppm. Importantly, only the signal of H_e shifted to low-field by 0.67 ppm. The largest shift of H_e can be attributable to the paratropic ring currents on the silepin rings, which is exclusive evidence of the hyperconjugative antiaromaticity.

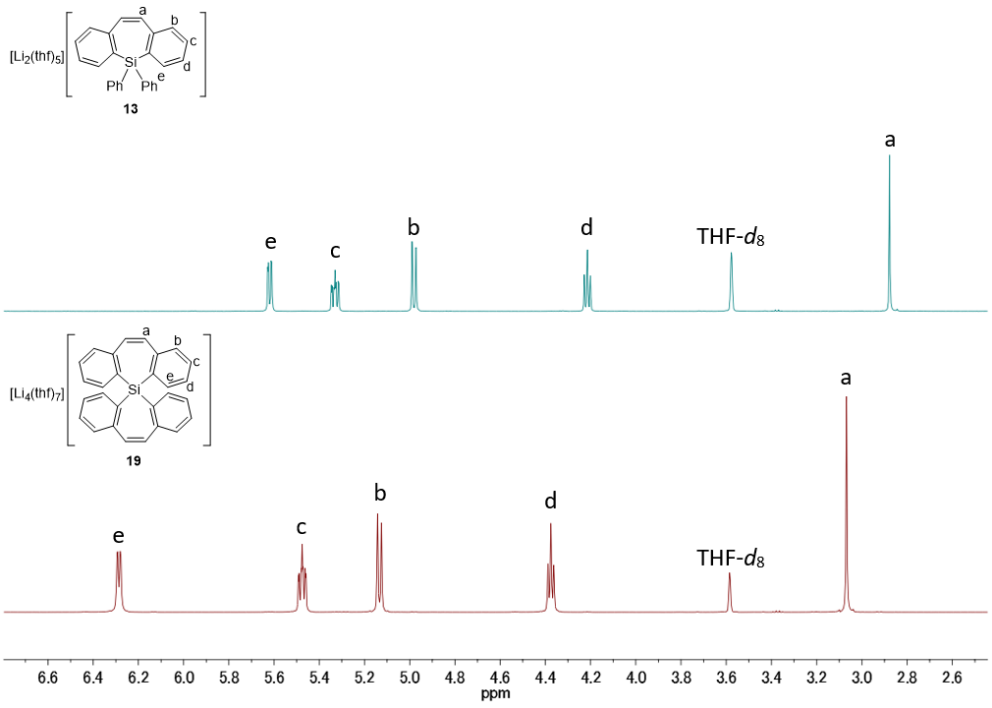

Figure 4-8. The ^{1}H NMR spectra of **13** (top) and **19** (bottom) recorded in THF-d_8.

Although high quality X-ray diffraction analysis data for **19** could not be obtained, crystal structures of **18** and **19** are illustrated in Figure 4-9, and the Si–C bond lengths are listed in Table 4-2. All Si–C bond lengths are almost the same (1.865(4)–1.875(4) Å). As mentioned in the previous research in this thesis, the shortenings and elongations of the endo and exocyclic Si–C bond lengths, respectively, were ones of the experimental diagnoses for hyperconjugation. However, in the case of spirosilepin, it is possible that the counterbalance of shortenings and elongations resulted in the equalization of Si–C bond lengths.

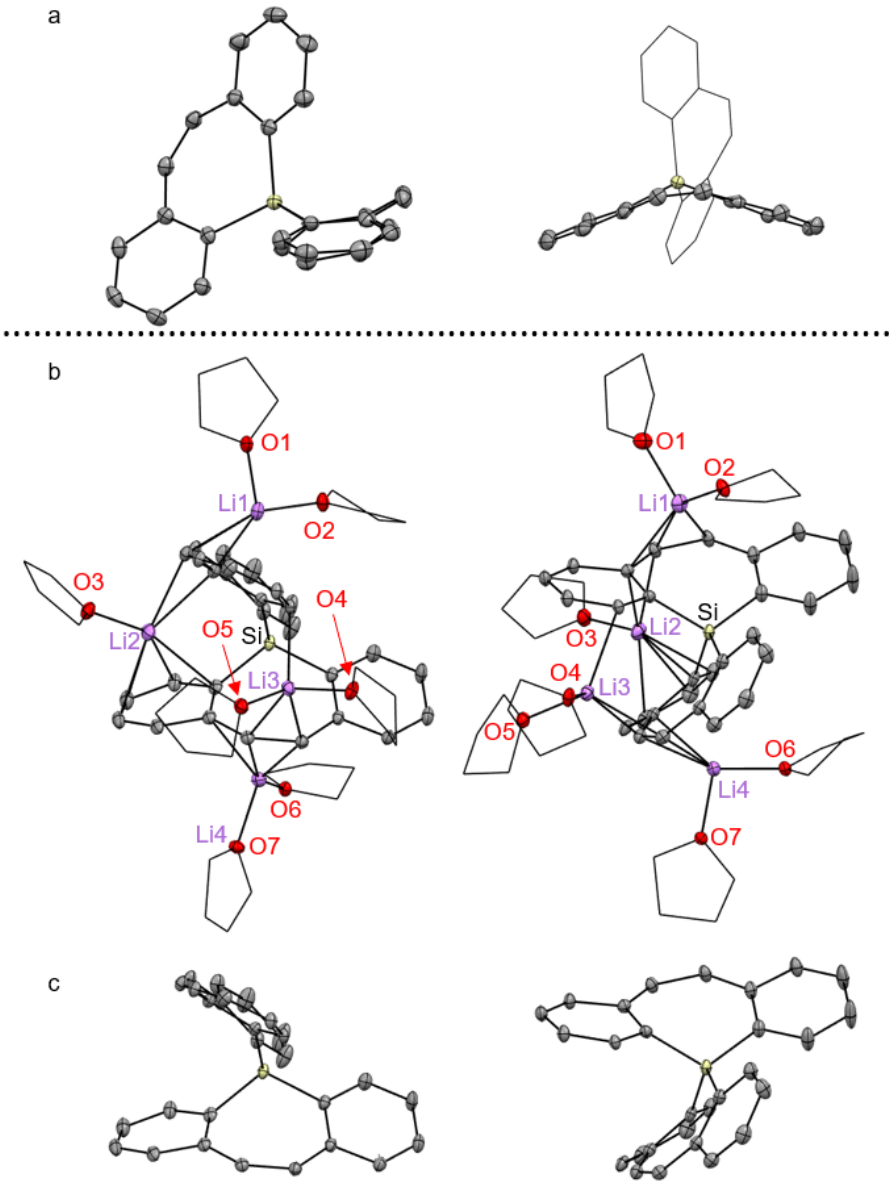

Figure 4-9. Solid state structures of **18** and **19** with thermal ellipsoids at 50% and 20% probability, respectively. Whole structures of **18** (top) and **19** (middle), and anionic parts of **19** (bottom).

Table 4-2. The Si–C bond lengths in **18** and **19**.

	18	**19**
Si−C1/Si−C2	1.873(3)/1.875(3)	1.871(4)/1.874(4)
Si−C3/Si−C4	1.865(3)/1.877(4)	1.865(4)/1.875(4)

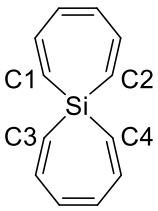

In conclusion, the author successfully synthesized and characterized tetrabenzospirosilepin **18** and its tetrareduced form **19**. Only the ^{1}H NMR signal assignable to the protons situated above the silepin rings in **19** (H_e in Figure 4-7) shifted to low-field in comparison to that of **13**, which can be attributable to the paratropic ring currents.

4-4 Experimental Section

4-4-1 Synthetic Procedures

General Procedure

All manipulations were carried out under an argon atmosphere by using standard Schlenk techniques or a glovebox unless otherwise stated. Et_2O, THF, toluene, toluene-d_8, and THF-d_8 were distilled over potassium mirror. Me_2SiCl_2 and $SiCl_4$ were purchased from Tokyo Chemical Industry (TCI). (*Z*)-2,2′-Dibromostilbene was synthesized according to the literature.[7] ^{1}H (500 MHz), ^{13}C{^{1}H} (126 MHz), ^{7}Li{^{1}H} (194 MHz), and ^{29}Si{^{1}H} (99 MHz) NMR spectra were recorded on a JEOL ECZ-500 spectrometer at 20°C unless otherwise stated. Chemical shifts are reported in δ and referenced to residual ^{1}H and ^{13}C signals of deuterated solvents as internal standards or to the ^{7}Li{^{1}H} and the ^{29}Si{^{1}H} NMR signal of LiCl in D_2O (δ = 0.00) and $SiMe_4$ in $CDCl_3$ (δ = 0.00), respectively, as external standards. Elemental analyses were performed on a Perkin Elmer 2400 series II CHN analyzer.

Synthesis of lithium salt of 5,5-dimethyldibenzo[*b*,*f*]silepinyl dianion 16.

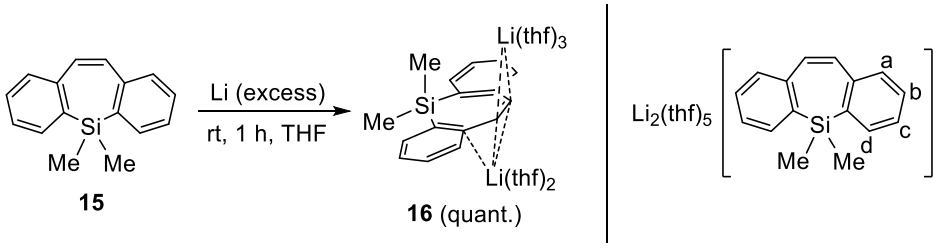

15 **16** (quant.)

Lithium (16.0 mg, 2.30 mmol) was added to a solution of **15** (50.0 mg, 0.212 mmol) in THF (2 mL) at room temperature. After 1 h, lithium was removed, and the solvent was removed in vacuo to yield **16** as a black-purple powder (130.3 mg, 0.213 mmol, quant.).

m.p. > 82 °C (decomp.); ^{1}H NMR (500 MHz, THF-d_8): δ = 5.80 (dd, $^{3}J_{H–H}$ = 7 Hz, $^{4}J_{H–H}$ = 1 Hz, 2H, *fused benzene-d*), 5.29 (ddd, $^{3}J_{H–H}$ = 8 Hz, $^{3}J_{H–H}$ = 6 Hz, $^{4}J_{H–H}$ = 1 Hz, 2H, *fused benzene-b*), 4.92 (d, $^{3}J_{H–H}$ = 9 Hz, 2H, *fused benzene-a*), 4.22 (t, $^{3}J_{H–H}$ = 7 Hz, 2H, *fused benzene-c*) , 2.81 (s, 2H, *vinyl*); ^{13}C{^{1}H} NMR (126 MHz, THF-d_8): δ = 146.3 (C_β), 138.4 (*fused benzene-d*), 127.7 (*fused benzene-b*), 119.1 (*fused benzene-a*), 109.3 (C_α), 96.3 (*fused benzene-c*), 75.9 (*vinyl*), 0.0 (*Me*); ^{7}Li{^{1}H} NMR (194 MHz, THF-d_8): δ = 0.29; ^{29}Si{^{1}H} NMR (99 MHz, THF-d_8): δ = −24.7.

Synthesis of trimer 17-THF.

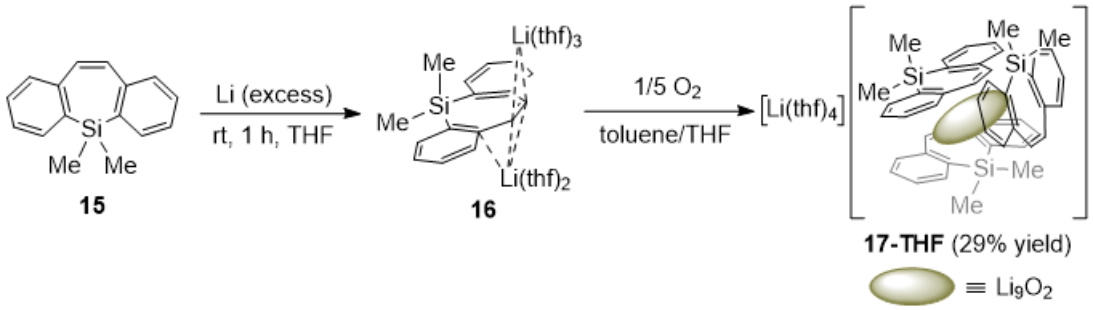

Lithium (16.0 mg, 2.30 mmol) was added to a solution of **15** (50.1 mg, 0.212 mmol) in THF (2 mL) at room temperature. After 1 h, the solvent was removed in vacuo, and the resulting black-purple powder was dissolved in a mixed solvent of toluene (6 mL) and THF (0.06 mL). The solution and the lithium were charged into a 100 mL Schlenk flask, then O_2 gas (0.2 mL, 0.008 mmol at 1 atom, 298 K) was injected to the flask every 10–12 h for five times (total O_2 amount: 1.0 mL, 0.04 mmol at 1 atom, 298 K). Standing the solution at room temperature deposited black crystals of **17-THF** (23.3 mg, 0.0205 mmol, 29% yield). m.p. > 156 °C (decomp.); ^{1}H NMR (500 MHz, toluene-d_8): δ = 5.93 (dd, $^{3}J_{H–H}$ = 7 Hz, $^{4}J_{H–H}$ = 1 Hz, 6H, *Ar*), 5.81 (brt, 6H, *Ar*), 4.89 (brs, 6H, *Ar*) 4.09 (t, $^{3}J_{H–H}$ = 6 Hz, 6H, *Ar*), 3.52 (brs, 6H, *vinyl*), 1.27 (brs, 9H, *Me*), 0.09 (brs, 9H, *Me*); ^{7}Li{^{1}H} NMR (194 MHz, toluene-d_8): δ = 6.29 (3Li, *middle of the Li_9O_2 cluster*), 4.44 (6Li, *edge of the Li_9O_2 cluster*), 0.62 (1Li, *solvent separated lithium cation*). Satisfactory elemental analysis data could not be obtained because of its instability towards moisture and oxygen. ^{13}C{^{1}H} and ^{29}Si{^{1}H} NMR in toluene-d_8 could not be measured due to its low solubility. The ^{1}H, ^{13}C{^{1}H}, and ^{7}Li{^{1}H} NMR spectra of **17-THF** in THF-d_8 are identical to those of **16**, suggesting **17-THF** is dissociated into three dibenzosilepinyl dianions in THF solution.

Synthesis of trimer 17-Et₂O.

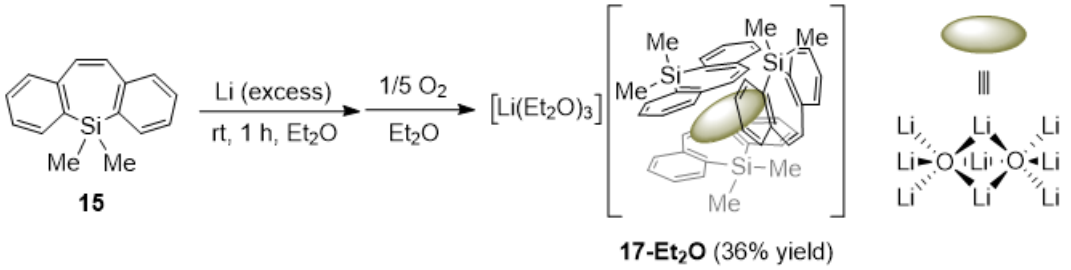

Lithium (19.7 mg, 2.83 mmol) was added to a solution of **15** (50.9 mg, 0.215 mmol) in Et_2O (2 mL) at room temperature. After 1 h, the solution and the lithium were charged into a 100 mL Schlenk flask, then O_2 gas (0.2 mL, 0.008 mmol at 1 atom, 298 K) was injected to the flask every 10–12 h for five times (total O_2 amount: 1.0 mL, 0.04 mmol at 1 atom, 298 K). Standing the solution at room temperature deposited black crystals of **17-Et₂O** (26.5 mg, 0.0257 mmol, 36% yield). The crystals are insoluble in C_6D_6. The ^1H, $^{13}C\{^1H\}$, and $^7Li\{^1H\}$ NMR spectra of **17-Et₂O** in THF-d_8 are identical to those of **16**, suggesting **17-Et₂O** is dissociated into three dibenzosilepinyl dianions in THF solution.

Synthesis of 5,5′-spirobi(5*H*-dibenzo[*b*,*f*]silepin) 18

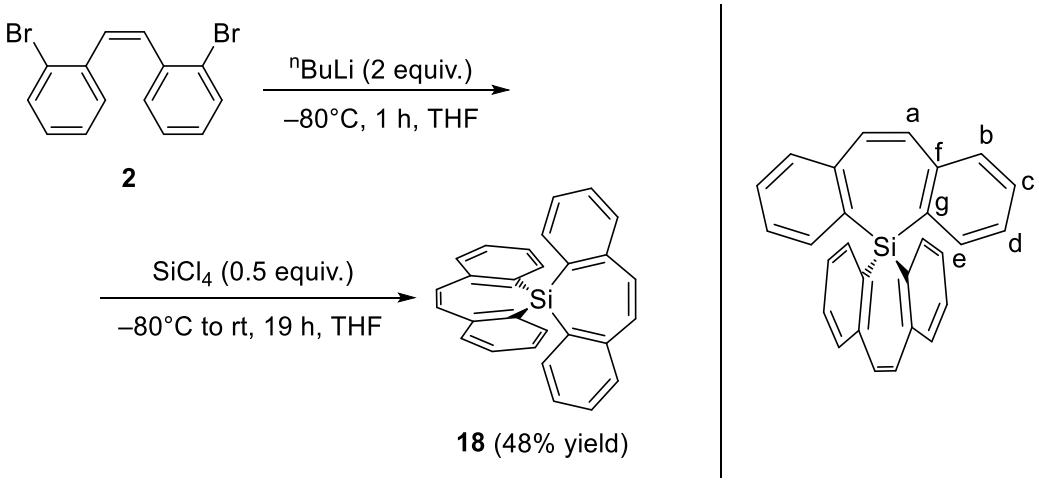

^{n}BuLi (1.59 M in hexanes, 1.50 mL, 2.38 mmol) was added to a THF solution (40 mL) of dibromostilbene **2** (0.400 g, 1.18 mmol) in THF at −80 °C. After 1 hour, $SiCl_4$ (0.07 mL, 0.105 g, 0.616 mmol) was added dropwise, then the mixture was allowed to gradually warm to room temperature and stirred for 19 hours. The solvent was removed in vacuo, and materials insoluble in CH_2Cl_2 were filtered off. The filtrate was concentrated and purified by column chromatography (eluent: hexane:CH_2Cl_2 = 3:1). Recrystallization of

the resulting white powder from Et_2O yielded **18** as colorless crystals (0.114 g, 0.296 mmol, 48% yield). ^{1}H NMR (500 MHz, $CDCl_3$): δ = 7.55 (td, $^3J_{H–H}$ = 7 Hz, $^4J_{H–H}$ = 1 Hz, 4H, H_b), 7.41 (dd, $^3J_{H–H}$ = 8 Hz, $^4J_{H–H}$ = 1 Hz, 4H, H_e), 7.37 (td, $^3J_{H–H}$ = 7 Hz, $^4J_{H–H}$ = 1 Hz, 4H, H_d), 7.20 (td, $^3J_{H–H}$ = 7 Hz, $^4J_{H–H}$ = 1 Hz, 4H, H_c) 6.79 (s, 4H, *vinyl*); ^{13}C{^{1}H} NMR (126 MHz, $CDCl_3$): δ = 147.2 (C_g), 136.8 (C_b), 133.3 (C_f), 132.9 (*vinyl*), 131.1 (C_e), 129.4 (C_d), 126.7 (C_c); ^{29}Si{^{1}H} NMR (99 MHz, $CDCl_3$): δ = −18.7; Elemental analysis calcd (%) for $C_{28}H_{20}Si$ (**5**): C 87.45, H 5.24; found: C 87.43, H 5.10.

Synthesis of tetralithium salt of 5,5′-spirobi(5*H*-dibenzo[*b*,*f*]silepinide) 19

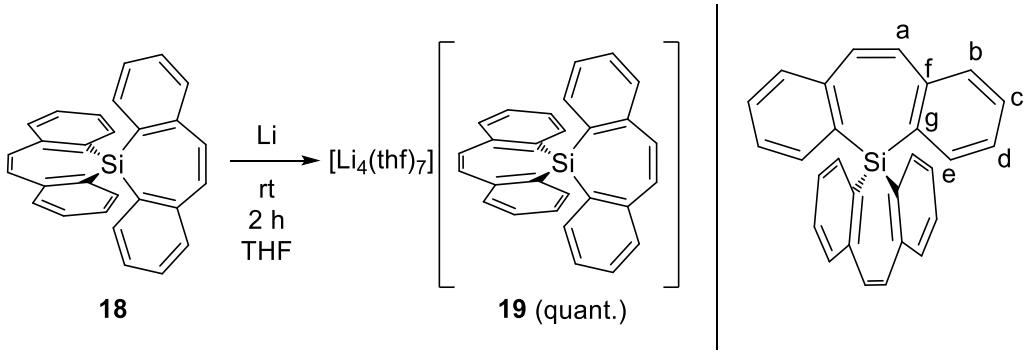

Lithium (16.0 mg, 2.30 mmol) was added to a solution of **18** (30.1 mg, 0.0783 mmol) in THF (2 mL) at room temperature. After 1 h, lithium was removed, and the solvent was removed in vacuo to yield **19** as a black-purple powder (71.6 mg, 0.0781 mmol, quant.) ^{1}H NMR (500 MHz, THF-d_8): δ = 6.29 (dd, $^3J_{H–H}$ = 7 Hz, $^4J_{H–H}$ = 1 Hz, 4H, H_e), 5.48 (ddd, $^3J_{H–H}$ = 8 Hz, $^3J_{H–H}$ = 6 Hz, $^4J_{H–H}$ = 2 Hz, 4H, H_c), 5.13 (d, $^3J_{H–H}$ = 8 Hz, 4H, H_b), 4.38 (t, $^3J_{H–H}$ = 6 Hz, 4H, H_d) , 2.81 (s, 2H, *vinyl*); ^{13}C{^{1}H} NMR (126 MHz, THF-d_8): δ = 146.3 (C_f), 138.4 (C_e), 127.7 (C_c), 119.1 (C_b), 109.3 (C_d), 96.3 (C_d), 75.9 (*vinyl*); ^{7}Li{^{1}H} NMR (194 MHz, THF-d_8): δ = 0.87; ^{29}Si{^{1}H} NMR (99 MHz, THF-d_8): δ = −38.2.

4-4-2 Theoretical studies

Theoretical calculations were performed by using the *Gaussian* 16 Rev.C.[8] All calculations were performed at the B3LYP[9] level of theory using 6-31+G(d)[10] basis sets except for the GIAO calculations for **17′** (6-311+G(2d,p)). The structural optimization has been carried out for **15**, $\mathbf{15^{2-}}$, **16**, and **17′**. The optimized structures of **16** and **17′** are

in good agreement with the corresponding X-ray structures. All local minima were confirmed by the vibrational frequency calculations with zero imaginary frequency. The NICS values for **15** and $\mathbf{15}^{2-}$, and molecular orbitals for **15** and **16** and **17′** were calculated using the optimized structures, while the NICS values for **17-THF** and $\mathbf{(15^{-2})_3}$ were obtained by single point energy calculations using the X-ray structures.

4-4-3 Crystal data

	16	**17-THF**	**17-Et_2O**
CCDC	2191231	2191232	2191233
formula	$C_{36}H_{56}Li_2O_5Si$	$C_{68}H_{85}Li_{10}O_5Si_3$	$C_{60}H_{78}Li_{10}O_5Si_3$
fw	610.77	1152.02	1032.89
crystal size	0.21 × 0.2 × 0.12	0.15 × 0.12 × 0.05	0.18 × 0.16 × 0.13
crystal system	monoclinic	triclinic	trigonal
space group	*Pc*	*P*-1	*R*3*c*
a [Å]	9.332(3)	11.117(6)	15.249(4)
b [Å]	10.610(3)	15.204(8)	15.249(4)
c [Å]	17.742(5)	19.765(10)	44.207(11)
α [deg]	90	85.97(2)	90
β [deg]	95.085(5)	79.66(2)	90
γ [deg]	90	79.45(2)	120
V [Å^3]	1749.7(8)	3228(3)	8902(5)
Z	2	2	6
ρ_{calcd} [g cm^{-3}]	1.159	1.185	1.156
F(000)	664	1226	3300
μ [cm^{-1}]	1.06	1.23	1.25
transmission factors range	0.8715 – 1	0.8544 – 1	0.8544 – 1
index range	-12 ≤ h ≤ 11	-13 ≤ h ≤ 14	-19 ≤ h ≤ 15
	-13 ≤ k ≤ 13	-19 ≤ k ≤ 19	-19 ≤ k ≤ 19
	-22 ≤ l ≤ 23	-25 ≤ l ≤ 25	-57 ≤ l ≤ 45
no. reflections	13870	26145	22798
unique (R_{int})	6403 (0.0364)	14088 (0.0419)	4195 (0.0565)
$I > 2\sigma(I)$	5102	9201	3660
no. parameters	400	792	239
R_1 ($I > 2\sigma(I)$)[a]	0.0515	0.0611	0.0513
wR_2 (all data)[b]	0.1280	0.1887	0.1340
GOF [c]	1.038	1.025	1.066
max diff peak / hole [e Å^{-3}]	0.54/-0.314	0.803/-0.601	0.521/-0.613

	18	**19**
CCDC		
formula	$C_{28}H_{20}Si$	$C_{60}H_{84}Li_4O_8Si$
fw	380.53	989.12
crystal size	0.18 × 0.08 × 0.07	0.15 × 0.11 × 0.04
crystal system	orthorhombic	triclinic
space group	*P*212121	*P*-1
a [Å]	7.5573(9)	12.666(3)
b [Å]	15.2356(18)	13.922(3)
c [Å]	34.335(4)	17.299(4)
α [deg]	90	96.870(2)
β [deg]	90	95.893(4)
γ [deg]	90	114.847(3)
V [Å^3]	3953.3(8)	2708.4(10)
Z	8	2
ρ_{calcd} [g cm^{-3}]	1.292	1.213
F(000)	1616	1068
μ [cm^{-1}]	1.30	0.98
transmission factors range	0.8602 – 1	0.8615 – 1
index range	-8 ≤ h ≤ 9	-15 ≤ h ≤ 13
	-19 ≤ k ≤ 19	-17 ≤ k ≤ 17
	-42 ≤ l ≤ 41	-21 ≤ l ≤ 21
no. reflections	30246	20724
unique (R_{int})	8160 (0.0539)	10906 (0.0435)
$I > 2\sigma$(I)	7271	6390
no. parameters	523	659
R_1 ($I > 2\sigma$(I))[a]	0.0522	0.1076
wR_2 (all data)[b]	0.1245	0.3880
GOF [c]	1.068	1.099
max diff peak / hole [e Å^{-3}]	0.341/-0.408	1.255/-1.225

[a] $R1 = \Sigma||F_o| - |F_c||/\Sigma|F_o|$. [b] $wR2 = [\Sigma\{w(F_o^2 - F_c^2)^2\}/\Sigma w(F_o^2)^2]^{1/2}$, w = 1/[□$^2F_o^2$ + (aP)^2 + bP] (a and b are constants suggested by the refinement program; P = [max(F_o^2,0) + 2F_c^2]/3). [c]GOF = $[\Sigma w(F_o^2 - F_c^2)^2/(N_{obs} - N_{params})]^{1/2}$.

4-5 References

(1) L. G. Mercier, S. Furukawa, W. E. Piers, A. Wakamiya, S. Yamaguchi, M. Parvez, R. W. Harrington and W. Clegg, *Organometallics*, 2011, **30**, 1719-1729.

(2) S. Ito, Y. Ishii, K. Ishimura and T. Kuwabara, *Chem. Commun.*, 2021, **57**, 11330-11333.

(3) (a) W. Clegg, R. W. Harrington, L. G. Mercier and W. E. Piers, *Acta Cryst.*, 2013, **C69**, 436-438; (b) K. Sprenger, C. Golz and M. Alcarazo, *Eur. J. Org. Chem.*, 2020, **2020**, 6245-6254. (17) A. Stanger, *J. Org. Chem.*, 2006, **71**, 883-893.

(4) M. Saito, T. Kuwabara, K. Ishimura and S. Nagase, *Chem. Asian J.*, 2011, **6**, 2907-2910.

(5) R. Gershoni-Poranne and A. Stanger, *Chem. Eur. J.*, 2014, **20**, 5673-5688.

(6) A. Stanger, *J. Org. Chem.*, 2006, **71**, 883-893.

(7) L. G. Mercier, W. E. Piers, M. Parvez, *Angew. Chem., Int. Ed.* **2009**, *48*, 6108-6111.

(8) M. J. Frisch, G. W. Trucks, H. B. Schlegel, G. E. Scuseria, M. A. Robb, J. R. Cheeseman, G. Scalmani, V. Barone, G. A. Petersson, H. Nakatsuji, X. Li, M. Caricato, A. V. Marenich, J. Bloino, B. G. Janesko, R. Gomperts, B. Mennucci, H. P. Hratchian, J. V. Ortiz, A. F. Izmaylov, J. L. Sonnenberg, Williams, F. Ding, F. Lipparini, F. Egidi, J. Goings, B. Peng, A. Petrone, T. Henderson, D. Ranasinghe, V. G. Zakrzewski, J. Gao, N. Rega, G. Zheng, W. Liang, M. Hada, M. Ehara, K. Toyota, R. Fukuda, J. Hasegawa, M. Ishida, T. Nakajima, Y. Honda, O. Kitao, H. Nakai, T. Vreven, K. Throssell, J. A. Montgomery Jr., J. E. Peralta, F. Ogliaro, M. J. Bearpark, J. J. Heyd, E. N. Brothers, K. N. Kudin, V. N. Staroverov, T. A. Keith, R. Kobayashi, J. Normand, K. Raghavachari, A. P. Rendell, J. C. Burant, S. S. Iyengar, J. Tomasi, M. Cossi, J. M. Millam, M. Klene, C. Adamo, R. Cammi, J. W. Ochterski, R. L. Martin, K. Morokuma, O. Farkas, J. B. Foresman, D. J. Fox, *Gaussian 16 Rev. C.01*, Gaussian, Inc., Wallingford, CT, **2016**.

(9) (a) C. Lee, W. Yang, R. G. Parr, *Phys. Rev. B* **1988**, *37*, 785-789; b) A. D. Becke, *J. Chem. Phys.* **1993**, *98*, 5648-5652. (16) M. Saito, T. Kuwabara, K. Ishimura and S. Nagase, *Chem. Asian J.*, 2011, **6**, 2907-2910.

(10) M. M. Francl, W. J. Pietro, W. J. Hehre, J. S. Binkley, M. S. Gordon, D. J. DeFrees, J. A. Pople, *J. Chem. Phys.* **1982**, *77*, 3654-3665.

Chapter 5

Weakened antiaromaticity of a dibenzosilepinyl dianion in a parallel stacked form

5-1 Introduction

In Chapter 4, the author demonstrated that a dibenzosilepinyl dianion remains its antiaromaticity in a form of a triangular pillar. However, interestingly, it is known that some parallel stacked antiaromatic molecules gain thermodynamic stability through face-to-face aromaticity. Theoreticians have proposed that the stacking of two antiaromatic systems such as pentalene dimer **AP**[1] and cyclobutadiene dimer **AQ**[2] can reduce their antiaromaticity via mutual π-interactions (Figure 5-1). Recently, Shinokubo's group synthesized tethered Ni(II) norcorrole dimer **AR**[3] and Ni(II) norcorrole cyclophane **AS**[4]. Since a norcorrole has an antiaromatic character due to the 16π-electron system, the aromatic character in each Ni(II) norcorrole unit in dimers was revealed by experimental methods such as low-field shifts of ^{1}H NMR signals induced by diatropic ring currents. However, synthetic research of face-to-face aromaticity is very limited, and to the best of the author's knowledge, such synthetic investigation for an anionic molecule has not been reported. In the final chapter, the synthesis of parallel stacked dibenzosilepinyl dianions and their through-space interactions are demonstrated.

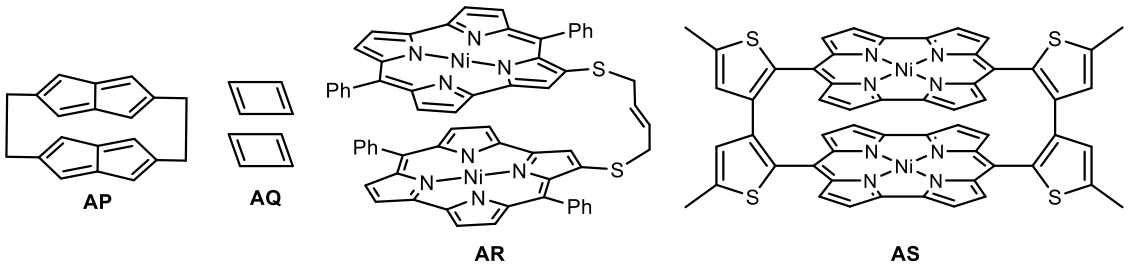

Figure 5-1. Selected examples of stacked antiaromatic molecules.

5-2 Dimerization of diphenyldibenzosilepinyl dianions

In chapter 3, the author revealed that recrystallization of **13** (diPh dianion) from a THF solution provided black crystals of monomeric form. In contrast, recrystallization of **13** from a toluene solution deposited black crystals of dimer **20** with a slipped dimeric structure in which two of the four lithium atoms are sandwiched by two dibenzosilepinide units (Scheme 5-1). DME-coordinated dimer **21** was also obtained by the reduction of **12** in Et_2O followed by recrystallization from a DME/toluene solution, which has higher

quality data for X-ray diffraction analysis than **20**. In dimer **21**, each sandwiched lithium atom is coordinated by one of the fused six-membered rings and the silepin ring in η^4- and η^3-fashions, respectively. Each other lithium atom is coordinated by a DME molecule and the vinyl carbon atoms.

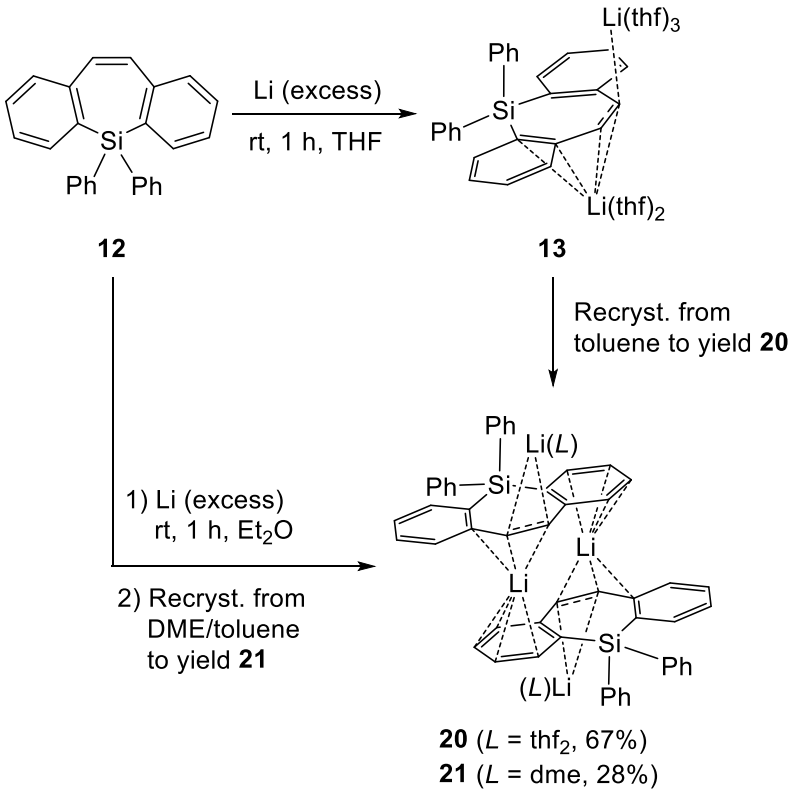

Scheme 5-1. Synthesis of dimers **20** and **21**.

The dibenzosilepinide cores in dimer **21** have structural features similar to those in monomer **13**. The shortening and elongation of the endocyclic and exocyclic Si–C bonds, respectively, are also observed in **21** (Table 5-1), thus, negative hyperconjugation also occurs effectively in dimer **21**. The HOMA values of fused benzene rings in **21** suggest that the degree of the aromatic character of the six-membered rings is reduced by the 16π-electron system even in dimeric form. However, the twisted angle of dimer **21** is obviously smaller than monomer **13** (20.49° vs. 32.46°), suggesting that dibenzosilepinyl dianions core obtain higher planarity in dimeric form (Figure 5-2), which can be attributable to weakened antiaromaticity in the dimer (*vide infra*).

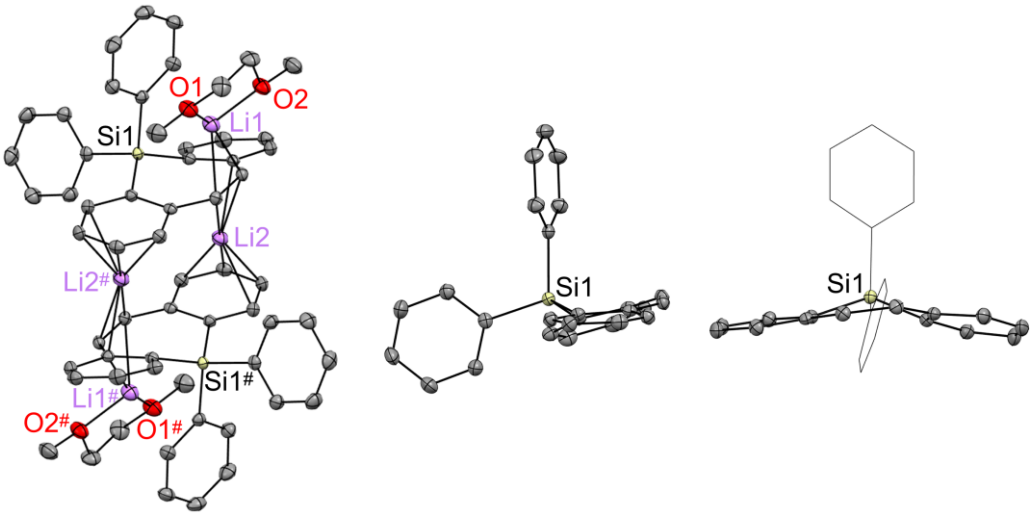

Figure 5-2. The whole structure of **21** (left), and anionic parts of **21** (middle and right).

Table 5-1. Selected bond lengths of **21**, and HOMA values for the six-membered rings.

	21
Si−C1/ Si−C6	1.8530(16)/1.8430(17)
Si−C15/Si−C21	1.8970(17)/1.8786(17)
C1−C2/C5−C6	1.469(2)/1.451(2)
C2−C3/C4−C5	1.407(2)/1.416(2)
C3−C4	1.469(2)
C1−C7/C6−C14	1.408(2)/1.407(2)
C7−C8/C14−C13	1.402(2)/1.389(2)
C8−C9/C13−C12	1.417(2)/1.403(3)
C9−C10/C12−C11	1.366(2)/1.369(3)
C10−C2/C5−C11	1.458(2)/1.442(2)
HOMA values of Ring a/b	0.90/0.83

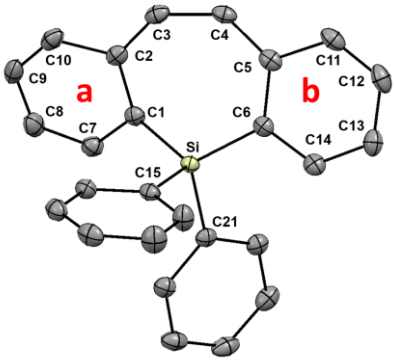

To gain more insight into the electronic properties, DFT calculations were conducted at the B3LYP/6-31+G(d) level of theory (details are written in Section 5-4-2). Through space interactions in **21** were confirmed by frontier molecular orbitals. The frontier MOs of **13** and **21** are illustrated in Figure 5-3. Both the HOMO and the HOMO−1 of **21** were constructed by the HOMO of **13**. However, the HOMO and the HOMO−1 of **21** are antibonding and bonding orbitals, respectively, thus the overlaps of orbitals between the two surfaces were confirmed only in HOMO−1 of **21**. Moreover, the energy level of HOMO−1 of **21** was lower than HOMO of **21**, suggesting that the orbital overlaps stabilize the system thermodynamically.

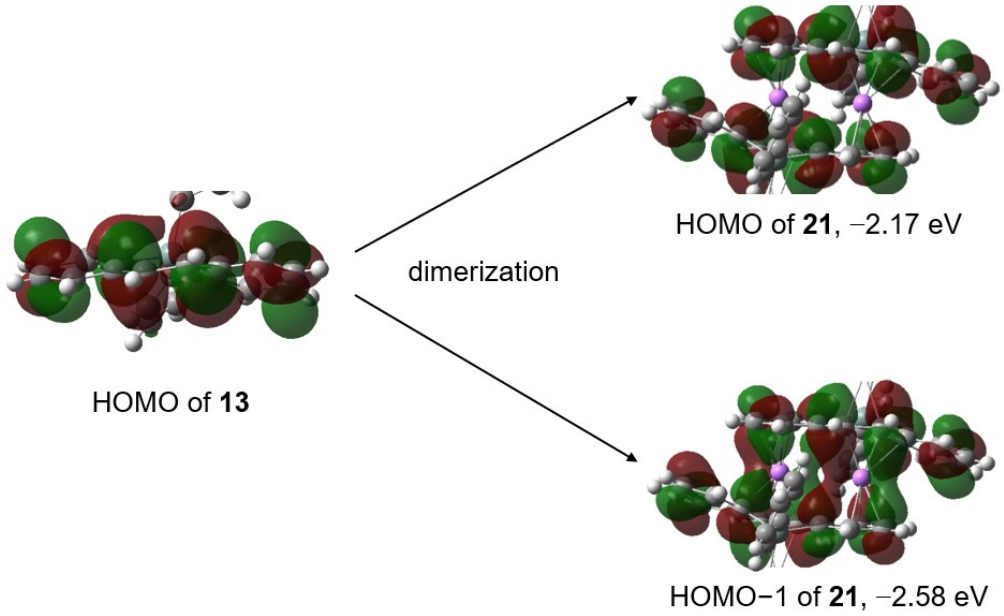

Figure 5-3. Frontier molecules for **13** and **21**.

$NICS_{iso}$ calculations were conducted on the lithium-free tetraanion of **21** (denoted as **21′**$_{dimer}$) and a model structure **21′**$_{monomer}$, which is defined as the monomeric dibenzosilepinyl dianion extracted from the structure of **21′**$_{dimer}$ (Table 5-2). The differences in the NICS values between **21′**$_{dimer}$ and **21′**$_{monomer}$ should be originated from face-to-face interactions. All NICS values for **21′**$_{dimer}$ were drastically smaller than the values of **21′**, whereas those for **21′**$_{monomer}$ are close to the values for **13′**. The smaller NICS values of **21′**$_{dimer}$ suggest that **21** is stabilized by face-to-face interactions to weaken its antiaromatic character.

Table 5-2. $NICS_{iso}(X)$ values for **13′**, **21′dimer**, and **21′monomer**.

	NICS(+1) NICS(0) NICS(−1)	
	six-membered rings	seven-membered rings
13′	7.0/8.0 13.6/12.8 8.2/7.5	2.1 5.1 4.2
21′dimer	−0.2[a]/−2.3[b] 4.1[a]/2.4[b] 0.4[a]/−2.6[b]	−3.1 1.1 −1.0
21′monomer	6.1/7.6 12.2/13.7 7.4/8.6	0.0 4.0 3.3

[a] The outer six-membered rings. [b] The inner six-membered rings.

To investigate differences in electronic properties between monomer **13** and dimer **21** experimentally, ^{1}H NMR signals of **13** and **21** were recorded in toluene-d_8. However, the signals of **13** and **21** were broadened and corresponded to each other, indicating that those are equilibrium in a solution. This result encouraged the author to design a new molecule that provides experimental facts of through-space interaction between stacked silepinyl dianions.

5-3 Synthesis of a tetralithium bissilepinide and weakened antiaromaticity

To synthesize stacked silepinyl dianions that do not dissociate in a solution, the author prepared a chlorophenylsilepin. ^{n}BuLi was added to a THF solution of (Z)-2,2′-dibromostilbene[5] at −80 °C, then the mixture was treated with $PhSiCl_3$ to yield 5-chloro-5-phenyldibenzo[*b*,*f*]silepin **22** (Scheme 5-2). Colorless crystals that are suitable for X-ray diffraction analysis were obtained by recrystallization of **22** from the Et_2O solution. The silepin ring of **22** has a boat-type structure, which is similar to those of reported dibenzosilepin skeletons (Figure 5-4).[6]

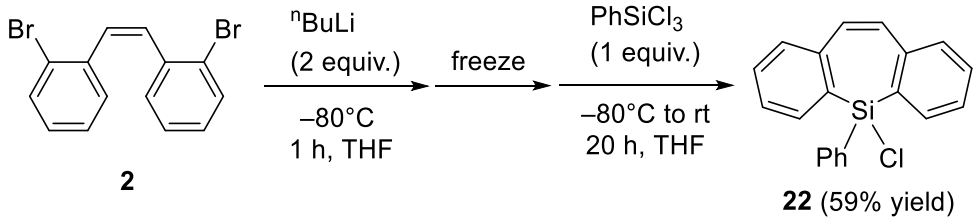

Scheme 5-2. Synthesis of phenylchlorosilepin **22**.

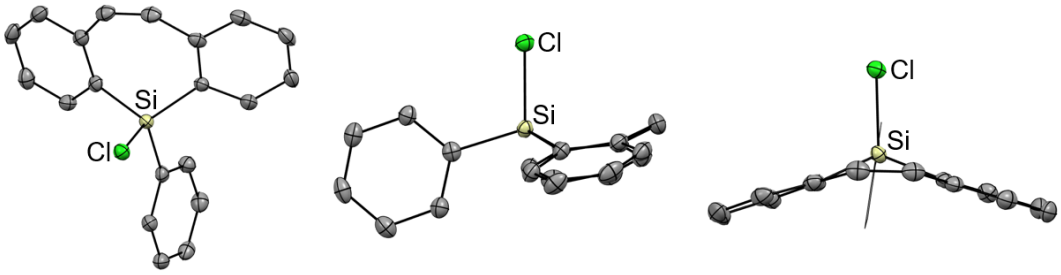

Figure 5-4. Whole molecular structures of **22**.

A reaction of **22** and excess lithium in Et_2O followed by oxygen oxidation afforded bis(phenyldibenzosilepin) **23** in which two silepin cores are bridged by the Si–Si single bond, which is expected that those silepin cores do not dissociate in a solution (Scheme 5-3). This is the first synthesis of a Si–Si bridged bissilepin. Compound **23** preferred gauche-form rather than anti-form presented by the dihedral angle of (*ipso*-Ph)–Si–Si–(*ipso*-Ph) of 63.9° (Figure 5-5, top). Treatment of colorless Et_2O solution of **23** with excess lithium generated black-purple solution. Recrystallization of the solution with the additive of DME deposited black crystals **24**. X-ray diffraction analysis revealed that the two dibenzosilepin cores were almost parallel and stacked to sandwich the two lithium cations.

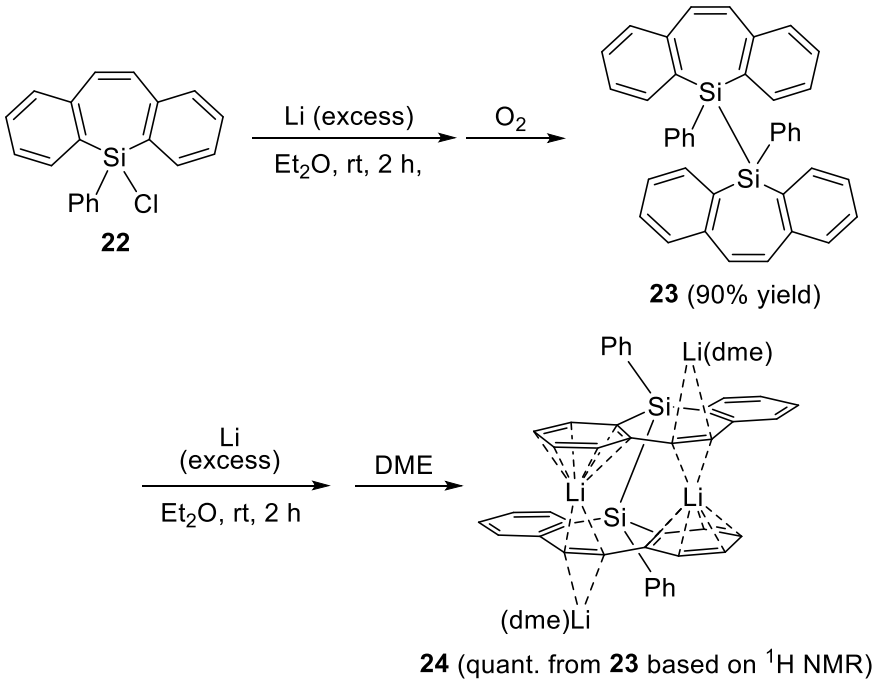

Scheme 5-3. Synthesis of bissilepin **23** and its tetrareduced species **24**.

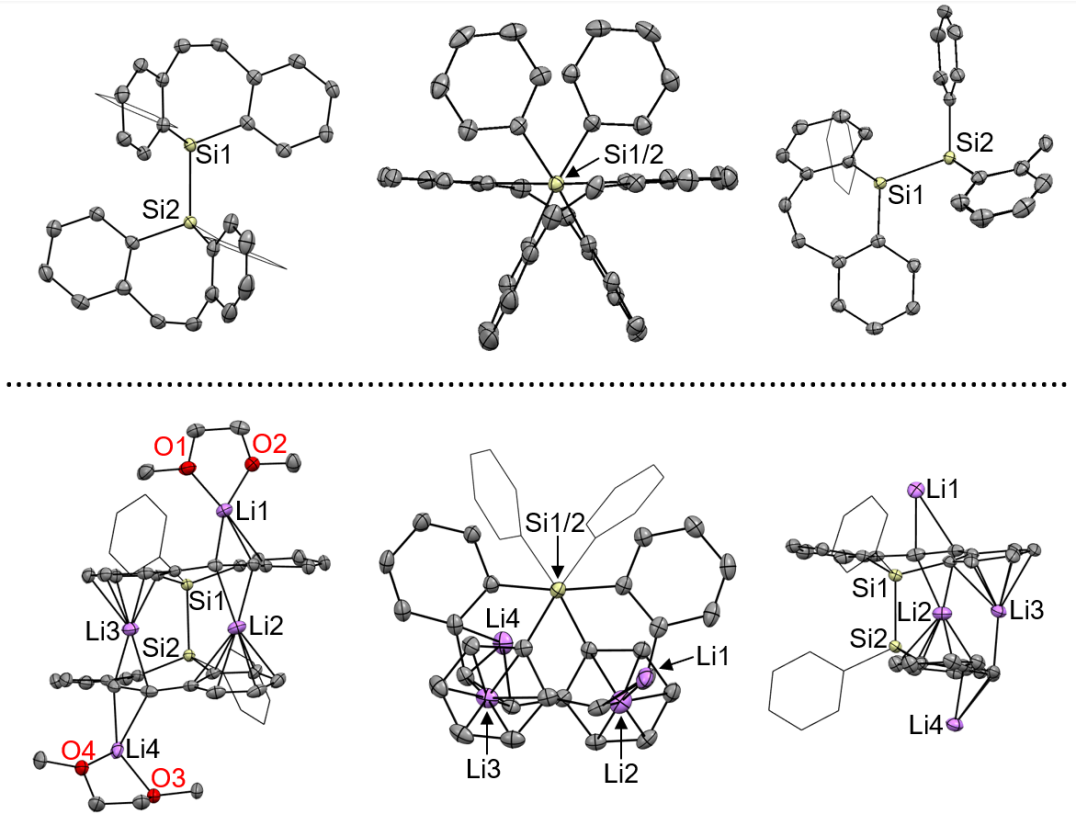

Figure 5-5. Whole molecule structures of **23** (top) and **24** (bottom left), and structures of **24** without DME molecules (bottom middle and bottom right).

As the other silepinyldianions written in this thesis, the shortening and elongation of the endocyclic and exocyclic Si–C bonds, respectively, are also observed in **24**, suggesting negative hyperconjugation also occurs in dimer **24**. The Si–Si bond length of **24** is shorter than that of precursor **23**, most likely for delocalized anionic charges via the sigma conjugation on the Si–Si bond of **24**. The smaller HOMA values of fused benzene rings in **24** than those of **23** suggest that the degree of the aromatic character of the six-membered rings is reduced by the 16π-electron system in dimeric form.

Table 5-3. Selected bond lengths of **23** and **24**, and HOMA values for the six-membered rings.

	23	**24**
Si1−C1/ Si1−C6	1.876(2)/1.877(2)	1.864(3)/1.874(3)
Si1−C15	1.886(2)	1.900(3)
Si1−Si2	2.3822(10)	2.3702(11)
C1−C2/C5−C6	1.414(3)/1.416(2)	1.450(4)/1.473(4)
C2−C3/C4−C5	1.472(3)/1.470(3)	1.413(4)/1.404(4)
C3−C4	1.347(3)	1.461(4)
C1−C7/C6−C14	1.399(3)/1.396(3)	1.423(4)/1.403(4)
C7−C8/C14−C13	1.391(3)/1.376(3)	1.378(4)/1.392(4)
C8−C9/C13−C12	1.383(3)/1.391(3)	1.415(4)/1.420(4)
C9−C10/C12−C11	1.380(3)/1.382(3)	1.359(4)/1.357(4)
C10−C2/C5−C11	1.402(3)/1.401(3)	1.449(4)/1.464(4)
HOMA values of Ring a/b	0.99/0.98	0.86/0.79

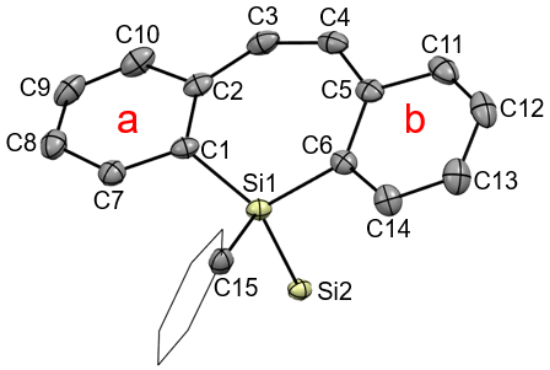

^{1}H NMR signals of **13** and **24** recorded in THF-d_8 are shown in Figure 5-6. The signals of the dibenzosilepinyl dianion scaffolds in **24** appeared at low-field in comparison to those of monomer **13** (Δδ0.12 to 0.53 ppm for fused benzene rings, Δδ0.90 ppm for vinyl protons). This phenomenon provides an experimental fact of weakened antiaromaticity in dimer **24**.

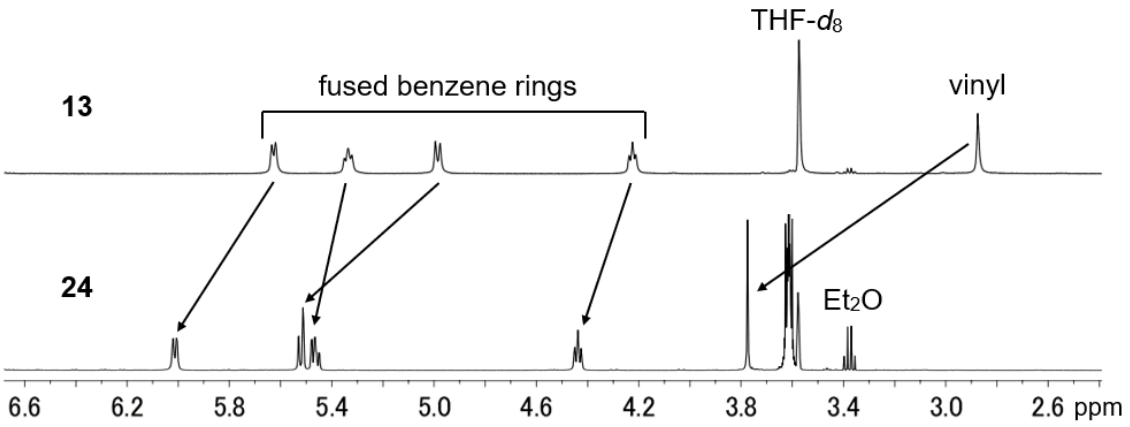

Figure 5-6. Comparison of ^{1}H NMR signals between **13** and **24**.

Although the two dibenzosilepinide units of **24** are slipped in the crystalline state, only five signals of dibenzosilepinyl dianion moieties were observed at room temperature, indicating fast rotation of the Si−Si bond in the solution state at room temperature, then the author investigated VT NMR of **24**. In the ^{1}H NMR spectra measured in THF-d_8, the signals of the dibenzosilepinide units were split at −90 °C (Figure 5-7), which can be attributable to a stacked structure. However, unfortunately, because the signals at a very low temperature were broadened, the assignment of those signals was unfruitable. The ^{7}Li{^{1}H} NMR spectra were also recorded in THF-d_8 (Figure 5-8). The signals of **24** appeared at higher-field than the signals of **17-THF** (trimer) even at low temperatures, which can be attributable to weakened antiaromaticity in the dimeric form. Indeed, theoretical calculations revealed that the calculated chemical shift of lithium cations sandwiched by dibenzosilepinide in a bissilepinyl tetraanion appeared at around 0.4 ppm when the chemical shift of $[Li(thf)_4]^+$ was set to 0 ppm.

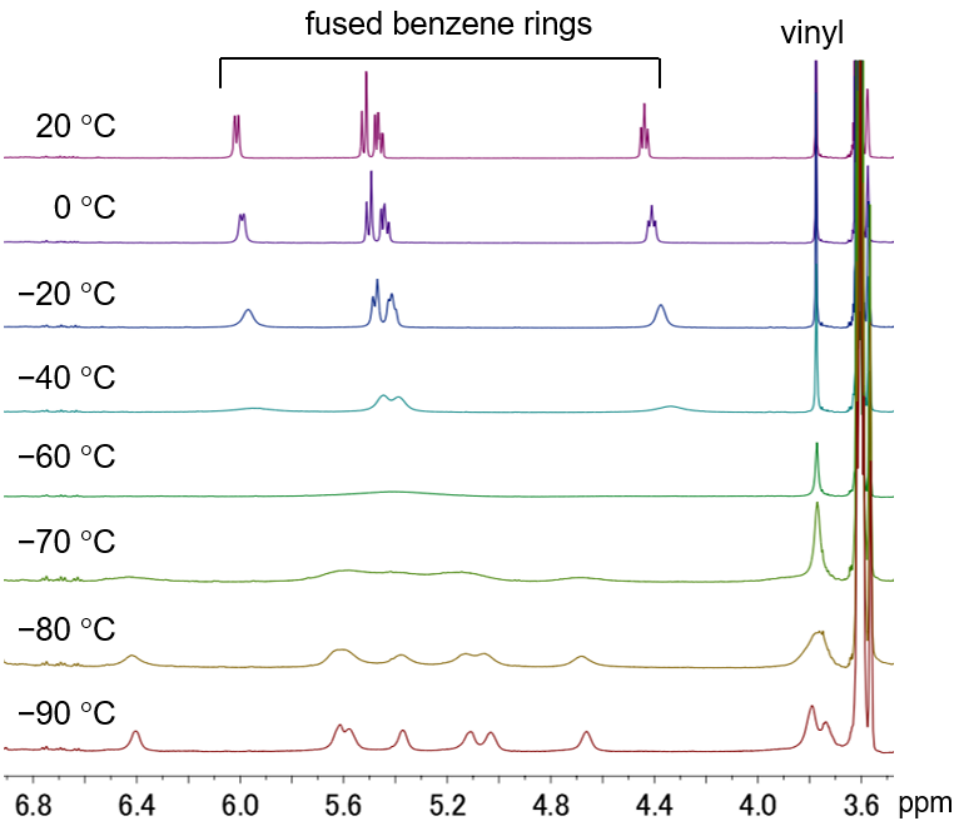

Figure 5-7. VT-^{1}H NMR spectra of **24** recorded in THF-d_8.

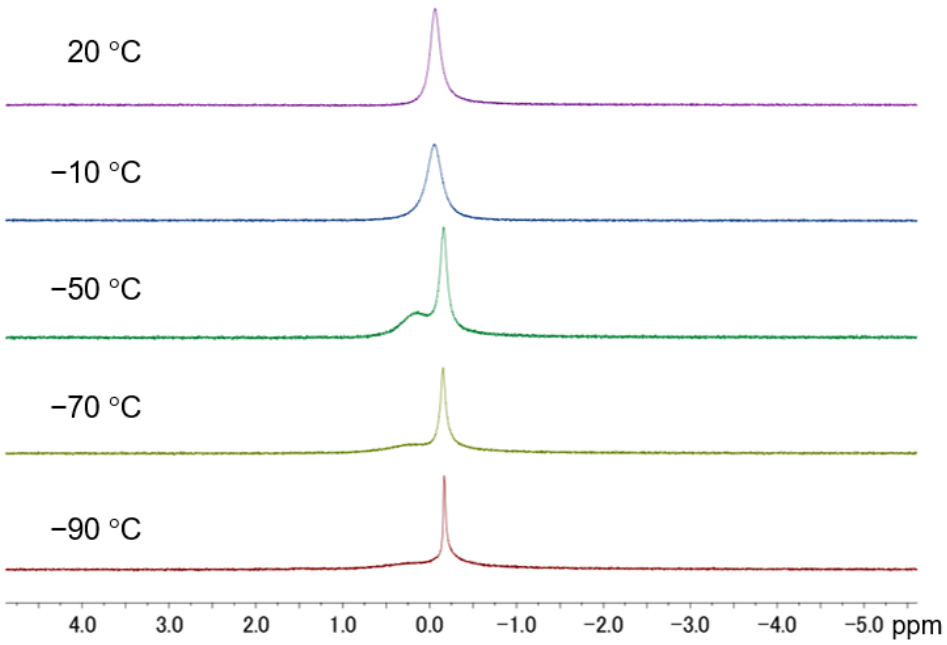

Figure 5-8. VT-^{7}Li{^{1}H} NMR spectra of **24** recorded in THF-d_8.

Through space interaction, which is the overlaps of π-orbitals between the two dibenzosilepinide, was found in the HOMO−1 of **24** as in the case of **21** (Figure 5-9). Importantly, a similar through-space interaction is also confirmed in the HOMO−1 of norcorrole cyclophane **AS** which has face-to-face aromaticity. Therefore, the author is estimating that compound **24** is also stabilized by face-to-face interaction.

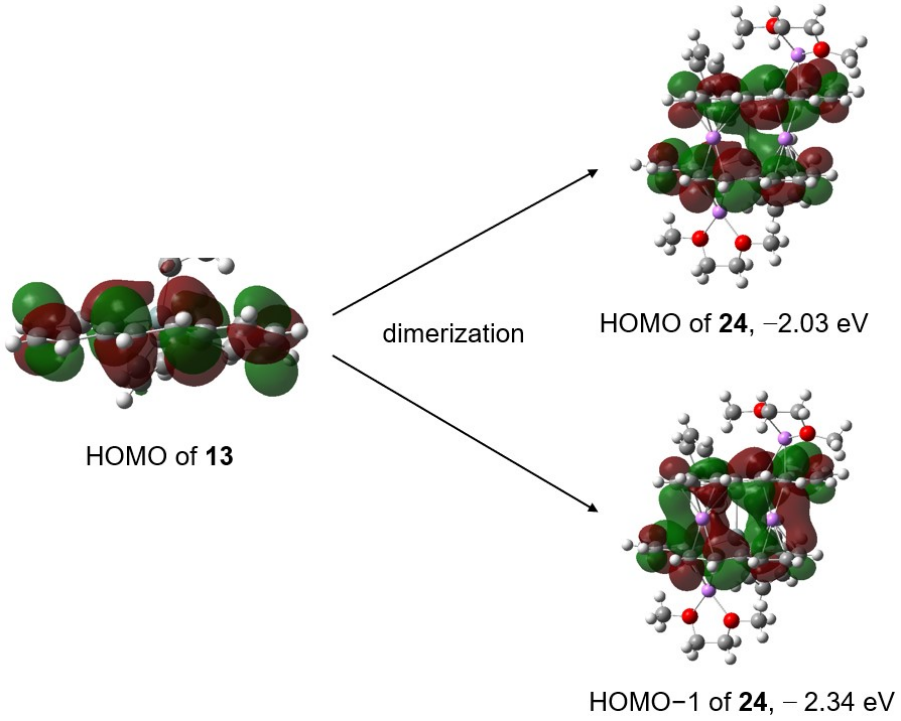

Figure 5-9. Frontier molecules for **13** and **24**.

All $NICS_{iso}$ values for **24′** were smaller than the values of **13′**, suggesting that the antiaromatic character in **24** was weakening by through-space interaction (Table 5-4), which agrees with the results of the ^{1}H NMR studies.

Table 5-4. $NICS_{iso}(X)$ values for **13′**, and **24′**.

	NICS(+1) NICS(0) NICS(−1)	
	six-membered rings	seven-membered rings
13′	7.0/8.0 13.6/12.8 8.2/7.5	2.1 5.1 4.2
24′	−0.5[a]/−2.9[b] 2.8[a]/−0.3[b] −2.8[a]/−6.2[b]	−3.4 −3.4 −6.3

[a] The outer six-membered rings. [b] The inner six-membered rings.

In conclusion, the author synthesized lithium salt of bissilepinyl tetraanion **24**. The mutual π-interactions between the two dibenzosilepinide in **24** were confirmed by molecular orbitals. Antiaromaticity of the dibenzosilepinyl dianion is weakened in its dimeric form as evidenced by the nearly zero NICS values in **21′$_{dimer}$** and **24′**, as well as the low-field shifts of ^{1}H NMR signals of **24** in comparison to those of **13** recorded in THF-d_8.

5-4 Experimental Section

5-4-1 Synthetic Procedures

General Procedure

All manipulations were carried out under an argon atmosphere by using standard Schlenk techniques or a glovebox unless otherwise stated. Et_2O, THF, DME, C_6D_6, toluene-d_8 and THF-d_8 were distilled over potassium mirror. $PhSiCl_3$ was purchased from Tokyo Chemical Industry (TCI). 2,2′-Dibromostilbene was synthesized according to the literature.[5] ^{1}H (500 MHz), $^{13}C\{^{1}H\}$(126 MHz), $^{7}Li\{^{1}H\}$ (194 MHz), and $^{29}Si\{^{1}H\}$ (99 MHz) NMR spectra were recorded on a JEOL ECZ-500 spectrometer at 20°C unless otherwise stated. Chemical shifts are reported in δ and referenced to residual ^{1}H and ^{13}C signals of deuterated solvents as internal standards or to the $^{7}Li\{^{1}H\}$ and the ^{29}Si NMR signal of LiCl in D_2O (δ = 0.00) and $SiMe_4$ in $CDCl_3$ (δ = 0.00), respectively, as external

standards. Elemental analyses were performed on a Perkin Elmer 2400 series II CHN analyzer.

Recrystallization of 13 from toluene.

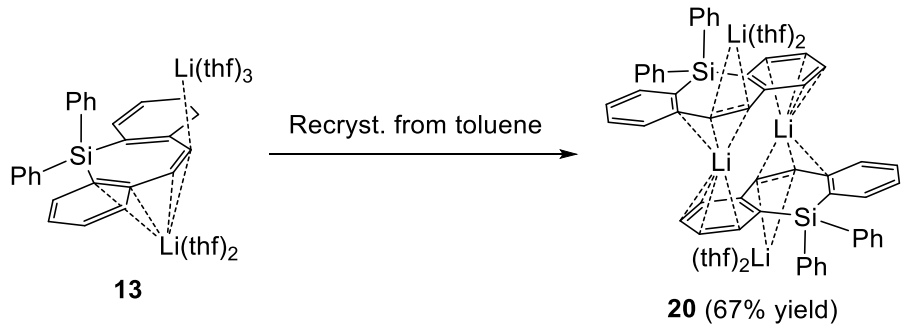

13 **20** (67% yield)

Recrystallization of the black powder of **13** (145.1 mg, 0.197 mmol) from toluene provided the black crystals of **20** (77.7 mg, 0.132 mmol, 67% yield). The ^{1}H NMR signals of **13** and isolated crystals of **20** in toluene-d_8 were both broadened and corresponded each other, suggesting that **13** and **20** are equilibrium in toluene.

Synthesis of dimer 21.

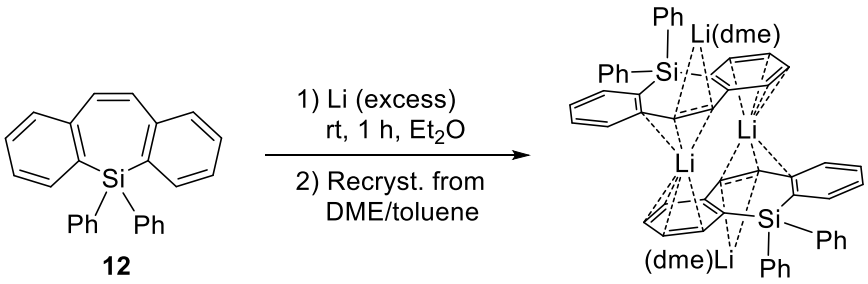

12 **21** (28% yield)

Lithium (28.1 mg, 4.05 mmol) was added to a solution of **12** (50.0 mg, 0.139 mmol) in Et_2O (2 mL) at room temperature. After 1 hour, lithium was removed and the solvent was removed in vacuo to yield black powder (145.1 mg, 0.197 mmol, quant.) Recrystallization of the black powder from DME and toluene provided the black crystals of **21** (17.8 mg, 0.0389 mmol, 28% yield).

Synthesis of chrolophenyldibenzosilepin 22.

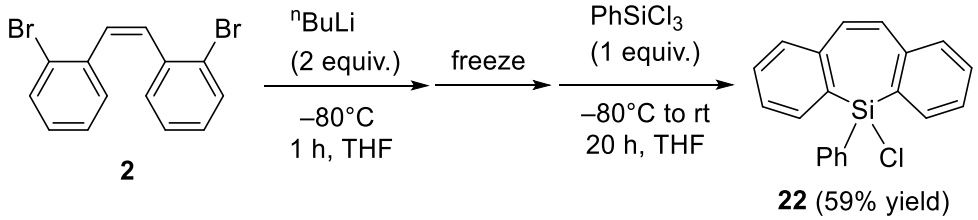

^{n}BuLi (1.59 M, 0.74 mL, 1.18 mmol) was added to a THF solution (20 mL) of dibromostilbene **2** (200.4 mg, 0.592 mmol) in THF at −80 °C. After 1 hour, the solution was frozen and $PhSiCl_3$ (0.14 mL, 184.8 mg, 0.874 mmol) was added dropwise, then the mixture was allowed to gradually warm to room temperature and stirred for 20 hours. The solvent was removed in vacuo, and materials insoluble in CH_2Cl_2 were filtered off. Recrystallization of the crude product from Et_2O yielded **22** as colorless crystals (112.1 mg, 0.352 mmol, 59% yield). ^{1}H NMR (500 MHz, $CDCl_3$): δ = 7.96 (dd, $^{3}J_{H–H}$ = 7 Hz, $^{4}J_{H–H}$ = 2 Hz, 2H, Ar), 7.50 (dt, $^{3}J_{H–H}$ = 7 Hz, $^{4}J_{H–H}$ = 2 Hz, 2H, Ar), 7.46-7.39 (m, 7H, Ar), 7.30 (t, $^{3}J_{H–H}$ = 8 Hz, 2H, vinyl), 6.90 (s, 2H, vinyl).; ^{13}C{^{1}H} NMR (126 MHz, $CDCl_3$): δ = 141.2, 134.8, 134.3, 132.9, 132.3, 132.0, 130.7, 130.6, 130.0, 127.9, 127.9.

Synthesis of bis(phenyldibenzosilepin) 23.

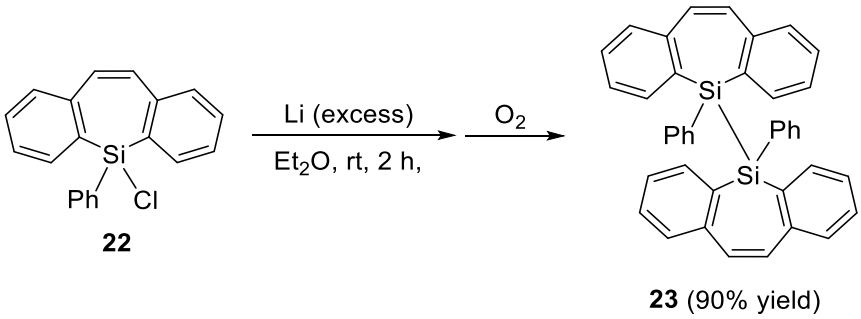

Lithium (31.3 mg, 4.51 mmol) was added to a solution of **22** (68.0 mg, 0.213 mmol) in Et_2O (3 mL) at room temperature. After 2 hour, lithium was removed and the solvent was oxidated by excess oxygen gas to generate the white suspension. The solvent was removed in vacuo, and materials insoluble in CH_2Cl_2 were filtered off. The filtrate was concentrated and purified by column chromatography (eluent: CH_2Cl_2) to yield **23** as white powder (54.3 mg, 0.192 mmol, 90% yield). ^{1}H NMR (500 MHz, $CDCl_3$): δ = 7.41 (dd, $^{3}J_{H–H}$ = 7 Hz, $^{4}J_{H–H}$ = 1 Hz, 2H, Ar), 7.37-7.32 (m, 3H, Ar), 7.29 (td, $^{3}J_{H–H}$ = 8 Hz, $^{4}J_{H–H}$ = 1 Hz, 2H, Ar), 7.22-7.15 (m, 4H, Ar), 7.13 (d, $^{3}J_{H–H}$ = 8 Hz, 2H, Ar), 6.20 (s, 2H, vinyl).; ^{13}C{^{1}H} NMR (126 MHz, $CDCl_3$): δ = 142.6, 137.5, 136.2, 135.2, 134.0, 133.3

(vinyl), 129.5, 129.3, 129.0, 127.7, 127.4.; ^{29}Si{^{1}H} NMR (99 MHz, $CDCl_3$): δ = −24.1.

Synthesis of tetralithium salt of bis(phenyldibenzosilepinide) 25 for NMR assignments.

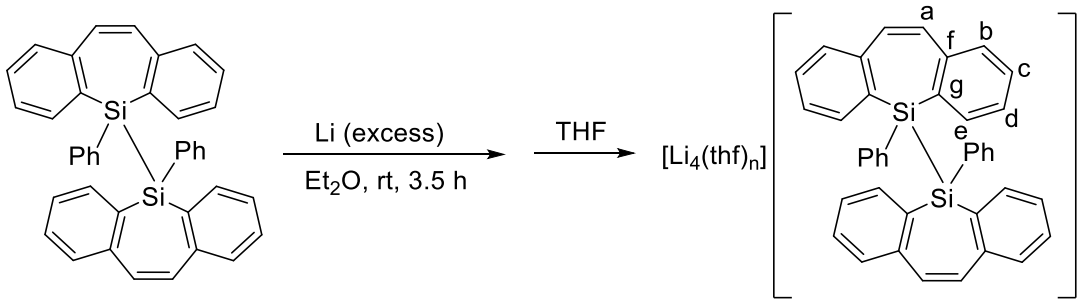

23 **25** (quant. based on NMR)

Lithium (19.0 mg, 2.26 mmol) was added to a solution of **23** (19.0 mg, 0.0670 mmol) in Et_2O (3 mL) at a room temperature. After 3.5 hour, lithium was removed and the solvent was removed in vacuo. THF (0.3 mL) was added to the solution and the solvent was removed in vacuo to yield black powder (36.1 mg, quant. based on NMR, the author does not have any structural information such as the number of coordinating THF molecules in black-powder of **25**). ^{1}H NMR (500 MHz, THF-d_8): δ = 7.52–7.50 (m, 4H, *Ph*), 7.00–6.98 (m, 6H, *Ph*), 6.01 (d, $^{3}J_{H–H}$ = 6 Hz, 4H, H_e), 5.52 (dd, $^{3}J_{H–H}$ = 9 Hz, $^{4}J_{H–H}$ = 1 Hz, 4H, H_b), 5.46 (t, $^{3}J_{H–H}$ = 7 Hz, 4H, H_c), 4.44 (t, $^{3}J_{H–H}$ = 6 Hz, 4H, H_d) , 3.77 (s, 4H, *vinyl*); ^{13}C{^{1}H} NMR (126 MHz, THF-d_8): δ = 144.1 (*ipso-Ph*), 140.9 (C_e), 138.9 (C_f), 137.6 (3°, *Ph*), 126.12 (3°, *Ph*), 126.10 (3°, *Ph*), 124.0 (C_c), 121.1 (C_b), 105.3 (C_g), 96.0 (C_d), 77.3 (*vinyl*); ^{7}Li{^{1}H} NMR (194 MHz, THF-d_8): δ = 0.06; ^{29}Si{^{1}H} NMR (99 MHz, THF-d_8): δ = −39.9.

5-4-2 Theoretical studies

Theoretical calculations were performed by using the *Gaussian* 16 Rev.C.[7] All calculations were performed at the B3LYP[8] level of theory using 6-31+G(d)[9] basis sets. The structural optimization has been carried out for **13′**. The optimized structures of **13′** are in good agreement with the corresponding X-ray structures. All local minima were confirmed by the vibrational frequency calculations with zero imaginary frequency. The NICS values and molecular orbitals for **13′** were calculated using the optimized structures,

while the NICS values and molecular orbitals for **21**, **21′**, **24**, and **24′** were obtained by single point energy calculations using the X-ray structures.

5-4-3 Crystal data

	21	22	23
CCDC			
formula	$C_{74}H_{76}Li_4O_4Si_2$	$C_{20}H_{15}ClSi$	$C_{40}H_{30}Si_2$
fw	1113.28	318.86	566.82
crystal size	0.16 × 0.14 × 0.09	0.09 × 0.07 × 0.06	0.12 × 0.08 × 0.06
crystal system	monoclinic	orthorhombic	monoclinic
space group	*P*21/*n*	*Pbca*	*P*21/*c*
a [Å]	12.1435(12)	9.1188(15)	21.114(5)
b [Å]	18.9003(18)	15.797(3)	9.042(2)
c [Å]	13.4767(13)	21.847(4)	16.875(4)
α [deg]	90	90	90
β [deg]	93.262(2)	90	111.266(4)
γ [deg]	90	90	90
V [Å^3]	3088.1(5)	3147.0(9)	3002.5(12)
Z	2	8	4
ρ_{calcd} [g cm^{-3}]	1.197	1.346	1.254
F(000)	1184	1328	1192
μ [cm^{-1}]	1.07	2.12	1.46
transmission factors range	0.8544 – 1	0.8548 – 1	0.8544 – 1
index range	-15 ≤ h ≤ 15	-11 ≤ h ≤ 11	-26 ≤ h ≤ 26
	-23 ≤ k ≤ 22	-19 ≤ k ≤ 16	-11 ≤ k ≤ 11
	-16 ≤ l ≤ 16	-27 ≤ l ≤ 27	-16 ≤ l ≤ 21
no. reflections	23089	22475	22320
unique (R_{int})	6387 (0.039)	3256 (0.0750)	6169 (0.0534)
$I > 2\sigma$(I)	5022	2777	4752
no. parameters	383	199	379
R_1 ($I > 2\sigma$(I))[a]	0.0511	0.0647	0.0574
wR_2 (all data)[b]	0.1470	0.1488	0.1542
GOF [c]	1.069	1.132	1.069
max diff peak / hole [e Å^{-3}]	0.961/-0.425	0.364/-0.424	0.364/-0.442

	24
CCDC	
formula	$C_{96}H_{60}Li_8O_8Si_4$
fw	1509.32
crystal size	0.21 × 0.14 × 0.05
crystal system	triclinic
space group	*P*-1
a [Å]	11.769(2)
b [Å]	18.155(3)
c [Å]	19.088(3)
α [deg]	86.268(5)
β [deg]	86.102(4)
γ [deg]	89.855(5)
V [Å^3]	4060.3(12)
Z	4
ρ_{calcd} [g cm^{-3}]	2.469
F(000)	3120
μ [cm^{-1}]	2.62
transmission factors range	0.8817 – 1
index range	-14 ≤ h ≤ 14
	-22 ≤ k ≤ 20
	-21 ≤ l ≤ 23
no. reflections	30845
unique (R_{int})	16341 (0.0488)
$I > 2\sigma$(I)	10517
no. parameters	1054
R_1 ($I > 2\sigma$(I))[a]	0.0711
wR_2 (all data)[b]	0.1993
GOF [c]	1.043
max diff peak / hole [e Å^{-3}]	0.540/-0.486

[a] $R1 = \Sigma||F_o| - |F_c||/\Sigma|F_o|$. [b] $wR2 = [\Sigma\{w(F_o^2 - F_c^2)^2\}/\Sigma w(F_o^2)^2]^{1/2}$, w = 1/[□$^2F_o^2$ + (aP)^2 + bP] (a and b are constants suggested by the refinement program; P = [max(F_o^2,0) + 2F_c^2]/3). [c]GOF = $[\Sigma w(F_o^2 - F_c^2)^2/(N_{obs} - N_{params})]^{1/2}$.

5-5 References

(1) M. C. Böhm, P. Bickert, K. Hafner, V. Boekelheide, *Proc. Natl. Acad. Sci.* **1984**, *81*, 2589-2591.

(2) C. Corminboeuf, P. von Ragué Schleyer, P. Warner, *Org. Lett.* **2007**, *9*, 3263-3266.

(3) R. Nozawa, H. Tanaka, W.-Y. Cha, Y. Hong, I. Hisaki, S. Shimizu, J.-Y. Shin, T. Kowalczyk, S. Irle, D. Kim, H. Shinokubo, *Nat. Commun.* **2016**, *7*, 13620.

(4) a) R. Nozawa, J. Kim, J. Oh, A. Lamping, Y. Wang, S. Shimizu, I. Hisaki, T. Kowalczyk, H. Fliegl, D. Kim, H. Shinokubo, *Nat. Commun.* **2019**, *10*, 3576; b) H. Kawashima, S. Ukai, R. Nozawa, N. Fukui, G. Fitzsimmons, T. Kowalczyk, H. Fliegl, H. Shinokubo, *J. Am. Chem. Soc.* **2021**, *143*, 10676–10685.

(5) L. G. Mercier, W. E. Piers, M. Parvez, *Angew. Chem., Int. Ed.* **2009**, *48*, 6108-6111.

(6) (a) E. R. Corey, J. Y. Corey and M. D. Glick, *J. Organomet. Chem.*, 1977, **129**, 17-25; (b) L. G. Mercier, S. Furukawa, W. E. Piers, A. Wakamiya, S. Yamaguchi, M. Parvez, R. W. Harrington and W. Clegg, *Organometallics*, 2011, **30**, 1719-1729; (c) W. Clegg, R. W. Harrington, L. G. Mercier and W. E. Piers, *Acta Crystallogr. Sec. C*, 2013, **69**, 436-438.

(7) M. J. Frisch, G. W. Trucks, H. B. Schlegel, G. E. Scuseria, M. A. Robb, J. R. Cheeseman, G. Scalmani, V. Barone, G. A. Petersson, H. Nakatsuji, X. Li, M. Caricato, A. V. Marenich, J. Bloino, B. G. Janesko, R. Gomperts, B. Mennucci, H. P. Hratchian, J. V. Ortiz, A. F. Izmaylov, J. L. Sonnenberg, Williams, F. Ding, F. Lipparini, F. Egidi, J. Goings, B. Peng, A. Petrone, T. Henderson, D. Ranasinghe, V. G. Zakrzewski, J. Gao, N. Rega, G. Zheng, W. Liang, M. Hada, M. Ehara, K. Toyota, R. Fukuda, J. Hasegawa, M. Ishida, T. Nakajima, Y. Honda, O. Kitao, H. Nakai, T. Vreven, K. Throssell, J. A. Montgomery Jr., J. E. Peralta, F. Ogliaro, M. J. Bearpark, J. J. Heyd, E. N. Brothers, K. N. Kudin, V. N. Staroverov, T. A. Keith, R. Kobayashi, J. Normand, K. Raghavachari, A. P. Rendell, J. C. Burant, S. S. Iyengar, J. Tomasi, M. Cossi, J. M. Millam, M. Klene, C. Adamo, R. Cammi, J. W. Ochterski, R. L. Martin, K. Morokuma, O. Farkas, J. B. Foresman, D. J. Fox, *Gaussian 16 Rev. C.01*, Gaussian, Inc., Wallingford, CT, **2016**.

(8) (a) C. Lee, W. Yang, R. G. Parr, *Phys. Rev. B* **1988**, *37*, 785-789; b) A. D. Becke, *J. Chem. Phys.* **1993**, *98*, 5648-5652.

(9) M. M. Francl, W. J. Pietro, W. J. Hehre, J. S. Binkley, M. S. Gordon, D. J. DeFrees, J. A. Pople, *J. Chem. Phys.* **1982**, *77*, 3654-3665.

Chapter 6

Conclusion and perspectives

In chapter 2, the author synthesized a heavier analog of cycloheptatrienyl anion, lithium dibenzostannepinide **4** which was concluded to be nonaromatic based on the NMR and X-ray diffraction studies. Moreover, the author synthesized thermally stable dilithium dinaphthostannepinide **11**. The ^{1}H NMR signals of **11** were observed at characteristic high-field, suggesting that the anionic charges are delocalized over the whole molecule. The NICS(0)$_{iso}$ values of **11** obtained from the optimized structure were calculated to be large positive values, suggesting its antiaromaticity derived from a 24π-electron system.

In chapter 3, the author has successfully synthesized and characterized dilithium dibenzosilepinide **13**. Hyperconjugation between the π-electrons of C_{α} and the σ*(Si–Ph) orbitals in **13** was revealed by structural features, molecular orbitals, and second-order perturbation theory analysis, and its antiaromaticity was evidenced by NICS values as well as ACID plot.

This is the first synthetic example of anionic hyperconjugative antiaromatic compound, thus generalization is required to obtain a wider knowledge of hyperconjugaive antiaromaticity. For instance, antiaromaticity would be enhanced by replacing the Si atom with other heavier group 14 atoms or using more electron-withdrawing substituents on the Si atom because an energy level of σ* orbital becomes lower.

In chapter 4, the author synthesized trimer **17-THF** encapsulating the Li_9O_2 core. The NMR studies revealed that the trimeric structure is maintained in toluene-d_8, and the antiaromatic character of **17-THF** has been elucidated by both experimental and theoretical ^{7}Li{^{1}H} NMR spectra with explicit downfield shifts due to the paratropic ring currents. Moreover, the author successfully synthesized and characterized tetrabenzospirosilepin tetraanion **19**. Only the ^{1}H NMR signal assignable to the protons situated above the silepin rings in **19** shifted to low-field, which can be attributable to the paratropic ring currents.

In this contribution, the author demonstrated that inorganic salt-assisted assembly of anionic antiaromatic rings is effective to construct a rigid supramolecular complex maintaining Li–π coordination in solution. It is interesting to apply this salt-assisted assembly toward other anionic π-conjugated system, which would result in the formation of unique supramolecular complexes. Using fluorine gas instead of oxygen gas would be also effective to diversify the structure of clusters.

In chapter 5, the author synthesized lithium salt of bissilepinyl tetraanion **24**. The face-to-face π-interactions between the two dibenzosilepinide in **24** were confirmed by molecular orbitals. Antiaromaticity of the dibenzosilepinyl dianion is weakened in its dimeric form as evidenced by the nearly zero NICS values in **21′$_{dimer}$** and **24′**, as well as the low-field shifts of ^{1}H NMR signals of **24** in comparison to those of **13** recorded in THF-d_8.

Face-to-face aromaticity is directly affected by the distance between two surfaces. In tetraanionic species **AT** (Figure 6-1), there are many parameters to control the distance. For example, the replacement of one or two Si atoms with Ge atoms elongates the distance between two surfaces. On the contrary, the removal of metal ions between two surfaces shortenings the distance between two surfaces, and possible methods are the replacement of the lithium cation with other bigger counter cations. The author is interested in the treatment of lithium salt of bissilepinyl tetraanion **24** with NaCl, KCl, or $MgCl_2$ to synthesize corresponding tetraanionic species via deposits of LiCl.

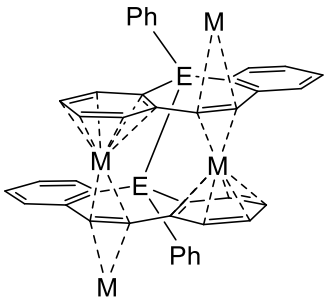

AT

Figure 6-1. Structure of tetraanionic species **AT** (E = heteroatoms, M = counter cations).

Publication list

(1) A Tin Analogue of the Cycloheptatrienyl Anion: Synthesis, Structure, and Further Reduction to Form a Dianionic Species
Shotaro Ito, Takuya Kuwabara, Yoichi Ishii
Organometallics **2020**, *39*, 640–644.

(2) A New Strategy for Hyperconjugative Antiaromatic Compounds Utilizing Negative Charges: a Dibenzo[*b*,*f*]silepinyl Dianion
Shotaro Ito, Kazuya Ishimura, Yoichi Ishii, Takuya Kuwabara
Chem. Commun. **2021**, *57*, 11330–11333.

(3) Inorganic Salt-assisted Assembly of Anionic π-Conjugated Rings Enabling ^{7}Li NMR-based Evaluation of Antiaromaticity
Shotaro Ito, Yoichi Ishii, Takuya Kuwabara
Dalton Trans. **2022**, *51*, 16397–16402.

(4) Synthesis of Dimerized Dibenzosilepinyl Dianion: Experimental Investigation of Face-to-Face Aromaticity in Anionic Compounds
Shotaro Ito, Yoichi Ishii, Takuya Kuwabara
Manuscript in preparation.